MARYLAND

COLLEGE PARK CAMPUS

VALIDATION OF RECIPES FOR THE RECOVERY OF STRESSES AND DERIVATIVES BY A COMPUTER-BASED APPROACH

by

I. Babuška
T. Strouboulis
S. K. Gangaraj
C. S. Upadhyay

94pp

Technical Note BN-1170

and

CMC Report No. 94-03
Texas Engineering Experiment Station
The Texas A&M University System

May 1994

INSTITUTE FOR PHYSICAL SCIENCE AND TECHNOLOGY

SECURITY CLASSIFICATION OF THIS PAGE (When Data Entered)

REPORT DOCUMENTATION PAGE		READ INSTRUCTIONS BEFORE COMPLETING FORM
1. REPORT NUMBER Technical Note BN-1170	2. GOVT ACCESSION NO.	3. RECIPIENT'S CATALOG NUMBER
4. TITLE (and Subtitle) Validation of Recipes for the Recovery of Stresses and Derivatives by a Computer-Based Approach		5. TYPE OF REPORT & PERIOD COVERED Final Life of Contract 6. PERFORMING ORG. REPORT NUMBER
7. AUTHOR(s) I. Babuska[1] - T. Strouboulis[2] - S. K. Gangaraj - C. S. Upadhyay		8. CONTRACT OR GRANT NUMBER(s) [1]N00014-90-J-1030 / ONR CCR-88-20279 / NSF [2]See Page 1
9. PERFORMING ORGANIZATION NAME AND ADDRESS Institute for Physical Science and Technology University of Maryland College Park, MD 20742-2431		10. PROGRAM ELEMENT, PROJECT, TASK AREA & WORK UNIT NUMBERS
11. CONTROLLING OFFICE NAME AND ADDRESS Department of the Navy Office of Naval Research Arlington, VA 22217		12. REPORT DATE May 1994 13. NUMBER OF PAGES 60 + Figs. 1 - 22
14. MONITORING AGENCY NAME & ADDRESS(if different from Controlling Office)		15. SECURITY CLASS. (of this report) 15a. DECLASSIFICATION/DOWNGRADING SCHEDULE

16. DISTRIBUTION STATEMENT (of this Report)

Approved for public release: distribution unlimited

17. DISTRIBUTION STATEMENT (of the abstract entered in Block 20, if different from Report)

18. SUPPLEMENTARY NOTES

19. KEY WORDS (Continue on reverse side if necessary and identify by block number)

20. ABSTRACT

In this paper we present a methodology for checking the local quality of recipes for the recovery of stresses or derivatives from finite element solutions of linear elliptic problems. The methodology accounts precisely for the factors which affect the local quality of the recovered quantities, namely: the geometry of the grid, the polynomial degree and the type of the elements, the coefficients of the differential equation and the class of solutions of interest. We give examples of how the methodology can be used to obtain precise conclusions about the quality of a class of recipes, based on *least-squares patch-recovery*, in the interior of complex grids, like the ones employed in engineering computations. By using this approach we were able to discover recipes which are much more robust than the ones which are currently in use in the various finite element codes.

DD FORM 1473 EDITION OF 1 NOV 65 IS OBSOLETE

Validation of recipes for the recovery of stresses and derivatives by a computer-based approach

I. Babuška*
Institute for Physical Science and Technology and Department of Mathematics,
University of Maryland, College Park, MD 20742, U.S.A.

T. Strouboulis†, S.K. Gangaraj† and C.S. Upadhyay†
Department of Aerospace Engineering, Texas A&M University,
College Station, TX 77843, U.S.A.

May 1994

*The work of this author was supported by the U.S. Office of Naval Research under Contract N00014-90-J-1030 and by the National Science Foundation under Grant CCR-88-20279.

†The work of these authors was supported by the U.S. Army Research Office under Grant DAAL03-G-028, by the National Science Foundation under Grant MSS-9025110 and by the Texas Advanced Research Program under Grant TARP-71071.

Abstract:

In this paper we present a methodology for checking the local quality of recipes for the recovery of stresses or derivatives from finite element solutions of linear elliptic problems. The methodology accounts precisely for the factors which affect the local quality of the recovered quantities, namely, the geometry of the grid, the polynomial degree and the type of the elements, the coefficients of the differential equation and the class of solutions of interest. We give examples of how the methodology can be used to obtain precise conclusions about the quality of a class of recipes, based on *least-squares patch-recovery*, in the interior of complex grids, like the ones employed in engineering computations. By using this approach we were able to discover recipes which are much more robust than the ones which are currently in use in the various finite element codes.

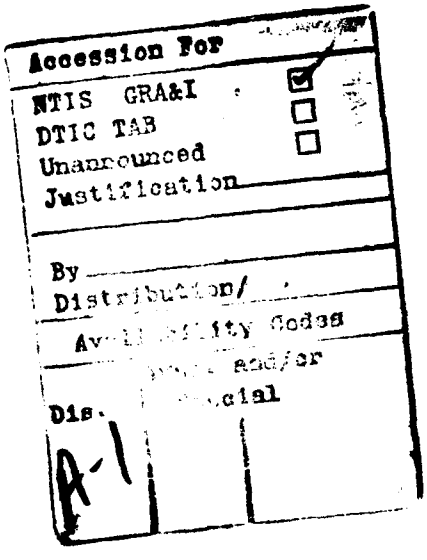

1 Introduction

The subject of superconvergence studies techniques which can be employed to increase, at a relatively small cost, the accuracy of quantities (derivatives of the solution, strains, stresses etc.) recovered from finite element solutions. Because of its obvious importance in finite element practice the superconvergence of finite element approximations has been studied by several investigators in the mathematical and the engineering literature; see for example [1-46] and the citations in these papers.

We distinguish two types of superconvergence according to the way that the values of the solution quantities are recovered, namely:

1. *Direct superconvergence*: The values of the solution quantities are obtained by *direct evaluation* from the finite element solution *at special points*, the superconvergence points for the solution quantity in the element (see, among others, [6], [10], [13], [14], [47] and [50]).

2. *Superconvergence via averaging*: The values of the solution quantities at a point are obtained by averaging the values of the finite element solution in a neighborhood of the point. According to the definition of the neighborhood, in which the averaging is computed, we have:

   a. *Global or subdomain averaging*: The neighborhood is either the entire domain (see [2], [3], [9], [11], [12], [15], [16-17], [42]) or a subdomain which does not depend on the mesh-size (see [15], [16-17], [42]).

   b. *Local or semilocal averaging*: The neighborhood is a *mesh-cell* of elements which are connected to a vertex, an edge or an element (local h-neighborhood) or such a mesh-cell and a few mesh-layers around it (semilocal h-neighborhood) (see also [46]).

In this paper we will study superconvergence via local averaging; the case of direct superconvergence will also be considered (as a special case where the averaging is the pointwise evaluation of the solution quantity directly from the finite element solution). For a detailed study of direct superconvergence for meshes of triangles and quadrilaterals see [47-50].

The objective of this paper is to develop computer-based methodologies for checking the quality of recipes for the recovery of solution quantities. We will apply the methodologies in the study of recipes based on least-squares patch-recovery of the type given in [35-40]; these recipes recover the solution quantities in an element from the finite element solution in the element and one mesh-layer around it. It is also possible to define various recipes (see [41] and [44] and Section 4 below) which take into account the information about the data (the body-force,

boundary-traction) and the differential operators (i.e. the differential equation, the traction boundary-condition) and the quality of these recipes can be checked by using exactly the same approach.

In the engineering literature the quality of recipes is often evaluated by observing their performance in a few example problems (*benchmarks*) (e.g. [24], [35-40], [41], [43] and [44]). This approach has serious shortcomings because the quality of recipes is sensitive to the structure of the solution and the meshes employed. The quality of the recovered solution quantities can be very different depending on whether the meshes are translation-invariant or general, whether the meshes are nearly equilibrated (or not) and whether the solution has singular points. The performance of a recipe can be very different in the neighborhood of a singular-point, at a smooth-boundary and in the interior of the mesh. Hence *benchmark computations could motivate misleading conclusions unless each benchmark is more or less representative of a precise class of computational problems and the conclusions are employed for this class of problems.*

In this paper we will define precisely the notion of the quality of the recipes and we will present a theory-based computational methodology for the assesment of the quality of the recipes in the interior of the domain and smooth solutions. Similar approaches for checking the quality of recipes at smooth boundaries and in the neighborhood of singular points will be given in forthcoming papers. The approach takes directly into account the factors which affect the quality of the recipes, namely:

a. *The local geometry of the grid*;

b. *The coefficients of the differential equation*;

c. *The polynomial degree and the type of the elements* (triangles, tensor-product quadrilaterals, serendipity squares etc.);

d. *The class of solutions of interest.*

Below we will give illustrative examples of how the quality of a recipe is influenced by these factors.

Following this Introduction we outline the model elliptic problems (Poisson's equation and the elasticity problem). We give a new definition of superconvergence and based on this definition we develop a theory for checking recipes in the interior of any class of meshes and for any class of material coefficients and we give several examples of application of the theory for studying the quality of recipes based on least-squares patch-recovery in the interior of complex finite element grids. We give examples of new recipes (which are similar, but less expensive, to the ones given in [35-40]) which also employ the available information about the differential equation and the right-hand side in the design of the recipe. By employing the

methodology of the paper we were able to show that one of these recipes is much more robust than the recipes in [35-40].

2 The model problems

We shall consider the vector-valued boundary-value problem

$$\left.\begin{aligned} L_i(\mathbf{u}) := -\sum_{j=1}^{2} \frac{\partial}{\partial x_j}\big(\sigma_{ij}(\mathbf{u})\big) = f_i \qquad & \text{in } \Omega \\ u_i = 0 \qquad & \text{on } \Gamma_D \\ \sum_{j=1}^{2} \sigma_{ij}(\mathbf{u}) n_j = \bar{t}_i \qquad & \text{on } \Gamma_N \end{aligned}\right\} \tag{1}$$

where $i = 1, 2$.

Here $\Omega \subset \mathbf{R}^2$ is a bounded domain with boundary $\partial\Omega = \Gamma_D \cup \Gamma_N$;

$\mathbf{n} := (n_1, n_2)$ is the outward pointing unit-normal on Γ_N;

f_i, $i = 1, 2$ are the components of the load-vector (*body-force*);

$\bar{t}_i$, $i = 1, 2$ are the components of the normal-flux vector (*traction*) applied on Γ_N;

$\Gamma_D \neq \emptyset$, $\Gamma_D \cap \Gamma_N = \emptyset$; $\mathbf{u} = (u_1, u_2)$ is the solution-vector (*displacement*);

$$\epsilon_{ij}(\mathbf{u}) := \frac{1}{2}\Big(\frac{\partial u_i}{\partial x_j} + \frac{\partial u_j}{\partial x_i}\Big), \qquad \sigma_{ij}(\mathbf{u}) := \sum_{k,\ell=1}^{2} a_{ijk\ell}\, \epsilon_{k\ell}(\mathbf{u}), \qquad i, j = 1, 2 \tag{2}$$

are the components of the flux (*strain, stress*);

$a_{ijk\ell}$, $i, j, k, \ell = 1, 2$, are the material-coefficients (*elastic constants*) which in the case of isotropic plane elasticity are given by $a_{ijk\ell} = \mu(\delta_{ij}\delta_{k\ell} + \delta_{i\ell}\delta_{kj}) + \lambda\delta_{ik}\delta_{j\ell}$ where δ_{ij} is Kronecker's delta and λ, μ are Lamé's constants.

We also introduce the scalar elliptic boundary-value problem (*heat-conduction in orthotropic medium*), namely

$$\left.\begin{aligned} L'(u) := -\sum_{k,\ell=1}^{2} \frac{\partial}{\partial x_k}\left(K_{k\ell}\frac{\partial u}{\partial x_\ell}\right) = f \qquad & \text{in } \Omega \\ u = 0 \qquad & \text{on } \Gamma_D \\ \sum_{k=1}^{2} q_k(u) n_k = \bar{g} \qquad & \text{on } \Gamma_N \end{aligned}\right\} \tag{3}$$

Here f is the source function (*heat-source*); $\bar{g}$ the boundary-flux (*heat-flux*); $q_k(u) := \sum_{\ell=1}^{2} K_{k\ell}\frac{\partial u}{\partial x_\ell}$, $k = 1,2$ are the components of the flux-vector (*heat-flux*); $K_{k\ell}$, $k,\ell = 1,2$, are the entries of the *thermal-conductivity* matrix which is symmetric, positive definite. Below we will let $K_{\min}, K_{\max}$ denote the principal values of the thermal-conductivity matrix.

Let us now cast the problems in the variational form. Let us denote the space of test-functions by

$$\mathbf{H}^1_{\Gamma_D} := \left\{ (v_1, v_2) \;\middle|\; v_i \in H^1(\Omega),\ v_i = 0 \text{ on } \Gamma_D \right\} \tag{4}$$

The variational form of the boundary-value problem (1) is now posed as:

Find $\mathbf{u} \in \mathbf{H}^1_{\Gamma_D}$ such that

$$B_\Omega(\mathbf{u}, \mathbf{v}) = \int_\Omega \sum_{i=1}^{2} f_i v_i + \int_{\Gamma_N} \sum_{i=1}^{2} \bar{t}_i v_i \qquad \forall\, \mathbf{v} \in \mathbf{H}^1_{\Gamma_D} \tag{5}$$

where the bilinear form $B_\Omega : \mathbf{H}^1_{\Gamma_D} \times \mathbf{H}^1_{\Gamma_D} \to \mathbf{R}$ is defined by

$$B_\Omega(\mathbf{u}, \mathbf{v}) := \int_\Omega \sum_{i,j,k,\ell=1}^{2} a_{ijk\ell} \frac{\partial u_j}{\partial x_\ell}\frac{\partial v_i}{\partial x_k} \tag{6}$$

The energy-norm over any subdomain $S \subseteq \Omega$ is defined by

$$|||\mathbf{v}|||_S := \sqrt{B_S(\mathbf{v}, \mathbf{v})} \tag{7}$$

where $B_S(\mathbf{u}, \mathbf{v})$ has the obvious meaning.

In the case of the scalar elliptic problem (3) the bilinear form is given by $b_\Omega(u, v) := \int_\Omega \sum_{k,\ell=1}^{2} K_{k\ell}\frac{\partial u}{\partial x_\ell}\frac{\partial v}{\partial x_k}$. The weak-solution of (3) satisfies:

Find $u \in H^1_{\Gamma_D} := \left\{ v \in H^1(\Omega) \;\middle|\; v = 0 \;\text{ on }\; \Gamma_D \right\}$ such that

$$b_\Omega(u,v) = \int_\Omega fv + \int_{\Gamma_N} \bar{t}v \qquad \forall\; v \in H^1_{\Gamma_D} \tag{8}$$

The energy-norm in any subdomain $S \subseteq \Omega$ is defined by $|||v|||_S := \sqrt{b_S(v,v)}$.

Let $\mathcal{T} = \{T_h\}$ be a family of meshes of triangles or quadrilaterals with straight edges. It is assumed that the family is regular (for the triangles the minimal angle of all the triangles is bounded below by a positive constant, the same for all the meshes; for the quadrilaterals see conditions (37.40) in Ciarlet [52]). The meshes are not assumed to be quasiuniform. We introduce the conforming finite-element spaces for the scalar model problem (the corresponding spaces of vector-valued functions for the elasticity problem are defined similarly):

$$S^p_h(T_h) := \left\{ u \in C^0(\Omega) \;\middle|\; u|_{\tau_k} \in S^p_h(\tau_k), \quad k = 1, \ldots, M(T_h) \right\}, \tag{9}$$

where $S^p_h(\tau_k) = \mathcal{P}_p(\tau_k)$, for the meshes of triangles, while for the meshes of quadrilaterals

$$S^p_h(\tau_k) := \left\{ w \in C^\infty(\tau_k) \;\middle|\; w \circ \mathbf{F}_{\tau_k} \in \hat{S}^{(p,p)}(\hat{\tau}) \right\} \tag{10}$$

where $\hat{\tau} := (-1,1)^2$ is the master-element and $\mathbf{F}_{\tau_k}$ is the bilinear mapping of $\hat{\tau}$ onto τ_k; $M(T_h)$ is the number of elements in T_h and

$$\hat{S}^{(p,p)}(\hat{\tau}) := \left\{ \hat{P} \;\middle|\; \hat{P}(\hat{x}_1, \hat{x}_2) = \sum_{\substack{i,j \\ 0 \le i,j \le p}} \alpha_{i,j}\, \hat{x}_1^i\, \hat{x}_2^j \right\} \tag{11}$$

Let $P(x_1,x_2) = \sum\limits_{0 \le m+n \le p} c_{mn}\, x_1^m x_2^n$ be a polynomial of degree p; noting that

$$x_1 = \sum_{i,j=0}^{1} a_{ij}\, \hat{x}_1^i\, \hat{x}_2^j\,, \qquad x_2 = \sum_{i,j=0}^{1} b_{ij}\, \hat{x}_1^i\, \hat{x}_2^j \tag{12}$$

we get

$$P(x_1,x_2) = \sum_{0 \le m+n \le p} c_{mn} \Big(\sum_{i,j=0}^{1} a_{ij}\, \hat{x}_1^i\, \hat{x}_2^j \Big)^m \Big(\sum_{k,l=0}^{1} b_{ij}\, \hat{x}_1^k\, \hat{x}_2^l \Big)^n = \sum_{\substack{0 \le s \le p \\ 0 \le t \le p}} d_{st}\, \hat{x}_1^s\, \hat{x}_2^t \tag{13}$$

Hence *any polynomial of degree p belongs to the span of the shape-functions* $S^p_h(\tau_k)$ *on every physical quadrilateral element* τ_k.

We let $S^p_{h,\Gamma_D} := S^p_h(T_h) \cap H^1_{\Gamma_D}$ denote the discrete test-space. The finite element solution u_h (for the heat-conduction problem) satisfies:

Find $u_h \in S^p_{h,\Gamma_D}$ such that

$$b_\Omega(u_h, v_h) = \int_\Omega f v_h + \int_{\Gamma_N} g v_h \qquad \forall\, v_h \in S^p_{h,\Gamma_D} \tag{14}$$

The error is $e_h := u - u_h$. The finite element solution and the error for the elasticity problem are defined similarly.

3 A new definition of superconvergence

The assessment of the quality of the recipes will be based on the following new definition of superconvergence (see also [47-50]): Let $\{u_h\}$ be a one parameter sequence of finite element solutions of a problem which are computed using a sequence of meshes $\mathcal{T} = \{T_h\}$ and let u denote the exact solution. Let us assume that we are interested in the values of the linear functional $F(u)(\bar{\mathbf{x}})$ (i.e. the values of the components of strain, stress or the gradient of the displacement) at a point $\bar{\mathbf{x}}$. We will let $\mathcal{F}(u_h)(\bar{\mathbf{x}})$ to denote the *recovered* value of $F(u)(\bar{\mathbf{x}})$ obtained from the *averaging* $\mathcal{F}$ which is assumed to be in the form

$$\mathcal{F}(u_h)(\bar{\mathbf{x}}) := \sum_{i=1}^{N} \beta_i^{F(u)}(\bar{\mathbf{x}}) u_h(\bar{\mathbf{x}}_i) \tag{15}$$

where $\{\bar{\mathbf{x}}_i\}_{i=1}^N$ is a set of points, which may include $\bar{\mathbf{x}}$, in an h-neighborhood of $\bar{\mathbf{x}}$ (as shown in Fig. 1) and $\{\beta_i^{F(u)}\}_{i=1}^N$ are the coefficients corresponding to the quantity $F(u)$. If $F(u)$ has several components it is understood that (15) holds with a different set of coefficients for each component. Let us denote by

$$\omega_{\bar{\mathbf{x}}} := \bigcup_{\bar{\mathbf{x}} \in \tau} \tau\,, \qquad \tau \in T_h \tag{16}$$

the mesh-cell which consists of the elements which include $\bar{\mathbf{x}}$ in their interior or boundary. (If $\bar{\mathbf{x}}$ is at a vertex (resp. on an edge) $\omega_{\bar{\mathbf{x}}}$ is the set of elements connected to the vertex (resp. to the edge)). We let

$$\Psi(\omega_{\bar{\mathbf{x}}}) := \max_{\mathbf{x} \in \omega_{\bar{\mathbf{x}}}} \left| F(u - u_h)(\mathbf{x}) \right| \tag{17}$$

Here $\left| \cdot \right|$ indicates the modulus employed for the quantity $F(u)$. (If $F(u)$ is a scalar-quantity (one component of stress, strain or of the gradient) $\left| \cdot \right|$ is the absolute value, if $F(u)$ is a vector-valued quantity $\left| \cdot \right|$ is the vector-modulus,

if $F(u)$ is a second-order tensor $|\cdot|$ denotes an invariant, like for example the second invariant, the second invariant of the deviator, etc.)

We will be interested in the values of *the error in the recovered quantity* $\mathcal{F}(u_h)(\bar{\mathbf{x}})$ *relative to the maximum error of the finite-element solution in* $\omega_{\bar{\mathbf{x}}}$, namely

$$\Theta(\bar{\mathbf{x}}; F; \mathcal{F}; u; \omega_{\bar{\mathbf{x}}}, T_h) := \begin{cases} \dfrac{\left| F(u)(\bar{\mathbf{x}}) - \mathcal{F}(u_h)(\bar{\mathbf{x}}) \right|}{\Psi(\omega_{\bar{\mathbf{x}}})} & , \quad \text{if } \Psi(\omega_{\bar{\mathbf{x}}}) \neq 0 \\ 0 & , \quad \text{if } \Psi(\omega_{\bar{\mathbf{x}}}) = 0 \end{cases} \tag{18}$$

Let us note that the relative error with respect to $\Psi(\omega_{\bar{\mathbf{x}}})$ has clear meaning. We compare the quality of the recovered value at $\bar{\mathbf{x}}$ with the maximum error in the quantity computed directly from the finite element solution in the mesh-cell $\omega_{\bar{\mathbf{x}}}$.

If the point $\bar{\mathbf{x}}$ and the averaging $\mathcal{F}$ are such that

$$\Theta(\bar{\mathbf{x}}; F; \mathcal{F}; u; \omega_{\bar{\mathbf{x}}}, T_h) \leq \frac{\eta}{100} \qquad \text{as} \quad h \longrightarrow 0 \tag{19}$$

then $\mathcal{F}(u_h)(\bar{\mathbf{x}})$ will be called u-η%-*superconvergent* relative to the exact solution u and the family of meshes $\mathcal{T}$. Given a class of solutions $\mathcal{U}$, we let

$$\mathcal{H}(\bar{\mathbf{x}}; F; \mathcal{F}; \mathcal{U}; \omega_{\bar{\mathbf{x}}}, T_h) = \max_{u \in \mathcal{U}} \Theta(\bar{\mathbf{x}}; F; \mathcal{F}; u; \omega_{\bar{\mathbf{x}}}, T_h) \tag{20}$$

denote *the maximum relative error in* $\mathcal{F}(u_h)$ *at* $\bar{\mathbf{x}}$ *for the class* $\mathcal{U}$. The dependence of $\mathcal{H}(\bar{\mathbf{x}}; F; \mathcal{F}; \mathcal{U}; \omega_{\bar{\mathbf{x}}}, T_h)$ on $\mathcal{U}$ is very essential. In practical computation we know *a-priori* some of the properties of the solution. For example if the distributed load is zero we know that the solution satisfies the homogeneous differential equation. Then we can restrict the set $\mathcal{U}$ to the set of solutions of the homogeneous differential equation. (Below we will see that the quality of a recipe can be very different for different classes $\mathcal{U}$. Of course it is preferable that the quality of a recipe is good for a large class $\mathcal{U}$; then we can say that the recipe is robust.)

We will say that the value $\mathcal{F}(u_h)(\bar{\mathbf{x}})$ is $\mathcal{U}$-η%-*superconvergent* if

$$\mathcal{H}(\bar{\mathbf{x}}; F; \mathcal{F}; \mathcal{U}; \omega_{\bar{\mathbf{x}}}, T_h) \leq \frac{\eta}{100} \qquad \text{as} \qquad h \longrightarrow 0 \tag{21}$$

If, in addition, we have

$$\mathcal{H}(\bar{\mathbf{x}}; F; \mathcal{F}; \mathcal{U}; \omega_{\bar{\mathbf{x}}}, T_h) \longrightarrow 0 \qquad \text{as} \qquad h \longrightarrow 0 \tag{22}$$

then $\mathcal{F}(u_h)(\bar{\mathbf{x}})$ is $\mathcal{U}$-superconvergent in the *classical sense*. It means that the rate of convergence of $\mathcal{F}(u_h)(\bar{\mathbf{x}})$ to the exact value $F(u)(\bar{\mathbf{x}})$ is higher than the global rate of convergence of the quantity $F(u_h)$.

It is well known that classical superconvergence is *very sensitive to the geometry of the grid, the class of solutions of interest and the coefficients of the differential operator* (see for example [48] and [50] for direct superconvergence; the situation is very similar for superconvergence via averaging). Let us note that if η in (21) is very small (smaller than a tolerance) we can still *practically* speak about a superconvergent value (with a given tolerance), which is the reason for introducing the notion of $\eta\%$-superconvergence. Note that $\eta\%$-superconvergence, as classical superconvergence, has asymptotic character for $h \longrightarrow 0$. *However, unlike classical superconvergence, which holds only for special grids and a fixed set of coefficients of the differential equation, $\eta\%$-superconvergence is well-defined for any classes of grids and for an entire class of coefficients.*

Remark 3.1. Note also that the notion of superconvergence can be understood in different ways. For example we can be interested in the quantity.

$$\Phi_q(\{\bar{\mathbf{x}}_\tau\}; F; \mathcal{F}; u; \{\tau\}, T_h) := \frac{\Big(\sum\limits_{\tau\in\{\tau\}}\sum\limits_{\bar{\mathbf{x}}_\tau\in\{\bar{\mathbf{x}}_\tau\}} \Big| F(u)(\bar{\mathbf{x}}_\tau) - \mathcal{F}(u_h)(\bar{\mathbf{x}}_\tau)\Big|^q\Big)^{\frac{1}{q}}}{\Big(\sum\limits_{\tau\in\{\tau\}} (\Psi(\tau))^q\Big)^{\frac{1}{q}}} \tag{22}$$

where $\{\tau\}$ is a set of elements, $\{\bar{\mathbf{x}}_\tau\}$ is a set of points in each element. Then the pointwise superconvergence is related to $q = \infty$. Very often (see [49] for concrete examples in the case of meshes with local refinements) we get $\Phi_q \longrightarrow 0$ as $h \longrightarrow 0$ (in fact $\Phi_q \approx h^{\frac{1}{q}}$). Various authors are also calling this effect superconvergence (see e.g. [13, 14]). The notion of superconvergence depends on its measure, e.g. if measured in L^q-norm, $q < \infty$, we may get superconvergence effects where for $q = \infty$ there may be no superconvergence (see [49] for further details). Hence *the term superconvergence has to be properly defined.*

Given a recipe $\mathcal{F}$ and $0 \leq \eta < \infty$ we will be interested in the *$\eta\%$-superconvergence regions of $\mathcal{F}(u_h)$ in the element $\tau \in T_h$ for the class of exact solutions $\mathcal{U}$:*

$$\mathcal{R}^{\eta\%}_{F(u)}(\mathcal{U}; \mathcal{F}; \tau, T_h) := \left\{\mathbf{x} \in \tau \;\middle|\; \mathcal{H}(\mathbf{x}; F; \mathcal{F}; \mathcal{U}; \tau, T_h) < \frac{\eta}{100}\right\} \tag{23}$$

Given two recipes $\mathcal{F}^1$ and $\mathcal{F}^2$ and a point $\bar{\mathbf{x}}$ we define the *index of relative robustness of the recipes at $\bar{\mathbf{x}}$.*

$$\mathcal{D}_{F(u)}(\bar{\mathbf{x}}; \mathcal{U}; \mathcal{F}^1, \mathcal{F}^2; \tau, T_h) = \frac{\mathcal{H}(\bar{\mathbf{x}}; F; \mathcal{F}^1; \mathcal{U}; \tau, T_h)}{\mathcal{H}(\bar{\mathbf{x}}; F; \mathcal{F}^2; \mathcal{U}; \tau, T_h)} \tag{24}$$

Here we will assume that the denominator can be equal to zero only at isolated points (this assumption that these points are isolated may be violated only for

very special mesh-geometries like meshes of squares, triangles arranged in a three-directional pattern, etc.) where the quotient is defined equal to ∞ (unless it is equal to $\frac{0}{0}$ in which case we will define it by continuity). We will be interested in the regions in the element $\tau \in T_h$ where $\mathcal{F}^2$ *is more robust than* $\mathcal{F}^1$, namely

$$\mathcal{A}_{F(u)}(\mathcal{U}; \mathcal{F}^1, \mathcal{F}^2; \tau, T_h) := \left\{ x \in \tau \;\middle|\; \mathcal{D}_{F(u)}(x; \mathcal{U}; \mathcal{F}^1, \mathcal{F}^2; \tau, T_h) > 1 \right\} \tag{25}$$

Obviously the above introduced notions are defining exactly the (asymptotic) quality of the recipe. *Comparisons of recipes should be based on computations of the above quantities, for the classes of meshes and solutions of interest, and not on arbitrarily selected benchmarks.*

One is interested to know a-priori the quantities defined above for classes of solutions of interest. (In the practical computations in plane elasticity and heat-conduction the class of solutions of interest is *the class of "harmonic" solutions* (i.e. the solutions which satisfy the homogeneous differential equation) with a finite number of algebraic point singularities of the type r^α at isolated points on the boundary and material-interfaces). In this paper we will determine a-priori the quantities defined in (18), (20), (23), (24), (25) under the following assumptions:

1. The grid is locally periodic with period h (details about how the limit $h \to 0$ is taken are given below);

2. We will study the superconvergence in mesh-patches in the interior of the domain where the solution is smooth (It is approximated well by its local Taylor-series expansion of degree $(p+1)$ where p is the polynomial degree of the elements);

3. The global modes of the error (pollutions), in the elements of interest, are negligible when compared with the magnitude of the error in the local best-approximation (see [51] and [53]).

The detailed theoretical setting and the precise assumptions are given in [47] (see also the outline given below). Our theory has an asymptotic character i.e. it gives the precise results when the mesh is sufficiently refined or the accuracy of the finite element solution is reasonably high. *The theory of this paper cannot be applied when the exact solution is unsmooth* (in the mesh-cell or element of interest) *or when the mesh is coarse.*

We now give an example to explain the meaning of the new definition of superconvergence. Let us consider the Dirichlet boundary-value problem for the Laplacian

$$\left.\begin{aligned} \Delta u = 0 \qquad & \text{in } \Omega := (0,1) \\ u = \bar{u} \qquad & \text{on } \partial\Omega \end{aligned}\right\}$$

where $\bar{u}$ is the boundary-value corresponding to the exact solution $u(x_1, x_2) = \sin(\pi x_1)\sinh(\pi x_2)$. We computed a sequence of finite element solutions $\{u_h\}$ using a sequence of meshes of skewed bilinear quadrilaterals $\{T_h\}$. These meshes were obtained by subdividing the square-domain Ω into a uniform three-directional mesh of triangles and by converting each triangle into three quadrilaterals by connecting the centroid of the triangle with the midpoints of its edges. The reason for choosing such a mesh instead of a regular mesh of bilinear squares is because we would like to give an illustrative example of the new definition in a case where it is different than the classical definition of superconvergence.

We considered the sequence of meshes $\{T_h\}$, $h = \frac{1}{4}, \frac{1}{8}, \frac{1}{16}, \frac{1}{32}$; the mesh $T_{\frac{1}{4}}$ is shown in Fig. 2a. We considered the mesh-cell $\omega_{2h} = (0.25 - h, 0.75 - h)\times(0.25 + h, 0.75 + h)$ which consists of four square subcells ω_h^i, $i = 1, \ldots, 4$, as shown in Fig. 2b. We identified points $\bar{\mathbf{x}}_K^{\omega_h^i}$, $K = 1, \ldots, 6$, in each subcell ω_h^i. The points with identical subscripts K have identical relative positions with respect to the corresponding subcell. We computed the value of

$$\Theta_K^h := \max_{i=1,\ldots,4} \Theta(\bar{\mathbf{x}}_K^{\omega_h^i}; \frac{\partial u}{\partial x_i}; \mathcal{F}; u; \tau_K^i, T_h), \qquad K = 1, \ldots, 6$$

where $\mathcal{F}$ is the ZZ-1 recipe given in Section 8, τ_K^i is the element where the point $\bar{\mathbf{x}}_K^{\omega_h^i}$ belongs. In Fig. 3 we show the graphs of Θ_K^h versus $\frac{1}{h}$ for $K = 1, 2, 5, 6$. These values converge, for $h \longrightarrow 0$, to the asymptotic values which were determined by the theoretical analysis of Section 5.

We also computed the rate of convergence for all the points. From theorem 2 and Remark 5.2 in Section 5 below we have

$$| F(u) - \mathcal{F}(u_h) | = \tilde{\Theta}_K \Psi(\bigcup_{i=1}^{4} \omega_h^i) + C_1 h^{1+\sigma_0'} + o(h^{1+\sigma_0'}), \qquad \sigma_0' > 0$$

where $\tilde{\Theta}_K$ denotes the asymptotic value of the relative error at the point which corresponds to K and $\Psi(\bigcup_{i=1}^{4} \omega_h^i)$ is the maximum error in $F(u)$ in the assembly of the four mesh-cells. We have $\Psi(\bigcup_{i=1}^{4} \omega_h^i) = C_0 h + o(h)$; hence we expect the error

in the recovered quantity to converge to zero linearly, unless $\tilde{\Theta}_K$ is zero (i.e. the point is a 0%-superconvergence point).

In Table 1 we give the values of the error in the recovered quantity $\max_{i=1,\ldots,4} |(F(u) - \mathcal{F}(u_h))(\bar{x}_K^{\omega_h^i})|$ versus h. For the points with $K = 1, 2, 3, 5, 6$ we employed $\mathcal{F} \equiv \mathcal{F}^{ZZ-1}$ while for the point with $K = 4$ we let $\mathcal{F} \equiv \mathcal{F}^{DIR}$. We note that we have $\tilde{\Theta}_3 = 0\%$ and the values of the error in the recovered quantity at the corners of the subcells are superconvergent with the rate two (i.e. $\sigma_0' = 1$). On the other hand at the points which correspond to $K = 1, 2$ the error in the recovered quantity converges to zero with the rate one. For $K = 4$ it appears that the rate is two. This is because $\tilde{\Theta}_K = 0.0162\%$ and $\tilde{\Theta}_K C_0 = 7.128\text{E-}03$ while $C_1 = 4.750$ and hence the true asymptotic rate of the error in the recovered quantity cannot be seen for the mesh-size considered here. We have

$$\max_{i=1,\ldots,4} |(F(u) - \mathcal{F}(u_h))(\bar{x}_4^{\omega_h^i})| = \left(\frac{0.007128}{h} + 4.75\right) h^2$$

We can detect the correct order of convergence when h is sufficiently small so that the first term in the parenthesis becomes of the same order or overcomes the second term; this is possible for $h \leq \frac{1}{1024}$. *Fig. 3 shows very clearly the preasymptotic phase* (for h large), *where our theory is not applicable, and the asymptotic phase* (for h sufficiently small), *where our theory predicts very well the pointwise values of the relative error.*

4 Recipes based on least-squares patch-recovery

Below we describe the ZZ-recipes which are now commonly used in finite element codes. We also describe a new class of recipes which are similar to the ZZ-recipes and also take into account the information about the differential operator and the source term.

4.1 Definition of the ZZ-recipes

We will now outline the definition of the ZZ-recipes for the elasticity problem. The ZZ-recipes for the orthotropic heat-conduction problem are defined analogously (see also [36-40] for further details).

Let $\omega_X := \bigcup_{X \in N(\tau')} \tau'$ denote the *patch* of elements connected to vertex X, as shown for example in Figs. 4a, 4b. For each patch ω_X we recover the *patch-projection* $\tilde{\sigma}_{ZZ}^X$, by solving the following problems:

a. Discrete least-squares:

$$\|\boldsymbol{\sigma}(\mathbf{u}_h) - \tilde{\boldsymbol{\sigma}}^X_{ZZ}\|_{L^2(\omega_X),c^{-1},\{\mathbf{y}_\ell\}_{\ell=1}^{nsp}} = \inf_{\substack{\sigma^X_{ij} \in \mathcal{P}_p(\omega_X) \\ i,j=1,2}} \|\boldsymbol{\sigma}(\mathbf{u}_h) - \boldsymbol{\sigma}^X\|_{L^2(\omega_X),c^{-1},\{\mathbf{y}_\ell\}_{\ell=1}^{nsp}} \quad (26)$$

where $\{\mathbf{y}_\ell\}_{\ell=1}^{nsp}$ denotes a set of *sampling points* in ω_X and

$$\|\boldsymbol{\sigma}\|^2_{L^2(\omega_X),c^{-1},\{\mathbf{y}_\ell\}_{\ell=1}^{nsp}} := \sum_{m=1}^{nsp} \left[\sum_{i,j,k,\ell=1}^{2} \sigma_{ij}(\mathbf{y}_m)\, c^{-1}_{ijk\ell}\, \sigma_{k\ell}(\mathbf{y}_m) \right] \quad (27)$$

b. Continuous least-squares:

$$\|\boldsymbol{\sigma}(\mathbf{u}_h) - \tilde{\boldsymbol{\sigma}}^X_{ZZ}\|_{L^2(\omega_X),c^{-1}} = \inf_{\substack{\sigma^X_{ij} \in \mathcal{P}_p(\omega_X) \\ i,j=1,2}} \|\boldsymbol{\sigma}(\mathbf{u}_h) - \boldsymbol{\sigma}^X\|_{L^2(\omega_X),c^{-1}} \quad (28)$$

where

$$\|\boldsymbol{\sigma}\|^2_{L^2(\omega_X),c^{-1}} := \int_{\omega_X} \sum_{i,j,k,\ell=1}^{2} \sigma_{ij}\, c^{-1}_{ijk\ell}\, \sigma_{k\ell} \quad (29)$$

In [36] $c_{ijk\ell}$ was chosen to be the material-tensor $a_{ijk\ell}$. It is also possible to define the patch-projections by letting $c_{ijk\ell} = \delta_{ik}\delta_{j\ell}$.

A continuous piecewise polynomial *recovered stress* $\boldsymbol{\sigma}^{ZZ}$ is obtained over each element by combining the patch-projections $\tilde{\boldsymbol{\sigma}}^X_{ZZ}$ which correspond to the vertices of the element. In the examples the quantity $\boldsymbol{\sigma}^{ZZ}$ was constructed as follows:

a. Linear (or bilinear) elements ($p = 1$).

The recovered C^0-continuous piecewise-linear (or bilinear) flux-field $\boldsymbol{\sigma}^{ZZ}$ over the domain is constructed as

$$\boldsymbol{\sigma}^{ZZ}(\mathbf{x}) = \sum_X \tilde{\boldsymbol{\sigma}}^X\Big|_X\, \Phi_X(\mathbf{x}) \quad (30)$$

Here $\tilde{\boldsymbol{\sigma}}^X\Big|_X$ is the value of the $\tilde{\boldsymbol{\sigma}}^X$ at the vertex X and Φ_X is the piecewise-linear (or bilinear) basis function associated with this vertex. Here and below we omitted the subscript ZZ from $\tilde{\boldsymbol{\sigma}}^X_{ZZ}$.

b. Quadratic (or biquadratic) elements ($p = 2$).

For the quadratic triangles a piecewise quadratic Langrangian representation of $\boldsymbol{\sigma}^{ZZ}$ is constructed from

$$\boldsymbol{\sigma}^{ZZ}(\mathbf{x}) = \sum_X \tilde{\boldsymbol{\sigma}}^X\big|_X \, \Phi_X(\mathbf{x}) + \sum_Y \frac{1}{2}\big(\tilde{\boldsymbol{\sigma}}^{X_1}\big|_Y + \tilde{\boldsymbol{\sigma}}^{X_2}\big|_Y\big) \, \Phi_Y(\mathbf{x}) \tag{31}$$

where Y denotes the midside node for the edge X_1X_2; Φ_X, Φ_Y are the Langrangian quadratic basis functions associated with the nodes X, Y, respectively. For the biquadratic quadrilaterals we let

$$\left.\begin{aligned} \boldsymbol{\sigma}^{ZZ}(\mathbf{x}) = &\sum_X \tilde{\boldsymbol{\sigma}}^X\big|_X \, \Phi_X(\mathbf{x}) + \sum_Y \frac{1}{2}\big(\tilde{\boldsymbol{\sigma}}^{X_1}\big|_Y + \tilde{\boldsymbol{\sigma}}^{X_2}\big|_Y\big) \, \Phi_Y(\mathbf{x}) \\ &+ \frac{1}{4}\big(\tilde{\boldsymbol{\sigma}}^{X_1}\big|_Z + \tilde{\boldsymbol{\sigma}}^{X_2}\big|_Z + \tilde{\boldsymbol{\sigma}}^{X_3}\big|_Z + \tilde{\boldsymbol{\sigma}}^{X_4}\big|_Z\big) \, \Phi_Z(\mathbf{x}) \end{aligned}\right\} \tag{32}$$

where X, Y, Φ_X, Φ_Y have the same meaning as before and Z and Φ_Z denote the internal node and the corresponding shape-function, respectively, for the biquadratic element.

The quantity $\boldsymbol{\sigma}^{ZZ}$ for cubic elements is defined similarly.

Remark 4.1. For the linear triangles we employed sampling points located at the centroids of the elements while for the quadratic triangles the sampling points are taken at the midpoints of the sides. These points are the same as the ones given in [36-39]. For the quadrilaterals we employed the mapped $p \times p$ Gauss-Legendre points as sampling points for the discrete recipe; for the continuous version of the recipe we employed the mapped 10×10 Gauss-Legendre quadrature rule.

4.2 Examples of "statically admissible" recipes

Here we give examples of alternative recipes which, like the ZZ-recipes, are based on local least-squares and also take into account the knowledge about the differential operator and the source term. Let us assume that we are recovering the stresses from a finite element solution of the elasticity problem with a given body force $\mathbf{f}$. For each patch ω_X we recover a "*statically admissible*" patch-projection $\tilde{\boldsymbol{\sigma}}^X$ by solving one of the following problems:

a. Least-squares fit for the stresses:

Find $\tilde{\boldsymbol{\sigma}}^X_{SA} \in \mathbf{S}^{SA}$ such that

$$\|\boldsymbol{\sigma}(\mathbf{u}_h) - \tilde{\boldsymbol{\sigma}}^X_{SA}\|_{L^2(\omega_X),\mathbf{c}^{-1},\{\mathbf{y}_\ell\}_{\ell=1}^{nsp}} = \inf_{\boldsymbol{\sigma}\in\mathbf{S}^{SA}} \|\boldsymbol{\sigma}(\mathbf{u}_h) - \boldsymbol{\sigma}^X_{SA}\|_{L^2(\omega_X),\mathbf{c}^{-1},\{\mathbf{y}_\ell\}_{\ell=1}^{nsp}} \tag{33}$$

where $\mathbf{S}^{SA}$ is the class of "statically admissible" stress-fields given by

$$\mathbf{S}^{SA} := \left\{ \boldsymbol{\sigma} = \boldsymbol{\sigma}(\mathbf{u}^{"H"} + \mathbf{u}^{P}) \mid \mathbf{u}^{"H"} \in \mathcal{P}^{p+1} \text{ and } \mathbf{L}(\mathbf{u}^{"H"}) = 0,\ \mathbf{L}(\mathbf{u}^{P}) = \mathbf{f} \right\} \quad (34)$$

Note that (33) defines a discrete statically admissible patch-projection. In the computations we employed the same sampling points as the ones given above for the ZZ-estimator. It is also possible to define a continuous statically admissible patch-projection analogously as in (28), (29).

b. Least-squares fit for the displacements:

Find $\tilde{\mathbf{u}}^{X}_{SA} \in \mathcal{U}^{SA}$ such that

$$\|\mathbf{u}_h - \tilde{\mathbf{u}}^{X}_{SA}\|_{L^2(\omega_X),\{\zeta_\ell\}_{\ell=1}^{nsp}} = \inf_{\mathbf{u}\in\mathbf{U}^{SA}} \|\mathbf{u}_h - \tilde{\mathbf{u}}^{X}_{SA}\|_{L^2(\omega_X),\{\zeta_\ell\}_{\ell=1}^{nsp}} \quad (35)$$

where $\mathcal{U}^{SA}$ is the class of "statically-admissible" displacement-fields given by

$$\mathcal{U}^{SA} := \left\{ \mathbf{u} = \mathbf{u}^{"H"} + \mathbf{u}^{P} \mid \mathbf{u}^{"H"} \in \mathcal{P}^{p+1} \text{ and } \mathbf{L}(\mathbf{u}^{"H"}) = \mathbf{0},\ \mathbf{L}(\mathbf{u}^{P}) = \mathbf{f} \right\} \quad (36)$$

The *corresponding stress-field* $\tilde{\boldsymbol{\sigma}}^{X}$ is computed from

$$\tilde{\boldsymbol{\sigma}}^{X} := \boldsymbol{\sigma}(\tilde{\mathbf{u}}^{X}_{SA}) \quad (37)$$

Here $\{\zeta_\ell\}_{\ell=1}^{nsp}$ denotes the set of sampling points for the displacement. For the quadrilateral elements we used the mapped $(p+1)\times(p+1)$ Lobatto-Legendre points. For the triangles we used as sampling points the nodes of the Lagrangian elements of degree p. It is also possible to define a continuous version of (35) by employing the usual L^2-norm.

After a recovered stress has been obtained for each patch from the above recipes a continuous piecewise polynomial recovered stress is obtained over the entire mesh by combining the patch-projections as given in (30)-(32).

Remark 4.2. It should be noted that the cost of constructing the recovered-fields using the above "statically-admissible" recipes is always less than the corresponding cost in the *ZZ*-recipes because we minimize over a smaller set. For example, in the case of elasticity and cubic elements the computation of $\tilde{\boldsymbol{\sigma}}^{X}_{ZZ}$ for a patch require the inversion of an 27×27 matrix. On the other hand the calculation of the $\tilde{\boldsymbol{\sigma}}^{X}_{SA}$ for both recipes given above requires only the inversion of a 12×12 matrix. This difference is more pronounced for higher-order elements.

Remark 4.3. It is obvious that the quality of a recipe can be improved if all the known properties of the exact solution are employed. Hence it is not surprising

that the quality of the "statically-admissible" recipes is better than the quality of the ZZ-recipes (see Section 8.6, below).

Remark 4.4. The fact that it is possible to recover fluxes with higher accuracy, than by direct computation, makes it possible to construct a-posteriori error estimates for the energy-norm of the error.

Remark 4.5. We do not address the higher-order recovery of the solution (i.e. the temperature or the displacement-vector) although it could be done in a similar way.

5 Outline of the theoretical setting

The theoretical setting will be outlined below for the *class of locally periodic meshes* which are defined as follows. Let $0 < H < H^0$, $\mathbf{x}^0 = (x_1^0, x_2^0) \in \Omega$,

$$S(\mathbf{x}^0, H) := \left\{ \mathbf{x} = (x_1, x_2) \;\middle|\; |x_i - x_i^0| < H, \quad i = 1,2 \right\} \tag{38}$$

and assume H^0 is sufficiently small such that $\bar{S}(\mathbf{x}^0, H^0) \subset \Omega$. Further, let γ be a set of multi-indices (i,j), $\mathbf{x}^{(i,j)} = (x_1^{(i,j)}, x_2^{(i,j)}) \in \Omega$ and

$$c(\mathbf{x}^{(i,j)}, h) := S(\mathbf{x}^{(i,j)}, h) \subset S(\mathbf{x}^0, H), \qquad (i,j) \in \gamma \tag{39}$$

be the set of the h-cells (or cells) which cover exactly $S(\mathbf{x}^0, H)$ as is for example shown in Fig. 2a, 2b. We will refer to $S(\mathbf{x}^0, H)$ as *the subdomain of periodicity of the mesh centered at* $\mathbf{x}^0$. We will denote by $\tilde{c} := S(\mathbf{0}, 1)$ the *unit-* (*master-*) cell $\tilde{c}$, the h-cell is an h-scaled and translated master-cell.

Let $\tilde{T}$ be a mesh of triangles or squares on the master-cell (the master-mesh) and $\tilde{T}_h^{(i,j)}$ be the mesh on $c(\mathbf{x}^{(i,j)}, h)$ which is the scaled and translated image of $\tilde{T}$. Let $T_h \in \mathcal{T}$ and $T_h(\mathbf{x}^0, H)$ be the restriction of T_h on $S(\mathbf{x}^0, H)$ and $T_h^{(i,j)}$ the restriction of $T_h(\mathbf{x}^0, H)$ on $c(\mathbf{x}^{(i,j)}, h)$. We assume that $T_h^{(i,j)} = \tilde{T}_h^{(i,j)}$, $(i,j) \in \gamma$ i.e. $T_h(\mathbf{x}^0, H)$ is made by the periodic repetition of the h-scaled master mesh. The family $\mathcal{T} = \{T_h\}$ is a class of meshes which are locally-periodic in the subdomain $S(\mathbf{x}^0, H)$. Outside the subdomain $S(\mathbf{x}^0, H)$ the mesh is arbitrary; it could have curved elements, refinements, etc.

Let Q be a polynomial of degree $(p+1)$ defined over the master-cell $\tilde{c}$ and let $\tilde{T}$ be the master-mesh. Then denote

$$\rho := Q - Q_1^{\mathrm{INT}} \tag{40}$$

where Q_1^{INT} is the interpolant of degree p of the function Q defined over the master-mesh $\tilde{T}$ (for which $h = 1$). Any polynomial of degree p on an element τ_k belongs to

$S_1^p(\tau_k)$ and hence any polynomial of degree p on $S(x^0, H)$ belongs to $S_1^p(T_h(x^0, H))$. It follows that ρ defined in (40) is $\tilde{c}$-periodic (this can be shown exactly as in [54]) and

$$\rho(1, \tilde{x}_2) = \rho(-1, \tilde{x}_2), \qquad |\tilde{x}_2| < 1 \tag{41a}$$

$$\rho(\tilde{x}_1, 1) = \rho(\tilde{x}_1, -1), \qquad |\tilde{x}_1| < 1 \tag{41b}$$

Let

$$H^1_{\mathrm{PER}}(\tilde{c}) := \left\{ u \in H^1(\tilde{c}) \;\middle|\; u \text{ satisfies (41)} \right\} \tag{42}$$

and

$$S^p_{1,\mathrm{PER}}(\tilde{c}) := \left\{ u \in H^1_{\mathrm{PER}}(\tilde{c}) \middle|\; u|_{\tilde{\tau}} \in S_1^p(\tilde{\tau}) \qquad \forall\ \tilde{\tau} \in \tilde{T} \right\} \tag{43}$$

Further let $\tilde{z}^\rho \in S^1_{\mathrm{PER}}(\tilde{c})$ such that

$$b_{\tilde{c}}(\tilde{z}^\rho, \tilde{v}) = b_{\tilde{c}}(\rho, \tilde{v}) \qquad \forall\ \tilde{v} \in S^p_{1,\mathrm{PER}}(\tilde{c}) \tag{44a}$$

and

$$\int_{\tilde{c}} (\rho - \tilde{z}^\rho) = 0 \tag{44b}$$

Note that the function $\tilde{z}^\rho$ exists and is uniquely determined (we will compute it numerically in the examples). Let us also define $\psi \in H^1(\tilde{c})$ by

$$\psi := \rho - \tilde{z}^\rho = Q - \tilde{w} \quad \text{where} \quad \tilde{w} := Q_1^{\mathrm{INT}} + \tilde{z}^\rho \tag{45}$$

Let $\psi_h \in H^1_{\mathrm{PER}}(c(x^{(i,j)}, h))$ be the function ψ, defined above, scaled and translated onto the cell $c(x^{(i,j)}, h)$ of the mesh in $S(x^0, H)$ i.e.

$$\psi_h(x) := h^{p+1}\, \psi(\tilde{x}), \qquad \frac{\partial \psi_h}{\partial x_i}(x) = h^p\, \frac{\partial \psi}{\partial \tilde{x}_i}(\tilde{x}), \quad i = 1, 2, \tag{46}$$

where $\tilde{x} = \dfrac{1}{h}(x - x^{(i,j)})$, $x \in c(x^{(i,j)}, h)$. It is easy to see that ψ_h can be periodically extended over $S(x^0, H_1)$.

In [47] we proved the following theorem for Poisson's equation based on the theory of interior estimates (see [53]):

Theorem 1. Let $H_1 < H < H^0$ and assume that the following assumptions hold with

$$\alpha = \frac{6p+1}{6p}, \qquad \beta = p+1-\epsilon, \qquad \epsilon = \sigma_0 = \frac{1}{6(6p+1)} \tag{47}$$

Assume that the exact solution u satisfies

$$\|D^\alpha u\|_{L^\infty(S(x^0,H))} \leq K < \infty, \qquad 0 \leq |\alpha| \leq p+2 \tag{48a}$$

where $\alpha := (\alpha_1, \alpha_2)$, $D^\alpha u := \dfrac{\partial^{|\alpha|} u}{\partial x_1^{\alpha_1} \partial x_2^{\alpha_2}}$, $|\alpha| := \alpha_1 + \alpha_2$, and

$$R^2 = \sum_{|\alpha|=p+1} a_\alpha^2 > 0 \qquad \text{where} \qquad a_\alpha := (D^\alpha u)(x^0) \tag{48b}$$

Further assume that the mesh T_h is such that

$$\|e_h\|_{L^2(S(x^0,H_1))} \leq C h^\beta H_1, \qquad \text{with} \quad \beta \geq (p+1) - \epsilon \tag{49}$$

Moreover assume that the meshes T_h in $S(x^0, H)$ are such that

$$C_1 H_1^\alpha \leq h \leq C_2 H_1^\alpha \tag{50}$$

Then for any $x \in S(x^0, H_1)$

$$\left|\frac{\partial e_h}{\partial x_i}(x)\right| = \left|\frac{\partial \psi_h}{\partial x_i}(x)\right| + \lambda C h^{p+\sigma_0} \tag{51}$$

with $\sigma_0 > 0$, $|\lambda| \leq 1$ and C independent of h.

Theorem 2. Let the assumptions of Theorem 1 hold; then

$$\left| F(u) - \mathcal{F}(u_h) \right| = \left| F(Q) - \mathcal{F}(\tilde{w}) \right| + \lambda C h^{p+\sigma_0'} \tag{52}$$

with $\sigma_0' > 0$, $|\lambda| \leq 1$ and C independent of h.

Remark 5.1. The theorems assume that the mesh is periodic and that the solution is smooth in a small subdomain (i.e. $S(x^0, H)$) in the interior of the domain. Outside the subdomain we assume neither periodicity of the mesh nor smoothness of the solution. The solution may have algebraic-type singularities at a finite number of corner points or points of abrupt change in the type of boundary-condition. Here it is only assumed that the pollution-error in a shrinking mesh-patch (i.e. $T_h(x^0, H_1)$) in the interior of the subdomain is controlled (see [51]). This implies that the mesh has been adequately refined in the neighborhood of all singular points.

Remark 5.2. If we further assume that

$$\Psi(\tau) := \left\| \left| F(u - u_h) \right| \right\|_{L^\infty(\tau)} \geq Ch^p, \qquad C > 0 \tag{53}$$

theorem 2 implies that: A point $\mathbf{x}_\tau$ in the element $\tilde{\tau}$ is an η%-superconvergence point for the averaging $\mathcal{F}$ if and only if $\tilde{\mathcal{H}}(\mathbf{x}_\tau; F; \mathcal{F}; \mathcal{Q}; \tilde{\tau}, \tilde{T}) \leq \frac{\eta}{100}$ where

$$\tilde{\mathcal{H}}(\bar{\mathbf{x}}; F; \mathcal{F}; \mathcal{Q}; \tilde{\tau}, \tilde{T}) := \max_{Q \in \mathcal{Q}} \tilde{\Theta}(\bar{\mathbf{x}}; F; \mathcal{F}; Q; \tilde{\tau}, \tilde{T}) \tag{54}$$

where

$$\tilde{\Theta}(\bar{\mathbf{x}}; F; \mathcal{F}; Q; \tilde{\tau}, \tilde{T}) := \begin{cases} \dfrac{\left| F(Q)(\bar{\mathbf{x}}) - \mathcal{F}(\tilde{w})(\bar{\mathbf{x}}) \right|}{\tilde{\Psi}(\tilde{\tau})} & , \quad \text{if } \tilde{\Psi}(\tilde{\tau}) \neq 0 \\ 0 & , \quad \text{if } \tilde{\Psi}(\tilde{\tau}) = 0 \end{cases} \tag{55}$$

with

$$\tilde{\Psi} := \max_{x \in \tilde{\tau}} \left| F(\psi)(x) \right| \tag{56}$$

Here $\mathcal{Q}$ denote the class of all $(p+1)$-degree monomials which occur in Taylor series expansions of functions from $\mathcal{U}$ (see also Section 6 below).

Remark 5.3. Assumption (53) can be realized by imposing additional restrictions on the values a_α of the $(p+1)$-derivatives of the solution at x_0. This assumption is reasonable because we are interested in a sufficiently large class of solutions $\mathcal{U}$.

Remark 5.4. The proof of theorem 1 in [47] was based on various interior estimates for the error in finite element approximations of Poisson's equation, especially the results given in [53]. It is very plausible that analogs of these results hold for finite element approximations of the elasticity equations and more general elliptic-systems because the main ideas of the proofs of these results carry to the general case. To our knowledge the precise details for the elasticity equations are not available in the open literature. Nevertheless we will assume the validity of the analog of Theorem 1 for the equations of elasticity.

Remark 5.5. The above theoretical setting was also employed to assess the quality of a-posteriori error estimators in [54] and [55].

6 The method of freezing the periodicity

Let us assume that for a given locally periodic grid with corresponding periodic master-mesh $\tilde{T}$, given material orthotropy and given class of solutions $\mathcal{U}$ which are smooth in the interior of the domain (i.e. the solutions which satisfy (48a)) we consider

$$\mathcal{Q} := \left\{ Q \,\middle|\, Q(x_1, x_2) = \sum_{k=1}^{nd} \alpha_k Q_k(x_1, x_2),\ Q_k(x_1, x_2) = \sum_{\ell=0}^{p+1} \beta_\ell\, x_1^\ell\, x_2^{p+1-\ell} \right\} \tag{57}$$

the class of $(p+1)$-degree monomials which occur in all $(p+1)$-degree Taylor-series expansions of functions from $\mathcal{U}$. Here Q_k, $k = 1, \ldots, nd$ denotes a set of linearly independent monomials which form a basis for $\mathcal{Q}$. For example, let us assume that $\mathcal{U}$ is the class of solutions $\mathcal{U}^G$ which are smooth in the neighborhood of the subdomain $S(\mathbf{x}^0, H)$; in this case we may choose

$$Q_k(x_1, x_2) := x_1^{p+2-k} x_2^{k-1}, \qquad 1 \le k \le nd = p+2 \tag{58}$$

and we obtain the class of all $(p+1)$-degree monomials $\mathcal{Q}^G$.

If we are interested only in the sub-class of harmonic solutions $\mathcal{U}^H$ (i.e. the solutions in $\mathcal{U}$ which satisfy $\Delta u = 0$) we will take $\mathcal{Q}$ as the two-dimensional linear space of harmonic monomials of degree $(p+1)$ denoted by $\mathcal{Q}^H$, namely,

$$\mathcal{Q}^H := \left\{ Q^H \,\middle|\, Q^H(x_1, x_2) = \sum_{k=1}^{2} \alpha_k Q_k^H(x_1, x_2) \right\}, \tag{59}$$

$$Q_1^H(x_1, x_2) = \mathcal{R}e(z^{p+1}), \quad Q_2^H(x_1, x_2) = \mathcal{I}m(z^{p+1}), \quad z = x_1 + i x_2\,. \tag{60}$$

For the elasticity problem the class of "harmonic" $(p+1)$-degree monomials $\mathcal{Q}^{"H"}$ is a four-dimensional linear space. Explicit expressions for a set of basis monomial are given in [50].

In the previous Section we outlined Theorem 2 which states that we can obtain the asymptotic values of the error in the recovered quantity for any smooth solution u in the interior of a periodic mesh-subdomain from the solution of the periodic boundary-value problem (44), obtained using the master-mesh $\tilde{T}$ over the master-cell $\tilde{c}$, with data obtained from the local $(p+1)$-degree Taylor-series expansion Q of the exact solution. In order to apply the results of the theoretical study to the practical meshes, for which the mesh is not locally periodic (like for example the mesh shown in Fig. 4a), the following technique of *freezing the periodicity* will be employed:

1. Let ω_0^h be an interior patch of elements of interest (shown shaded gray in Fig. 4a). Define the *s-layered patch* of elements ω_s^h, $s \geq 1$, surrounding the patch ω_0^h by

$$\omega_s^h := \bigcup_{\substack{X \in N(\tau') \\ \tau' \subseteq \omega_h^{s-1}}} \omega_X \,, \qquad \omega_X := \bigcup_{X \in N(\tau')} \tau' \tag{61}$$

where $N(\tau')$ denotes the set of the vertices of element τ', ω_X is the patch of the elements connected to vertex X. The patch ω_s^h is shown with thick black perigram in Fig. 4a. Note that *the patch ω_0^h with its surrounding s-layers is meant as a pattern which may be repeated in other places in the grid.*

2. Complete the patch ω_s^h to a periodic-grid over a slightly larger square periodic-cell which encloses the patch as shown in Fig. 4b. The periodic-cell is then scaled and translated to the unit master-cell $\tilde{c}$.

3. Assume that the mesh in the neighborhood of element τ is made from the periodic repetition of h-cells obtained from the master-cell as shown in Fig. 4c (by h-scaling and translation) and let h tend to zero. Based on the results of the theoretical study, we have

$$\lim_{h \to 0} \mathcal{R}_{F(u)}^{\eta\%}(\mathcal{U}; \mathcal{F}; \tau, T_h) = \tilde{\mathcal{R}}_{F(u)}^{\eta\%}(\mathcal{Q}; \mathcal{F}; \tilde{\tau}, \tilde{T}) \tag{62}$$

$$\lim_{h \to 0} \mathcal{A}_{F(u)}(\mathcal{U}; \mathcal{F}^1, \mathcal{F}^2; \tau, T_h) = \tilde{\mathcal{A}}_{F(u)}(\mathcal{Q}; \mathcal{F}^1, \mathcal{F}^2; \tilde{\tau}, \tilde{T}) \tag{63}$$

where $\tilde{\mathcal{R}}$, $\tilde{\mathcal{A}}$ denote the quantities defined in the master-mesh in the master-cell.

Remark 6.1. The above limits hold for the locally periodic meshes under the assumptions of the theoretical analysis outlined in Section 5 (see [47] for the details). Hence *for the general grids the limit should be understood for the mesh which is constructed by freezing the periodicity* (as is, for example, shown in Fig. 4c).

7 Determination of the η%-superconvergence quantities

The asymptotic values of $\tilde{\mathcal{H}}(\mathrm{x}; \mathcal{F}; \mathcal{F}^1; \mathcal{Q}; \tilde{\tau}, \tilde{T})$ for a recipe $\mathcal{F}$ for a class of solutions $\mathcal{Q}$ can be determined using numerical optimization. Let us consider a uniform subdivision of the element τ into subtriangles with vertices at the set of points $\Xi := \{\tilde{\xi}_k\}_{k=1}^{np}$. The value of the relative-error function for the class $\mathcal{Q}$ at the point $\tilde{\xi}_k$ is

$$\tilde{\mathcal{H}}^{\Xi}(\tilde{\boldsymbol{\xi}}_k; F; \mathcal{F}; \mathcal{Q}; \tilde{\tau}, \tilde{T}) := \max_{\alpha_i} \frac{|\sum_{i=1}^{nd} \alpha_i (F(Q_i)(\tilde{\boldsymbol{\xi}}_k) - \mathcal{F}(\tilde{w}_i)(\tilde{\boldsymbol{\xi}}_k))|}{\max_{j=1,\ldots,np} |\sum_{i=1}^{nd} \alpha_i F(\psi_i)(\tilde{\boldsymbol{\xi}}_j)|} \cdot 100 \qquad (64)$$

where $\{Q_i\}_{i=1}^{nd}$ is a basis of $\mathcal{Q}$ and $\{\tilde{w}_i\}_{i=1}^{nd}$ denote the set of finite-element solutions corresponding to the Q_i's according to (45). The function $\tilde{\mathcal{H}}^{\Xi}(\tilde{\mathbf{x}}; F; \mathcal{F}; \mathcal{Q}; \tilde{\tau}, \tilde{T})$ can be defined for any point $\tilde{\mathbf{x}} \in \tilde{\tau}$ by using linear interpolation in the subtriangles. The $\eta\%$-superconvergence regions for the recipe $\mathcal{F}$ in the element τ can be approximated from

$$\tilde{\mathcal{R}}^{\eta\%}_{F(u)}(\mathcal{Q}; \mathcal{F}; \tilde{\tau}, \tilde{T}) \approx \left\{ \tilde{\mathbf{x}} \in \tilde{\tau} \;\middle|\; \mathcal{H}^{\Xi}(\tilde{\mathbf{x}}; F; \mathcal{F}; \mathcal{Q}; \tilde{\tau}, \tilde{T}) < \eta\% \right\} \qquad (65)$$

We will call the above approach the *direct approach*. It is also possible to use a ***simplified approach*** which avoids the use of numerical optimization at every point. We define the function

$$\widehat{\tilde{\mathcal{H}}}^{\Xi}(\tilde{\mathbf{x}}; F; \mathcal{F}; \mathcal{Q}; \tilde{\tau}; \tilde{T}) := \frac{1}{Z_{\Xi}} \sqrt{\sum_{i=1}^{nd} \Big(F(Q_i)(\tilde{\mathbf{x}}) - \mathcal{F}(\tilde{w}_i)(\tilde{\mathbf{x}})\Big)^2}, \qquad (66)$$

where

$$Z_{\Xi} := \min_{\alpha_i} \left(\frac{\max_{j=1,\ldots,np} |\sum_{i=1}^{nd} \alpha_i F(\psi_i)(\boldsymbol{\xi}_j)|}{(\sum_{i=1}^{nd} \alpha_i^2)^{\frac{1}{2}}} \right) \qquad (67)$$

The quantity Z_{Ξ} can be computed using numerical optimization. Let

$$\widehat{\tilde{\mathcal{R}}}^{\eta\%}_{F(u)}(\mathcal{Q}; \mathcal{F}; \tau, \tilde{T}) := \left\{ \tilde{\mathbf{x}} \in \tau \;\middle|\; \widehat{\tilde{\mathcal{H}}}^{\Xi}(\tilde{\mathbf{x}}; F; \mathcal{F}; \mathcal{Q}; \tilde{\tau}, \tilde{T}) < \frac{\eta}{100} \right\} \qquad (68)$$

denote the approximate regions of $\eta\%$-superconvergence for the class of solutions $\mathcal{Q}$ obtained by the simplified approach.

Remark 7.1. Note that

$$\widehat{\tilde{\mathcal{R}}}^{\eta\%}_{F(u)}(\mathcal{Q}; \mathcal{F}; \tilde{\tau}, \tilde{T}) \subseteq \tilde{\mathcal{R}}^{\eta\%}_{F(u)}(\mathcal{Q}; \mathcal{F}; \tilde{\tau}, \tilde{T}) \,. \qquad (69)$$

Therefore the simplified approach results to a conservative estimate for the $\eta\%$-superconvergence regions.

The function $\mathcal{D}_{F(u)}(\tilde{\mathbf{x}};\mathcal{U};\mathcal{F}^1;\mathcal{F}^2;\tilde{\tau},\tilde{T})$, defined in (24), can be approximated by computing the numerator and the denominator in (24) as in (59). Then approximations of the region $\tilde{\mathcal{A}}(\mathcal{U};\mathcal{F}^1;\mathcal{F}^2;\tilde{\tau},\tilde{T})$, defined in (25), can be obtained.

Remark 7.2. The functions defined in (64) and (66) depend on the set of points Ξ. To ensure good accuracy in the approximation of the η%-superconvergence regions a sufficient number of points must be employed.

Remark 7.3. In eq. (64) we define the relative error by taking the maximum over the class of solutions $\mathcal{Q}$ because we do not know the solution a-priori. Obviously we have to use all the information about the solution that we have in our disposition. This is the reason that in (64) we compute the maximum for the class $\mathcal{Q}$ (i.e. the class of polynomials of degree $(p+1)$ which satisfy the differential equation).

8 A model numerical study of recipes

We will now present a model study of the recipes given in Section 4 based on the definition of superconvergence given in Section 3. We will compare the quality of the recipes with respect to *direct sampling* (i.e. direct evaluation of the quality $F(u)$ from the finite element solution) based on the following criteria:

1. The gain in the value of the minimum relative error.

For a given recipe we will define the minimum value of the maximum relative error for the class of solutions $\mathcal{U}$ in the element.

$$\eta^{\%}_{min}(F;\mathcal{F};\mathcal{U};\tau,T_h) = \min_{x\in\tau}\mathcal{H}(x;F;\mathcal{F};\mathcal{U};\tau,T_h) \tag{70}$$

In this measure we will say that recipe $\mathcal{F}^1$ is superior to recipe $\mathcal{F}^2$ in the element τ for the class of solutions $\mathcal{U}$, if

$$\eta^{\%}_{min}(F;\mathcal{F}^1;\mathcal{U};\tau,T_h) < \eta^{\%}_{min}(F;\mathcal{F}^2;\mathcal{U};\tau,T_h) \tag{71}$$

2. Gain in the η%-superconvergence regions.

For a given recipe $\mathcal{F}$ and given η, $0<\eta<100$ we define the percentage area of the element in which the relative error in the recovered quantity is less than η%, namely

$$\tau^{\%}_{\mathcal{H}<\eta\%}(F;\mathcal{F};\mathcal{U};\tau,T_h) := \frac{|\mathcal{R}^{\eta\%}_{F(u)}(\mathcal{U};\mathcal{F};\tau,T_h)|}{|\tau|}\,100 \tag{72}$$

Here the symbol $|\cdot|$ indicates the area of the set. Given a value of η, we will say that $\mathcal{F}^1$ is superior to $\mathcal{F}^2$ in the element τ, for the class of solutions $\mathcal{U}$ if

$$\tau^{\%}_{\mathcal{H}<\eta\%}(F;\mathcal{F}^1;\mathcal{U};\tau,T_h) > \tau^{\%}_{\mathcal{H}<\eta\%}(F;\mathcal{F}^2;\mathcal{U};\tau,T_h) \tag{73}$$

3. Robustness of a recipe $\mathcal{F}^1$ relative to the recipe $\mathcal{F}^2$ at an arbitrary point relative to direct sampling

For a given recipe $\mathcal{F}^1$ we define the percentage area of the element in which the recipe is less robust than recipe $\mathcal{F}^2$, namely,

$$\tau^{\%}_{\mathcal{D}>1}(F;\mathcal{U};\mathcal{F}^1,\mathcal{F}^2;\tau,T_h) = \frac{|\mathcal{A}_{F(u)}(\mathcal{U};\mathcal{F}^1;\mathcal{F}^2;\tau,T_h)|}{|\tau|}\,100 \tag{74}$$

In this measure we will say that the recipe $\mathcal{F}^1$ is more robust than the recipe $\mathcal{F}^2$ in the element τ if

$$\tau^{\%}_{\mathcal{D}>1}(\mathcal{U};\mathcal{F}^1,\mathcal{F}^2;\tau,T_h) < \tau^{\%}_{\mathcal{D}>1}(\mathcal{U};\mathcal{F}^2,\mathcal{F}^1;\tau,T_h) \tag{75}$$

We will also define the maximum value of the relative robustness in an element, namely,

$$\mathcal{D}^{max}_{F(u)}(\mathcal{U};\mathcal{F}^1,\mathcal{F}^2;\tau,T_h) = \max_{x\in\tau}\mathcal{D}_{F(u)}(\mathrm{x};\mathcal{U};\mathcal{F}^1,\mathcal{F}^2;\tau,T_h) \tag{76}$$

Below we will investigate the quality of the several recipes by employing the above defined measures.

In the numerical examples we will employ three versions of the ZZ-recipe, and the "statically-admissible" recipes introduced in Section 4. We will use the following abbreviations:

1. *ZZ-1: Discrete ZZ recipe, $\mathcal{F}^{ZZ-1}$, defined in (26) with $c_{ijk\ell} = a_{ijk\ell}$.*
2. *ZZ-2: Continuous ZZ recipe, $\mathcal{F}^{ZZ-2}$, defined in (28) with $c_{ijk\ell} = a_{ijk\ell}$.*
3. *ZZ-3: Discrete ZZ recipe, $\mathcal{F}^{ZZ-3}$, defined in (26) with $c_{ijk\ell} = \delta_{ik}\delta_{j\ell}$.*
4. *SA-1: "Statically-admissible" recipe, $\mathcal{F}^{SA-1}$, based on least-squares fit for the displacements defined in (33)-(34).*
5. *SA-2: "Statically-admissible" recipe, $\mathcal{F}^{SA-2}$, based on least-squares fit for the displacements defined in (35)-(36).*
6. *DIR: Direct sampling recipe, $\mathcal{F}^{DIR}$, which means that the solution quantity is evaluated directly from the finite-element solution.*

We will employ the methodology of the paper in the study of these recipes.

8.1 Influence of the choice of the solution quantity $F(u)$ and its modulus $|\cdot|$

In this Section we will show that the quality of a recipe depends on the solution quantity of interest and the modulus employed. We considered the case of elasticity problem in which one could be interested in the error in one stress component or the errors in all the stress components. We employed three types of measures and moduli to compute the errors in the stress components, namely:

(i) $F(\mathbf{u}) = \sigma_{11}(\mathbf{u})$ and $\left|\sigma_{11}(\mathbf{u})\right| := |\sigma_{11}(\mathbf{u})|$.

(ii) $F(\mathbf{u}) = I_1(\sigma_{ij}(\mathbf{u}))$ and $\left|I_1(\sigma_{ij}(\mathbf{u}))\right| := |I_1(\sigma_{ij}(\mathbf{u}))|$, where $I_1(\sigma_{ij}) := \sigma_{11} + \sigma_{22} + \sigma_{33}$.

(iii) $F(\mathbf{u}) = \sigma_{ij}(\mathbf{u})$ and $\left|\sigma_{ij}(\mathbf{u})\right| = J_2(\sigma_{ij}(\mathbf{u}))$, where $J_2(\sigma_{ij}) = \sqrt{\sum_{i,j=1}^{3} \sigma'_{ij}\sigma'_{ij}}$ where $\sigma'_{ij} := \sigma_{ij} - \frac{1}{3} I_1(\sigma_{ij})$.

We computed the $\eta\%$-superconvergence regions in the elements in ω_1^h (shown in Fig. 4a) for the stresses computed using the finite element solution (i.e. direct sampling). In Figs. 6a, 6b, 6c we show the regions of $\eta\%$-superconvergence $\mathcal{R}^{\eta\%}_{F(u)}(\mathcal{Q}^{\text{"}H\text{"}}; \mathcal{F}^{DIR}; \tau_i, T_h)$ for $F(\mathbf{u}) = \sigma_{11}(\mathbf{u})$, $I_1(\sigma_{ij}(\mathbf{u}))$ and $\sigma_{ij}(\mathbf{u})$, respectively. The values of $\eta^{\%}_{min}(F; \mathcal{F}^{DIR}; \mathcal{Q}^{\text{"}H\text{"}}; \tau_i, T_h)$ and $\tau^{\%}_{\mathcal{H}<\eta\%}(F; \mathcal{F}^{DIR}; \mathcal{Q}^{\text{"}H\text{"}}; \tau_i, T_h)$ for the three measures used in Figs. 6a-6c are given in Table 2a. It can be seen that when $F(\mathbf{u}) = I_1(\sigma_{ij}(\mathbf{u}))$ or $\sigma_{ij}(\mathbf{u})$, the percentage area of the element with less than 10% relative error is small or zero. We also computed the $\eta\%$-superconvergence regions for the stresses recovered using the recipe $\mathcal{F}^{ZZ-1}$. In Figs. 7a, 7b, 7c we give the regions $\mathcal{R}^{\eta\%}_{F(u)}(\mathcal{Q}^{\text{"}H\text{"}}; \mathcal{F}^{ZZ-1}; \tau_i, T_h)$ for $F(\mathbf{u}) = \sigma_{11}(\mathbf{u})$, $I_1(\sigma_{ij}(\mathbf{u}))$ and $\sigma_{ij}(\mathbf{u})$, respectively. In Table 2b we give the values of $\eta^{\%}_{min}(F; \mathcal{F}^{ZZ-1}; \mathcal{Q}^{\text{"}H\text{"}}; \tau_i, T_h)$ and $\tau^{\%}_{\mathcal{H}<\eta\%}(F; \mathcal{F}^{ZZ-1}; \mathcal{Q}^{\text{"}H\text{"}}; \tau_i, T_h)$ for the three measures employed in Fig. 6a-6c. It can be observed that when the three different measures are employed different gains in the value of the minimum relative error and the $\eta\%$-superconvergence regions are obtained. By comparing Tables 2a, 2b we observe that the ZZ-recipe is much superior than the direct sampling in all the measures i.e. there are significant gains in the minimum relative error and the $\eta\%$-superconvergence regions especially for small $\eta\%$. For example, in the J_2-measure, which takes into account all stress-components, we have for $\mathcal{F}^{ZZ-1}$

$$\eta^{\%}_{min}(\sigma_{ij}; \mathcal{F}^{ZZ-1}; \mathcal{Q}^{\text{"}H\text{"}}; \tau_i, T_h) < 2.5\%, \qquad \tau^{\%}_{\mathcal{H}<25\%}(\sigma_{ij}; \mathcal{F}^{ZZ-1}; \mathcal{Q}^{\text{"}H\text{"}}; \tau_i, T_h) > 85\%$$

while for direct sampling

$$\eta^{\%}_{min}(\sigma_{ij};\mathcal{F}^{DIR};\mathcal{Q}^{"H"};\tau_i,T_h) > 10\%, \qquad \tau^{\%}_{\mathcal{H}<25\%}(\sigma_{ij};\mathcal{F}^{DIR};\mathcal{Q}^{"H"};\tau_i,T_h) < 9.5\%$$

Similar gains are also observed in the other measures. Note however that the minimum value of the maximum relative error in each element obtained from the ZZ-recipes and the direct sampling are very similar.

8.2 Influence of the choice of the definition of the ZZ-recipe

We now give an example to show how the methodology can be employed to compare the quality of different recipes. In particular we considered the three versions of the ZZ-recipe, namely $\mathcal{F}^{ZZ-1}$, $\mathcal{F}^{ZZ-2}$ and $\mathcal{F}^{ZZ-3}$.

We considered the elasticity problem and the elements in ω^h_{II} (shown in Fig. 4b) assuming biquadratic elements ($p = 2$). We first computed the $\eta\%$-superconvergence regions for stresses which are recovered using $\mathcal{F}^{ZZ-1}$ and $\mathcal{F}^{ZZ-2}$. In Figs. 8a and 8b we show the regions $\mathcal{R}^{\eta\%}_{\sigma_{11}(\mathbf{u})}(\mathcal{Q}^{"H"};\mathcal{F};\tau_i,T_h)$ for $\mathcal{F} = \mathcal{F}^{ZZ-1}$ and $\mathcal{F} = \mathcal{F}^{ZZ-2}$, respectively. In Figs. 8c and 8d we give the regions $\mathcal{R}^{\eta\%}_{\sigma_{ij}(\mathbf{u})}(\mathcal{Q}^{"H"};\mathcal{F};\tau_i,T_h)$ for $\mathcal{F} = \mathcal{F}^{ZZ-1}$ and $\mathcal{F} = \mathcal{F}^{ZZ-2}$. In Table 3a we give the values of $\eta^{\%}_{min}(\sigma_{ij};\mathcal{F};\mathcal{Q}^{"H"};\tau_i,T_h)$ and $\tau^{\%}_{\mathcal{H}<\eta\%}(\sigma_{ij};\mathcal{F};\mathcal{Q}^{"H"};\tau_i,T_h)$ for the three recipes $\mathcal{F}^{ZZ-1}$, $\mathcal{F}^{ZZ-2}$ and $\mathcal{F}^{ZZ-3}$. It can be seen that the quality of $\mathcal{F}^{ZZ-1}$ and $\mathcal{F}^{ZZ-3}$, using this measure, is almost the same whereas the quality of $\mathcal{F}^{ZZ-2}$ is superior to the other two, in this measure.

We also computed the regions in the elements where the recipes $\mathcal{F}^{ZZ-1}$, $\mathcal{F}^{ZZ-2}$ and $\mathcal{F}^{ZZ-3}$ are less robust than the direct sampling. In Figs. 9a, 9b, 9c we show the regions $\mathcal{A}_{\sigma_{11}(\mathbf{u})}(\mathcal{Q}^{"H"};\mathcal{F};\mathcal{F}^{DIR};\tau,T_h)$ for $\mathcal{F} = \mathcal{F}^{ZZ-1}$, $\mathcal{F}^{ZZ-2}$ and $\mathcal{F}^{ZZ-3}$, respectively. The dark regions in Figs. 9a-9c are the regions where the recipe $\mathcal{F}$ is less robust than direct sampling. In this measure, $\mathcal{F}^{ZZ-3}$ appears to be superior to $\mathcal{F}^{ZZ-1}$ and $\mathcal{F}^{ZZ-2}$. However, this is not true when we employ $F(\mathbf{u}) = \sigma_{ij}$ to compute the regions of relative robustness $\mathcal{A}_{\sigma_{ij}}(\mathcal{Q}^{"H"};\mathcal{F};\mathcal{F}^{DIR};\tau,T_h)$ which are given in Figs. 9d, 9e, 9f we show the regions for $\mathcal{F} = \mathcal{F}^{ZZ-1}$, $\mathcal{F}^{ZZ-2}$ and $\mathcal{F}^{ZZ-3}$. In Table 3b we report the values of $\mathcal{D}^{max}_{F(\mathbf{u})}(\mathcal{Q}^{"H"};\mathcal{F};\mathcal{F}^{DIR};\tau,T_h)$ and $\tau^{\%}_{\mathcal{D}>1}(\sigma_{ij}\mathcal{Q}^{"H"};\mathcal{F};\mathcal{F}^{DIR};\tau,T_h)$ for $\mathcal{F} = \mathcal{F}^{ZZ-1}$, $\mathcal{F}^{ZZ-2}$ and $\mathcal{F}^{ZZ-3}$, respectively. It can be seen from Figs. 9d, 9f and from Table 3b that the quality of $\mathcal{F}^{ZZ-1}$ and $\mathcal{F}^{ZZ-3}$ is about the same while the $\mathcal{F}^{ZZ-2}$ is superior to the other two, in this measure.

8.3 Influence of the class of solutions and the material-orthotropy

In this Section we give examples to show that the quality of the recipes depends on the type of solution ("harmonic" or general) and the material orthotropy. We

considered the problem of orthotropic heat conduction and the elements in ω_{II}^h (shown in Fig. 4b) assuming biquadratic elements ($p = 2$). We computed the $\eta\%$-superconvergence regions $\mathcal{R}_{q_i(u)}^{\eta\%}(\mathcal{Q}; \mathcal{F}^{ZZ-1}; \tau_i, T_h)$ and the regions of relative robustness $\mathcal{A}_{q_i(u)}(\mathcal{Q}; \mathcal{F}^{ZZ-1}; \mathcal{F}^{DIR}; \tau_i, T_h)$ for the recipe $\mathcal{F}^{ZZ-1}$.

We first considered the case of isotropic heat conduction and studied the quality of the recipe for the class of harmonic and general solutions. In Figs. 10a, 10b we give the $\eta\%$-superconvergence regions $\mathcal{R}_{\frac{\partial u}{\partial x_i}}^{\eta\%}(\mathcal{Q}; \mathcal{F}^{ZZ-1}; \tau_i, T_h)$ for $\mathcal{Q} = \mathcal{Q}^H$ and $\mathcal{Q} = \mathcal{Q}^G$, respectively. Note that in this case $q_i(u) = \dfrac{\partial u}{\partial x_i}$, and $\left|\dfrac{\partial u}{\partial x_i}\right| := \sqrt{\left(\dfrac{\partial u}{\partial x_1}\right)^2 + \left(\dfrac{\partial u}{\partial x_2}\right)^2}$. It can be seen that for class of general solutions the $\eta\%$-superconvergence regions are smaller than those for the class of harmonic solutions. In Figs. 10c, 10d we give the regions of relative robustness $\mathcal{A}_{\frac{\partial u}{\partial x_i}}(\mathcal{Q}; \mathcal{F}^{ZZ-1}, \mathcal{F}^{DIR}; \tau_i, T_h)$ for $\mathcal{Q} = \mathcal{Q}^H$ and $\mathcal{Q} = \mathcal{Q}^G$, respectively. We observe that the regions $\mathcal{A}_{\frac{\partial u}{\partial x_i}}(\mathcal{Q}; \mathcal{F}^{ZZ-1}, \mathcal{F}^{DIR}; \tau_i, T_h)$ for $\mathcal{Q} = \mathcal{Q}^H$ are much smaller and are included in the corresponding regions for $\mathcal{Q} = \mathcal{Q}^G$.

We now consider the case of orthotropic heat conduction with the principal material directions oriented along the coordinate axes and $\left(\dfrac{K_{22}}{K_{11}}\right) = 2$. In Figs. 11a, 11b we show the regions of $\eta\%$-superconvergence $\mathcal{R}_{q_i(u)}^{\eta\%}(\mathcal{Q}; \mathcal{F}^{ZZ-1}; \tau_i, T_h)$ for $\mathcal{Q} = \mathcal{Q}^H$ and $\mathcal{Q} = \mathcal{Q}^G$, respectively. In Figs. 11c, 11d we give the regions of relative robustness $\mathcal{A}_{q_i(u)}(\mathcal{Q}; \mathcal{F}^{ZZ-1}, \mathcal{F}^{DIR}; \tau_i, T_h)$ for $\mathcal{Q} = \mathcal{Q}^H$ and $\mathcal{Q} = \mathcal{Q}^G$, respectively. We reported the values of $\eta_{min}^{\%}(q_i; \mathcal{F}^{ZZ-1}; \mathcal{Q}; \tau_i; T_h)$ and $\tau_{\mathcal{H}<10\%}^{\%}(q_i; \mathcal{F}^{ZZ-1}; \mathcal{Q}; \tau_i; T_h)$ in Table 4a and the values of $\tau_{\mathcal{D}>1}^{\%}(q_i; \mathcal{F}^{ZZ-1}, \mathcal{F}^{DIR}; \mathcal{Q}; \tau_i; T_h)$ in Table 4b. From Table 4a, it can be seen that the quality of the $\mathcal{F}^{ZZ-1}$ recipe deteriorates when the exact solution is not "harmonic" and also when material orthotropy is introduced. In Table 4b we observe that regions of relative robustness $\mathcal{A}_{q_i(u)}(\mathcal{Q}; \mathcal{F}^{ZZ-1}, \mathcal{F}^{DIR}; \tau_i, T_h)$ are relatively large when general solutions are employed or when the material is orthotropic. Thus, *the robustness of the recipe $\mathcal{F}^{ZZ-1}$ is reduced when a larger class of solutions and material-orthotropy are admitted.*

We also studied the influence of material orthotropy on the recipe $\mathcal{F}^{ZZ-1}$ in meshes of triangular elements shown in Fig. 12. Here we considered the periodic mesh of triangles shown in Fig. 12d (Criss-Cross Pattern) with $p = 2$ and computed the values of $\eta_{min}^{\%}(q_i, \mathcal{F}; \mathcal{Q}^G; \tau_i, T_h)$ and $\tau_{\mathcal{H}<10\%}^{\%}(q_i, \mathcal{F}; \mathcal{Q}^G; \tau_i, T_h)$ for $\mathcal{F} = \mathcal{F}^{ZZ-1}$ and $\mathcal{F} = \mathcal{F}^{DIR}$. These are given in Table 5 for $\dfrac{K_{11}}{K_{22}} = 1$ and $\dfrac{K_{11}}{K_{22}} = 10$ with the principal material directions oriented along the coordinate-axes. In Table 5 we also report the values of $\mathcal{D}_{F(u)}^{max}(\mathcal{Q}^G; \mathcal{F}^{ZZ-1}, \mathcal{F}^{DIR}; \tau_i, T_h)$ and

$\tau^{\%}_{\mathcal{D}>1}(q_i; \mathcal{Q}^G; \mathcal{F}^{ZZ-1}, \mathcal{F}^{DIR}; \tau_i, T_h)$ for the case of $\frac{K_{11}}{K_{22}} = 10$. We observe that when the $ZZ-1$ recipe is employed there is a significant gain in the minimum relative error; for example the minimum relative error obtained with direct sampling is greater than 25% while that of the $ZZ-1$ recipe is less than 3%. Moreover there are no 10%-superconvergence regions for the direct recipe while there are regions of significant size for the $ZZ-1$ recipe.

8.4 Influence of the polynomial degree of the elements and the topology of the mesh and the element-type

We now give some examples to demonstrate the influence of element type (quadrilateral or triangle, the degree p of the element) and the local mesh topology.

We first considered the elasticity problem and the elements in ω^h_{II} (shown in Fig. 4b). In Section 8.2, we used this mesh patch with biquadratic elements to report the regions of relative robustness for $\mathcal{F}^{ZZ-1}$. We now computed these regions for $p = 1$ and $p = 3$. In Figs. 13a, 13b we show the regions $\mathcal{A}_{\sigma_{ij}(\mathbf{u})}(\mathcal{Q}^{"H"}; \mathcal{F}^{ZZ-1}; \mathcal{F}^{DIR}; \tau_i, T_h)$ for $p = 1$ and $p = 3$, respectively. In Table 6 we give the values of $\mathcal{D}^{max}_{\mathbf{F}(\mathbf{u})}(\mathcal{Q}^{"H"}; \mathcal{F}^{ZZ-1}; \mathcal{F}^{DIR}; \tau_i, T_h)$ and $\tau^{\%}_{\mathcal{D}>1}(\mathcal{Q}^{"H"}; \mathcal{F}^{ZZ-1}; \mathcal{F}^{DIR}; \tau_i, T_h)$ for $p = 1$, 2 and 3. It can be observed that the regions of relative robustness $\mathcal{A}^{\%}_{\sigma_{ij}(\mathbf{u})}(\mathcal{Q}^{"H"}; \mathcal{F}^{ZZ-1}; \mathcal{F}^{DIR}; \tau_i, T_h)$ where the $ZZ-1$ recipe is less robust than the direct sampling increase in size as p is increased.

We now consider the problem of isotropic heat conduction and the elements in the mesh patch shown in Fig. 4c assuming $p = 1$. We first computed the η%-superconvergence regions of the derivative $\frac{\partial u}{\partial x_1}$ of the finite element solution (direct sampling) for the class of harmonic and general solutions. These are shown in Figs. 14a and 14b. It can be observed that the η%-superconvergence regions for the class of general solutions are smaller than those for the class of harmonic solutions. In Figs. 15a, 15b we show the η%-superconvergence regions of $\frac{\partial u}{\partial x_1}$ which is recovered using the recipe $\mathcal{F}^{ZZ-1}$ for the class of harmonic and general solutions, respectively. We also computed the regions of relative robustness $\mathcal{A}_{\frac{\partial u}{\partial x_1}}(\mathcal{Q}; \mathcal{F}^{ZZ-1}; \mathcal{F}^{DIR}; \tau_i, T_h)$ in these elements; we observe that the regions where the $ZZ-1$ recipe is less robust than the direct sampling increase in size as the class of solutions is enlarged. In Figs. 15c, 15d we give these regions for $\mathcal{Q} = \mathcal{Q}^H$ and $\mathcal{Q} = \mathcal{Q}^G$, respectively. It can be clearly seen that η%-superconvergence regions and the regions of relative robustness depend not only on the geometry of the element but also on the topology of its neighborhood.

In order to study the effect of mesh topology in triangular elements, we considered the four periodic patterns shown in Fig. 12 (Regular, Chevron, Union-Jack and Criss-Cross patterns). We solved the problem of isotropic heat conduction

using these patterns. For $p = 1$, the ZZ-recipes give 0%-superconvergent derivatives at all points in the elements of Regular, Union-Jack and Criss-Cross patterns. For the Chevron pattern and $p = 1$, the derivatives recovered using the ZZ-recipe are 0%-superconvergent only along the lines which pass through the midpoints of the horizontal sides. In Fig. 16 we give the η%-superconvergence regions $\mathcal{R}^{\eta\%}_{\frac{\partial u}{\partial x_i}}(Q^G; \mathcal{F}^{ZZ-1}; \tau_i, T_h)$ in the elements of the Chevron pattern. The values of $\eta^{\%}_{min}(\frac{\partial u}{\partial x_i}; \mathcal{F}; Q^G; \tau_i, T_h)$ and $\tau^{\%}_{\mathcal{H}<10\%}(\frac{\partial u}{\partial x_i}; \mathcal{F}; Q^G; \tau_i, T_h)$ for $\mathcal{F} = \mathcal{F}^{ZZ-1}$ and $\mathcal{F} = \mathcal{F}^{DIR}$ are given in Table 7. It can be observed that for $\mathcal{F}^{ZZ-1}$

$$\tau^{\%}_{\mathcal{H}<10\%}(\frac{\partial u}{\partial x_i}; \mathcal{F}^{ZZ-1}; Q^G; \tau_i, T_h) > 43\%$$

whereas for direct sampling

$$\tau^{\%}_{\mathcal{H}<10\%}(\frac{\partial u}{\partial x_i}; \mathcal{F}^{DIR}; Q^G; \tau_i, T_h) = 0\%$$

Thus, the recovered derivatives in the elements of the Chevron pattern are not exact at all points. However there is a significant gain in the minimum relative error and percentage area of the element with 10%-relative error.

For $p = 2$, the recovered derivatives in the elements in all the four patterns are not 0%-superconvergent except, perhaps, at isolated points in the elements. In Figs. 17a-d we give the η%-superconvergence regions $\mathcal{R}^{\eta\%}_{\frac{\partial u}{\partial x_i}}(Q^G; \mathcal{F}^{ZZ-1}; \tau_i, T_h)$ for the four patterns. In Table 8 we give the values of $\eta^{\%}_{min}(\frac{\partial u}{\partial x_i}; \mathcal{F}; Q^G; \tau_i, T_h)$ and $\tau^{\%}_{\mathcal{H}<10\%}(\frac{\partial u}{\partial x_i}; \mathcal{F}; Q^G; \tau_i, T_h)$ for $\mathcal{F} = \mathcal{F}^{ZZ-1}$ and $\mathcal{F} = \mathcal{F}^{DIR}$. We also report the values of $\mathcal{D}^{max}_{F(u)}(Q^G; \mathcal{F}^{ZZ-1}; \mathcal{F}^{DIR}; \tau_i, T_h)$ and $\tau^{\%}_{\mathcal{D}>1}(Q^G; \mathcal{F}^{ZZ-1}; \mathcal{F}^{DIR}; \tau_i, T_h)$ in all the elements of the four periodic patterns. In Fig. 17e we show the regions $\mathcal{R}^{\eta\%}_{\frac{\partial u}{\partial x_i}}(Q^G; \mathcal{F}^{ZZ-1}; \tau_i, T_h)$ for the distorted Criss-Cross pattern. By comparing Figs. 17c and 17e we observe that a small distortion of the uniform mesh has caused the disappearance of 5%-superconvergence regions in one of the elements.

8.5 An example which shows that the results obtained using the method of freezing the periodicity hold in the actual meshes

We now give some examples to show that the numerical results obtained by the method of freezing the periodicity are observed in actual finite element calculations.

We first give an example to show that the pointwise values of the maximum relative error obtained by the periodic-mesh methodology are also observed in

actual computations. We considered the problem of isotropic heat conduction and studied the superconvergence in the patch ω_{II}^h assuming biquadratic elements ($p = 2$). We used the methodology of Sections 6 and 7 to compute the $\eta\%$-superconvergence in the modulus of the gradient for recipe $\mathcal{F}^{ZZ-1}$. The points $\bar{\mathbf{x}}_k$ where the maximum relative error takes a minimum value in the element are shown in Fig. 18, i.e. $\tilde{\mathcal{H}}(\bar{\mathbf{x}}_k; \frac{\partial u}{\partial x_i}; \mathcal{F}^{ZZ-1}; \mathcal{Q}^{"H"}; \tilde{\tau}_i, \tilde{T}_h) = \eta^{\%}_{min}(\frac{\partial u}{\partial x_i}; \mathcal{F}^{ZZ-1}; \mathcal{Q}^{"H"}; \tilde{\tau}_i, \tilde{T}_h)$. The values of the maximum relative error at these points and the coefficients of the harmonic monomials which correspond to the extremal values of the error at these points are given in Table 9. We now check if these values of relative errors can be observed in the mesh patch when solving a boundary-value problem in the mesh shown in Fig. 5a. We solved a Dirichlet boundary value problem with the data consistent with the exact solution

$$u_{EX}(x_1, x_2) = \alpha_1(x_1^3 - 3x_1x_2^2) + \alpha_2(x_2^3 - 3x_1^2x_2)$$

where the values of α_1 and α_2 are given in Table 9. The values of α_1 and α_2 were obtained to correspond to the maximum relative-error at the point $\bar{\mathbf{x}}_k$ in the periodic mesh. The values of the relative error at $\bar{\mathbf{x}}_k$, computed using the mesh of Fig. 5a, are given in Table 9. It can be observed that the relative errors at these points are close to the values of $\tilde{\mathcal{H}}(\bar{\mathbf{x}}_k; \frac{\partial u}{\partial x_i}; \mathcal{F}^{ZZ-1}; \mathcal{Q}^{"H"}; \tilde{\tau}_i, \tilde{T}_h)$ (which are computed from the periodic-mesh). Therefore the conclusions made from the methodology are also valid for finite meshes.

We now give an example to show that the error in the recovered quantity $\mathcal{F}^{ZZ-1}(u_h)$ can be more than the error in quantity $F(u_h)$ computed directly from the finite element solution at some points and for some solutions. We considered the problem of isotropic heat conduction and studied the superconvergence in the mesh-cell ω_{II}^h assuming biquadratic elements. We used the methodology to compute the regions $\tilde{\mathcal{A}}_{\frac{\partial u}{\partial x_i}}(\mathcal{Q}^G; \mathcal{F}^{ZZ-1}, \mathcal{F}^{DIR}; \tilde{\tau}_i, \tilde{T}_h)$, i.e. the regions where $\mathcal{F}^{ZZ-1}$ is less robust than the direct sampling $\mathcal{F}^{DIR}$. We chose one point $\bar{\mathbf{x}}_k$ in each element in ω_{II}^h which lies in $\tilde{\mathcal{A}}_{\frac{\partial u}{\partial x_i}}(\mathcal{Q}^G; \mathcal{F}^{ZZ-1}, \mathcal{F}^{DIR}; \tilde{\tau}_i, \tilde{T}_h)$ (as shown in Fig. 19) and determined the coefficients of the monomials which correspond to the maximum relative error in the recovered quantity $\mathcal{F}^{ZZ-1}(u_h)$ at this point, $\tilde{\mathcal{H}}(\bar{\mathbf{x}}_k; \frac{\partial u}{\partial x_i}; \mathcal{F}^{ZZ-1}; \mathcal{Q}^G; \tilde{\tau}_i; \tilde{T})$. These coefficients are given in Table 10b. We then solved the Dirichlet boundary value problems using the mesh shown in Fig. 5a. The data for each problem is consistent with the exact solution

$$u_{EX}(x_1, x_2) = a_1x_1^3 + a_2x_1^2x_2 + a_3x_1x_2^2 + a_4x_2^3$$

where the values of $\{a_i\}_{i=1}^4$ are given in Table 10b. In order to compute the error at the point $\bar{\mathbf{x}}_k$ we chose the exact solution with the coefficients of the monomials

corresponding to this point given in Table 10b. The values of the errors in the solution quantity computed directly from the finite element solution and the errors in the recovered quantity are given in Table 10a. We also computed the ratio of the error in the recovered quantity $|\mathcal{F}^{ZZ-1}(u_h) - F(u)|$ to the error in the quantity computed directly from the finite element solution $|\mathcal{F}^{DIR}(u_h) - F(u)|$; these values are given in the last column of Table 10a. It can be observed that error in the recovered quantity exceeds the error in the finite element solution by a large factor, as it was predicted by the method of freezing the periodicity.

8.6 The quality of the "statically admissible" recipes

We will now give examples to illustrate that the "statically-admissible" recipes defined in Section 4.2 are more robust than the ZZ-recipes described in Section 4.1.

We first considered Laplace's equation and the elements in the mesh-cell ω_I^h (resp. ω_{II}^h) shown in Fig. 4a (resp. Fig. 4b) assuming bi-cubic elements. We computed the regions $\mathcal{R}^{\eta\%}_{\frac{\partial u}{\partial x_i}}(Q^H; \mathcal{F}; \tau_i, T_h)$ for the levels $\eta = 0.5\%, 1\%, 2\%$ for $\mathcal{F} = \mathcal{F}^{ZZ-1}, \mathcal{F}^{SA-1}, \mathcal{F}^{SA-2}$. These regions are given in Fig. 20a, 20b, 20c (resp. Figs. 21a, 21b, 21c). We note that for the recipe $\mathcal{F}^{ZZ-1}$ the 2%-superconvergence regions are very small or non-existent in most of the elements while for the recipes $\mathcal{F}^{SA-1}$ and $\mathcal{F}^{SA-2}$ the 2%-superconvergence regions cover most of the elements.

We also considered the elasticity problem and the elements in the mesh-cell ω_{III}^h which is shown in Fig. 4c. We employed biquadratic elements and computed the regions $\mathcal{R}^{\eta\%}_{\sigma_{ij}(u)}(Q^{"H"}; \mathcal{F}; \tau_i, T_h)$ with $\eta\% = 0.1\%, 0.5\%, 1\%$ for $\mathcal{F}^{ZZ-1}, \mathcal{F}^{SA-1}, \mathcal{F}^{SA-2}$; these regions are given in Fig. 22a, b, c. We observed that the recipe $SA-2$ which employs the least-squares fit of the displacement is the most robust. For this recipe the 1%-superconvergence regions cover almost completely all the elements in ω_{III}^h. Note also that both "statically-admissible" recipes are more robust than the ZZ-recipe at all the points in all the elements.

9 Summary of conclusions

This study presented a new definition of superconvergence which extends the classical definition to practical meshes. Using this definition we constructed a methodology for checking recipes for the recovery of the stresses, fluxes or derivatives from the finite element solutions. We employed the theory to assess the quality of a class of recipes known as ZZ-recipes and improved "statically-admissible" recipes. The following conclusions were drawn:

1. The regions of small relative error (i.e. less than 10%) for the ZZ-recipes are much larger than the corresponding regions for direct sampling.

2. The performance of the recipes depends on the class of meshes, solutions and materials of interest.

3. In general, we cannot say that a particular version of the ZZ-recipe is the best.

4. Depending on the geometry of the mesh, the class of solutions and the material-orthotropy significant regions of large relative error (greater than 50%) may exist for the ZZ-recipes.

5. The robustness of the ZZ-recipe relative to direct sampling decreases when the class of solution is enlarged or material-orthotropy is considered.

6. It is possible to improve significantly the quality of the recipes by employing the available information about the classes of admissible data. Among the recipes tested in this paper the recipe SA–2, which employs a "harmonic" least-squares fit for the displacement, is the best.

7. We recommend the use of any of the recipes tested here, especially the recipe SA–2, for practical computations.

8. The conclusions obtained using the methodology of the paper, to validate the recipes, hold for practical computations.

9. The methodology should be used, instead of random benchmarks, to assess the quality any concrete recipe used in practical finite element codes for the classes of meshes, solutions and materials of interest.

10. By employing the methodology of freezing the periodicity we can find the regions of least-error for any recipe in the interior of any practical mesh for the various solution quantities in the element.

11. The presented theory has asymptotic character. Hence the above conclusions are practically valid when the solution is smooth and the mesh is sufficiently refined. The cases of unsmooth solutions and coarse meshes will be addressed in forthcoming papers.

References

1. L.A. Oganesyan and L.A. Rukhovets, 'Study of the rate of convergence of variational difference schemes for second-order elliptic equations in a two-dimensional field with a smooth boundary', *U.S.S.R. Comput. Math. and Math. Phys.*, **9**, 153-183 (1968).

2. J.T. Oden and H. Brauchli, 'On the calculation of consistent stresses distributions in finite element approximations', *Internat. J. Numer. Methods Engrg.*, **3**, 317-325 (1971).

3. J.T. Oden and J.N. Reddy, 'Note on an approximate method for computing consistent conjugate stresses in elastic finite elements', *Internat. J. Numer. Methods Engrg.*, **6**, 55-61 (1973).

4. J. Douglas, Jr. and T. Dupont, 'Superconvergence for Galerkin methods for the two point boundary problem via local projections', *Numer. Math.*, **21**, 270-278 (1973).

5. J. Douglas, Jr., and T. Dupont, 'Galerkin approximations for the two point boundary problem using continuous piecewise polynomial spaces', *Numer. Math.*, **22**, 99-109 (1974).

6. J. Douglas, Jr., T. Dupont, and M.F. Wheeler, 'An L^∞ estimate and a superconvergence result for a Galerkin method for elliptic equations based on tensor products of piecewise polynomials', *RAIRO Anal. Numér.*, **8**, 61-66 (1974).

7. E. Hinton and J.S. Campbell, 'Local and global smoothing of discontinuous finite element functions using a least-squares method', *Internat. J. Numer. Methods Engrg.*, **8**, 461-480 (1974).

8. E. Hinton, F.C. Scott and R.E. Ricketts, 'Local least squares smoothing for parabolic isoparametric elements', *Internat. J. Numer. Methods Engrg.*, **9**, 235-238 (1975).

9. T. Dupont, 'A unified theory of superconvergence for Galerkin methods for two-point boundary problems', *SIAM J. Numer. Anal.*, **13**, 362-368 (1976).

10. J. Barlow, 'Optimal stress location in finite element models', *Internat. J. Numer. Methods Engrg.*, **10**, 243-251 (1976).

11. J.H. Bramble and A.H. Schatz, 'Higher order local accuracy by averaging in the finite element method', *Math. Comp.*, **31**, 94-111 (1977).

12. V. Thomée, 'High order local approximations to derivatives in the finite element method', *Math. Comp.*, **31**, 652-660 (1977).

13. M. Zlámal, 'Superconvergence and reduced integration in the finite element method', *Math. Comp.*, **32**, 663-685 (1978).

14. P. Lesaint and M. Zlámal, 'Superconvergence of the gradient of finite element solutions', *RAIRO Anal. Numér.*, **13**, 139-166 (1979).

15. A. Louis, 'Acceleration of convergence for finite element solutions of the Poisson equation', *Numer. Math.*, **33**, 43-53 (1979).

16. I. Babuška and A. Miller, 'The post-processing approach in the finite element method. Part 1: Calculation of displacements, stresses and other higher derivatives of the displacements', *Internat. J. Numer. Methods Engrg.*, **20**, 1085-1109 (1984).

17. I. Babuška, K. Izadpanah and B. Szabo, 'The postprocessing technique in the finite element method. The theory and experience', in *Unification of Finite Element Methods*, H. Kardestuncer, Ed., Elsevier Science Publishers B.V., 97-121 (1984).

18. M. Křižek and P. Neitaanmäki, 'Superconvergence phenomenon in the finite element method arising from averaging gradients', *Numer. Math.*, **45**, 105-116 (1984).

19. N. Levine, 'Superconvergent recovery of the gradient from piecewise linear finite element approximations', *IMA J. Numer. Anal.*, **5**, 407-427 (1985).

20. M.F. Wheeler and J.R. Whiteman, 'Superconvergent recovery of gradient on subdomains from piecewise linear finite-element approximations', *Numer. Methods for PDEs*, **3**, 65-82 (1987).

21. M. Křižek and P. Neitaanmäki, 'On superconvergence techniques', *Acta Applic. Math.*, **9**, 175-198 (1987).

22. M.T. Nakao, 'Superconvergence of the gradient of Galerkin approximations for elliptic problems', *RAIRO Math. Model. Numer. Anal.*, **21**, 679-695 (1987).

23. M.T. Nakao, 'Superconvergence of the gradient of Galerkin approximations for elliptic problems', *J. Comput. Appl. Math.*, **20**, 341-348 (1987).

24. O.C. Zienkiewicz and J.Z. Zhu, 'A simple error estimator and adaptive procedure for practical engineering analysis', *Internat. J. Numer. Methods Engrg.*, **24**, 337-357 (1987).

25. M. Křížek and P. Neittaanmäki, 'On a global superconvergence of the gradient of linear triangular elements', *J. Comput. Appl. Math.*, **18**, 221-233 (1987).

26. I. Hlaváček and M. Křížek, 'On a superconvergent finite element scheme for elliptic systems. I. Dirichlet boundary condition', *Aplik. Mat.*, **32**, 131-154 (1987).

27. I. Hlaváček and M. Křížek, 'On a superconvergent finite element scheme for elliptic systems. II. Boundary conditions of Newton's or Neumann's type', *Aplik. Mat.*, **32**, 200-213 (1987).

28. I. Hlaváček and M. Křížek, 'On a superconvergent finite element scheme for elliptic systems. III. Optimal interior estimates', *Aplik. Mat.*, **32**, 276-289 (1987).

29. W. Rachowicz, 'An evaluation and comparison of post-processing methods for finite element solutions of elliptic boundary value problems', *TICOM Report 87-11*, The Texas Institute for Computational Mechanics, The University of Texas at Austin, Austin, Texas, 1987.

30. A.B. Andreev and R.D. Lazarov, 'Superconvergence of the gradient for quadratic triangular finite elements', *Numer. Methods for PDEs*, **4**, 15-32 (1988).

31. W. Rachowicz and J.T. Oden, 'On the accuracy and convergence of conjugate flux approximations', *Numer. Methods for PDEs*, **5**, 143-156 (1989).

32. Q.D. Zhu and Q. Lin, 'Superconvergence theory of FEM', *Hunan Science Press*, (1989).

33. G. Goodsell and J.R. Whiteman, 'A unified treatment of superconvergent recovered gradient functions for piecewise linear finite element approximations', *Internat. J. Numer. Methods Engrg.*, **27**, 469-481 (1989).

34. G. Goodsell and J.R. Whiteman, 'Pointwise superconvergence of recovered gradients for piecewise linear finite element approximations to problems of planar linear elasticity', *Numer. Methods for PDEs*, **6**, 59-74 (1990).

35. J.Z. Zhu and O.C. Zienkiewicz, 'Superconvergence recovery technique and a posteriori error estimators', *Internat. J. Numer. Methods Engrg.*, **30**, 1321-1339 (1990).

36. O.C. Zienkiewicz and J.Z. Zhu, 'The superconvergence patch recovery and a posteriori error estimates. Part 1: The recovery technique', *Internat. J. Numer. Methods Engrg.*, **33**, 1331-1364 (1992).

37. O.C. Zienkiewicz and J.Z. Zhu, 'The superconvergence patch recovery and a posteriori error estimates. Part 2: Error estimates and adaptivity', *Internat. J. Numer. Methods Engrg.*, **33**, 1365-1382 (1992).

38. O.C. Zienkiewicz and J.Z. Zhu, 'The superconvergence patch recovery (SPR) and adaptive finite element refinement', *Comput. Methods Appl. Mech. Engrg.*, **101**, 207-224 (1992).

39. O.C. Zienkiewicz, J.Z. Zhu and J. Wu, 'Superconvergent patch recovery techniques. Some further tests', *Comm. Numer. Methods Engrg.*, **9**, 251-258 (1993).

40. J.Z. Zhu, 'Further tests on the derivative recovery technique and a posteriori error estimator', in *Finite Elements in the 90's*, E. Oñate, J. Periaux, A. Samuelson, Eds., Springer-Verlag/CIMNE, Barcelona, 594-604 (1991).

41. N.E. Wiberg and F. Abdulwahab, 'A posteriori error estimation based on superconvergent derivatives and equilibrium', *Internat. J. Numer. Methods Engrg.*, **36**, 2703-2724 (1993).

42. Q. Niu and M.S. Shephard, 'Superconvergent extraction techniques for finite element analysis', *Internat. J. Numer. Methods Engrg.*, **36**, 811-836 (1993).

43. A. Samuelson, N.E. Wiberg and L.F. Zeng, 'The effectivity of the Zienkiewicz-Zhu error estimate and two 2D adaptive mesh generators', *Commun. Num. Methods Engrg.*, **9**, 687-699 (1993).

44. T. Blacker and T. Belytschko, 'Superconvergent patch recovery with equilibrium and conjoint interpolant enhancements', *Internat. J. Numer. Methods Engrg.*, **37**, 517-536 (1994).

45. A.H. Schatz, I.H. Sloan and L.B. Wahlbin, 'Superconvergence in finite element methods and meshes which are symmetric with respect to a point', preprint (1993).

46. I. Babuška and R. Rodriguez, 'The problem of the selection of an a posteriori error indicator based on smoothening techniques', *Internat. J. Numer. Methods Engrg.*, **36**, 539-567 (1993).

47. I. Babuška, T. Strouboulis, C.S. Upadhyay and S.K. Gangaraj, 'Study of superconvergence by a computer-based approach. Superconvergence of the gradient in finite element solutions of Laplace's and Poisson's equation', Technical Note BN-1155, Institute for Physical Science and Technology, University of Maryland, College Park, November 1993.

48. I. Babuška, T. Strouboulis and C.S. Upadhyay, 'η%-superconvergence of finite element approximations in the interior of general meshes of triangles', Technical Note BN-1160, Institute for Physical Science and Technology, University of Maryland, College Park, December 1993.

49. I. Babuška, T. Strouboulis, S.K. Gangaraj and C.S. Upadhyay, 'η%-superconvergence in the interior of locally refined meshes of quadrilaterals. Superconvergence of the gradient in finite element solutions of Laplace's and Poisson's equations', Technical Note BN-1161, Institute for Physical Science and Technology, University of Maryland, College Park, January 1994.

50. I. Babuška, T. Strouboulis, C.S. Upadhyay and S.K. Gangaraj, 'Superconvergence of the gradient of the displacement, the strain and stress in finite element solutions for plane elasticity', Technical Note BN-1164, Institute for Physical Science and Technology, University of Maryland, College Park, February 1994.

51. I. Babuška, T. Strouboulis, A. Mathur and C.S. Upadhyay, 'Pollution-error in the h-version of the finite element method and the local quality of a-posteriori error estimators', Technical Note BN-1163, Institute for Physical Science and Technology, University of Maryland, College Park, February 1994.

52. P.G. Ciarlet, 'Basic error estimates for elliptic problems', in: P.G. Ciarlet and J.L. Lions, eds., *Handbook of Numerical Anaylsis*, *Vol. II*, North-Holland, Amsterdam, 17-351 (1991).

53. L.B. Wahlbin, 'Local behavior in finite element methods', in P.G. Ciarlet and J.L. Lions, eds., *Handbook of Numerical Analysis*, *Vol. II*, North-Holland, Amsterdam, 357-522 (1991).

54. I. Babuška, T. Strouboulis and C.S. Upadhyay, 'A model study of the quality of a posteriori error estimators for linear elliptic problems. Error estimation in the interior of patchwise uniform grids of triangles', Comput. Methods Appl. Mech. Engrg. (1994), to appear.

55. I. Babuška, T. Strouboulis, C.S. Upadhyay, S.K. Gangaraj and K. Copps, 'Validation of a posteriori error estimators by numerical approach', Internat. J. Numer. Methods Engrg., **37**, 1073-1123 (1994).

List of Figures

Fig. 1. *Examples of geometrical quantities used in the definition of the recipes.* The value of the recovered quantity at the point $\bar{\mathbf{x}}$, shown here in the interior of mesh-cell of bilinear elements, is obtained as a linear combination of the values of the solution at the vertices $\{\bar{\mathbf{x}}\}_{i=1}^{16}$.

Fig. 2. *An example to explain the new definition of superconvergence.* (a) A typical finite element mesh, bilinear elements, in the sequence of meshes. The point (0.25, 0.75) and the mesh-cell consisting of four sub-cells (shown shaded); (b) The mesh-cell of size $(2h \times 2h)$ and the $\mathbf{x}_K^{\omega_i^h}$. Here we show the points $\mathbf{x}_1^{\omega_1^h}$, $\mathbf{x}_2^{\omega_1^h}$, $\mathbf{x}_3^{\omega_2^h}$, $\mathbf{x}_4^{\omega_2^h}$, $\mathbf{x}_5^{\omega_2^h}$, $\mathbf{x}_6^{\omega_2^h}$.

Fig. 3. *An example to explain the new definition of superconvergence.* Exact solution $u_{EX}\ (x_1, x_2) = \sin(\pi x_1)\sinh(\pi x_2)$; bilinear Elements. Graphs of the relative error at the points marked in Fig. 2b for various values of the mesh-cell size h. Note that the values of the relative error converge to the theoretical values obtained from the periodic mesh.

Fig. 4. *The interior mesh-cells employed in the study of the quality of the recipes.* (a) Mesh-cell ω_I^h consisting of three elements shown with four surrounding mesh-layers; (b) Mesh-cell ω_{II}^h consisting of seven elements shown with seven surrounding mesh-layers; (c) Mesh-cell ω_{III}^h consisting of 20 elements surrounded by three mesh-layers.

Fig. 5. *The method of freezing the periodicity.* (a) Mesh of skewed quadrilateral with the mesh-cell ω_0^h shown shaded gray; (b) The periodic grid obtained by completing the mesh-cell ω_4^h; (c) The locally periodic mesh obtained by the method of freezing the periodicity.

Fig. 6. *Influence of the choice of the solution quantity $F(u)$ and its modulus $\left|\cdot\right|$ on the quality of the recipes*: Elasticity problem, biquadratic elements, "harmonic" solutions, mesh-cell ω_I^h.
(a) The regions $\mathcal{R}^{\eta\%}_{\sigma_{11}(u)}(\mathcal{Q}^{\text{"}H\text{"}}; \mathcal{F}^{DIR}; \tau_i, T_h)$;
(b) The regions $\mathcal{R}^{\eta\%}_{I_1(u)}(\mathcal{Q}^{\text{"}H\text{"}}; \mathcal{F}^{DIR}; \tau_i, T_h)$, $I_1(\mathbf{u}) := \sigma_{11}(\mathbf{u}) + \sigma_{22}(\mathbf{u})$;
(c) The regions $\mathcal{R}^{\eta\%}_{\sigma_{ij}(u)}(\mathcal{Q}^{\text{"}H\text{"}}; \mathcal{F}^{DIR}; \tau_i, T_h)$ where $\left|\sigma_{ij}\right| = J_2(\sigma_{ij})$.
The levels of $\eta\%$ employed are: 10%, 25%, 50% (dark, light and lighter gray, respectively).

Fig. 7. *Influence of the choice of the solution quantity $F(u)$ and its modulus $\left|\cdot\right|$ on the quality of the recipes*: Elasticity problem, biquadratic elements, "harmonic" solutions, mesh-cell ω_I^h.

(a) The regions $\mathcal{R}^{\eta\%}_{\sigma_{11}(u)}(\mathcal{Q}^{"H"};\mathcal{F}^{ZZ-1};\tau_i,T_h)$;
(b) The regions $\mathcal{R}^{\eta\%}_{I_1(u)}(\mathcal{Q}^{"H"};\mathcal{F}^{ZZ-1};\tau_i,T_h)$, $I_1(\mathbf{u}) := \sigma_{11}(\mathbf{u}) + \sigma_{22}(\mathbf{u})$;
(c) The regions $\mathcal{R}^{\eta\%}_{\sigma_{ij}(u)}(\mathcal{Q}^{"H"};\mathcal{F}^{ZZ-1};\tau_i,T_h)$ where $\left|\sigma_{ij}\right| = J_2(\sigma_{ij})$.
The levels of $\eta\%$ employed are: 5%, 10%, 25% (dark, light, lighter gray, respectively).

Fig. 8. *Influence of the choice of the definition of the ZZ-recipe*: $\eta\%$-superconvergence regions for the ZZ-recipes. Elasticity problem, biquadratic elements, "harmonic" solutions, mesh-cell ω^h_{II}.
(a) The regions $\mathcal{R}^{\eta\%}_{\sigma_{11}(u)}(\mathcal{Q}^{"H"};\mathcal{F}^{ZZ-1};\tau_i,T_h)$;
(b) The regions $\mathcal{R}^{\eta\%}_{\sigma_{11}(u)}(\mathcal{Q}^{"H"};\mathcal{F}^{ZZ-2};\tau_i,T_h)$;
(c) The regions $\mathcal{R}^{\eta\%}_{\sigma_{ij}(u)}(\mathcal{Q}^{"H"};\mathcal{F}^{ZZ-1};\tau_i,T_h)$ where $\left|\sigma_{ij}\right| = J_2(\sigma_{ij})$;
(d) The regions $\mathcal{R}^{\eta\%}_{\sigma_{ij}(u)}(\mathcal{Q}^{"H"};\mathcal{F}^{ZZ-2};\tau_i,T_h)$ where $\left|\sigma_{ij}\right| = J_2(\sigma_{ij})$.
The levels of $\eta\%$ employed are: 5%, 10%, 25% (dark, light, lighter gray, respectively).

Fig. 9. *Influence of the choice of the definition of the ZZ-recipe*: Regions of relative robustness of the ZZ-recipes with respect to the direct recipe. Elasticity problem, biquadratic elements, "harmonic" solutions, mesh-cell ω^h_{II}.
(a) The regions $\mathcal{A}_{\sigma_{11}(u)}(\mathcal{Q}^{"H"};\mathcal{F}^{ZZ-1};\mathcal{F}^{DIR};\tau_i,T_h)$;
(b) The regions $\mathcal{A}_{\sigma_{11}(u)}(\mathcal{Q}^{"H"};\mathcal{F}^{ZZ-2};\mathcal{F}^{DIR};\tau_i,T_h)$;
(c) The regions $\mathcal{A}_{\sigma_{11}(u)}(\mathcal{Q}^{"H"};\mathcal{F}^{ZZ-3};\mathcal{F}^{DIR};\tau_i,T_h)$;
(d) The regions $\mathcal{A}_{\sigma_{ij}(u)}(\mathcal{Q}^{"H"};\mathcal{F}^{ZZ-1};\mathcal{F}^{DIR};\tau_i,T_h)$;
(e) The regions $\mathcal{A}_{\sigma_{ij}(u)}(\mathcal{Q}^{"H"};\mathcal{F}^{ZZ-2};\mathcal{F}^{DIR};\tau_i,T_h)$;
(f) The regions $\mathcal{A}_{\sigma_{ij}(u)}(\mathcal{Q}^{"H"};\mathcal{F}^{ZZ-3};\mathcal{F}^{DIR};\tau_i,T_h)$.
The dark-regions indicate the areas where the ZZ-recipes are less robust than direct sampling. In the regions given in (d), (e) and (f) the modulus $\left|\sigma_{ij}\right| := J_2(\sigma_{ij})$ was employed.

Fig. 10. *Influence of the class of solutions*: Regions of $\eta\%$-superconvergence and of relative robustness (with respect to direct sampling) for the ZZ-recipes. Isotropic heat-conduction, biquadratic elements, mesh-cell ω^h_{II}.
(a) The regions $\mathcal{R}^{\eta\%}_{\frac{\partial u}{\partial x_i}}(\mathcal{Q}^{H};\mathcal{F}^{ZZ-1};\tau_i,T_h)$;
(b) The regions $\mathcal{R}^{\eta\%}_{\frac{\partial u}{\partial x_i}}(\mathcal{Q}^{G};\mathcal{F}^{ZZ-1};\tau_i,T_h)$;
(c) The regions $\mathcal{A}_{\frac{\partial u}{\partial x_i}}(\mathcal{Q}^{H};\mathcal{F}^{ZZ-1},\mathcal{F}^{DIR};\tau_i,T_h)$;
(d) The regions $\mathcal{A}_{\frac{\partial u}{\partial x_i}}(\mathcal{Q}^{G};\mathcal{F}^{ZZ-1},\mathcal{F}^{DIR};\tau_i,T_h)$.
The dark-regions indicate the areas where the ZZ-recipes are less robust than direct sampling. Here the modulus $\left|\frac{\partial u}{\partial x_i}\right| := \sqrt{\left(\frac{\partial u}{\partial x_1}\right)^2 + \left(\frac{\partial u}{\partial x_2}\right)^2}$ was employed.

Fig. 11. *Influence of the class of solutions*: Regions of η%-superconvergence and of relative robustness (with respect to direct sampling) for the ZZ-recipes. Orthotropic heat-conduction with $\frac{K_{22}}{K_{11}} = 2$, biquadratic elements, mesh-cell ω_{II}^h.
(a) The regions $\mathcal{R}_{q_i(u)}^{\eta\%}(\mathcal{Q}^H; \mathcal{F}^{ZZ-1}; \tau_i, T_h)$;
(b) The regions $\mathcal{R}_{q_i(u)}^{\eta\%}(\mathcal{Q}^G; \mathcal{F}^{ZZ-1}; \tau_i, T_h)$;
(c) The regions $\mathcal{A}_{q_i(u)}(\mathcal{Q}^H; \mathcal{F}^{ZZ-1}, \mathcal{F}^{DIR}; \tau_i, T_h)$;
(d) The regions $\mathcal{A}_{q_i(u)}(\mathcal{Q}^G; \mathcal{F}^{ZZ-1}, \mathcal{F}^{DIR}; \tau_i, T_h)$.
The dark-regions indicate the areas where the ZZ-recipes are less robust than direct sampling. Here the modulus $\left| q_i \right| := \sqrt{q_1^2 + q_2^2}$ was employed.

Fig. 12. *Periodic meshes of triangles.* (a) Regular pattern; (b) Union-Jack pattern; (c) Chevron pattern; (d) Criss-Cross pattern.

Fig. 13. *Influence of the polynomial degree of the elements*: Elasticity problem, tensor-product quadrilaterals "harmonic"; solutions mesh-cell ω_{II}^h. The regions $\mathcal{A}_{\sigma_{ij}(u)}(\mathcal{Q}^{"H"}; \mathcal{F}^{ZZ-1}; \mathcal{F}^{DIR}; \tau_i, T_h)$.
(a) Bilinear elements ($p = 1$);
(b) Bicubic elements ($p = 3$).
The dark regions indicate the areas where the ZZ recipes are less robust than direct sampling.

Fig. 14. *Influence of the topology of the mesh and the class of solutions*: Isotropic heat-conduction, bilinear elements, direct sampling.
(a) The regions $\mathcal{R}_{\frac{\partial u}{\partial x_1}}^{\eta\%}(\mathcal{Q}^H; \mathcal{F}^{DIR}; \tau_i, T_h)$;
(b) The regions $\mathcal{R}_{\frac{\partial u}{\partial x_1}}^{\eta\%}(\mathcal{Q}^G; \mathcal{F}^{DIR}; \tau_i, T_h)$;
The levels of η% employed are: 10%, 30%, 50% (dark, light, lighter gray, respectively). Note the η%-superconvergence regions for the general class of solutions shown in (b) are smaller than the corresponding regions for the harmonic class of solutions shown in (a).

Fig. 15. *Influence of the topology of the mesh and the class of solutions*: Isotropic heat-conduction, bilinear elements, mesh-cell ω_{III}^h.
(a) The regions $\mathcal{R}_{\frac{\partial u}{\partial x_1}}^{\eta\%}(\mathcal{Q}^H; \mathcal{F}^{ZZ-1}; \tau_i, T_h)$;
(b) The regions $\mathcal{R}_{\frac{\partial u}{\partial x_1}}^{\eta\%}(\mathcal{Q}^G; \mathcal{F}^{ZZ-1}; \tau_i, T_h)$;
The levels of η% employed are: 5%, 10%, 25% (dark, light, lighter gray, respectively). Note in contrast to the η%-superconvergence regions for direct sampling shown in Fig. 11 the 25%-region practically covers all the elements.
(c) The regions $\mathcal{A}_{\frac{\partial u}{\partial x_1}}^{\eta\%}(\mathcal{Q}^H; \mathcal{F}^{ZZ-1}; \mathcal{F}^{DIR}; \tau_i, T_h)$;

(d) The regions $\mathcal{A}^{\eta\%}_{\frac{\partial u}{\partial x_i}}(\mathcal{Q}^G; \mathcal{F}^{ZZ-1}; \mathcal{F}^{DIR}; \tau_i, T_h)$.

The dark-regions in (c) and (d) indicate the areas where the ZZ-recipes are less robust than direct sampling. Note that the dark-regions for the general class of solutions are larger than the corresponding regions for the harmonic solutions.

Fig. 16. *Influence of the element type*: Isotropic heat-conduction, linear triangular elements, Chevron-pattern, discrete ZZ-recipe.

Fig. 17. *Influence of the element type*: Isotropic heat-conduction, quadratic triangular elements, discrete ZZ-recipe.
(a) The regions $\mathcal{R}^{\eta\%}_{\frac{\partial u}{\partial x_i}}(\mathcal{Q}^G; \mathcal{F}^{ZZ-1}; \tau_i, T_h)$ for the Chevron pattern;

(b) The regions $\mathcal{R}^{\eta\%}_{\frac{\partial u}{\partial x_i}}(\mathcal{Q}^G; \mathcal{F}^{ZZ-1}; \tau_i, T_h)$ for the Union-Jack pattern;

(c) The regions $\mathcal{R}^{\eta\%}_{\frac{\partial u}{\partial x_i}}(\mathcal{Q}^G; \mathcal{F}^{ZZ-1}; \tau_i, T_h)$ for the Criss-Cross pattern;

(d) The regions $\mathcal{R}^{\eta\%}_{\frac{\partial u}{\partial x_i}}(\mathcal{Q}^G; \mathcal{F}^{ZZ-1}; \tau_i, T_h)$ for the Regular pattern;

(e) The regions $\mathcal{R}^{\eta\%}_{\frac{\partial u}{\partial x_i}}(\mathcal{Q}^G; \mathcal{F}^{ZZ-1}; \tau_i, T_h)$ for the distorted Criss-Cross pattern. Note that the slight displacement of the central node caused the disappearance of the 5%-regions from two of the elements.
The levels of $\eta\%$ employed are: 5%, 10%, 15% (dark, light, lighter gray, respectively). Here the modulus $\left|\frac{\partial u}{\partial x_i}\right| := \sqrt{\left(\frac{\partial u}{\partial x_1}\right)^2 + \left(\frac{\partial u}{\partial x_2}\right)^2}$ was employed.

Fig. 18. *An example to show that the conclusions hold for general meshes.* Mesh-cell ω^h_{II} and the regions $\mathcal{R}^{\eta\%}_{\frac{\partial u}{\partial x_i}}(\mathcal{Q}^G; \mathcal{F}^{ZZ-1}; \tau_i, T_h)$ for biquadratic elements shown in Fig. 10b. The points of interest in these regions are marked and enumerated for studying the relative error in the ZZ-recipe.

Fig. 19. *An example to show that the conclusions hold for general meshes.* Mesh-cell ω^h_{II} and the regions $\mathcal{A}^{\eta\%}_{\frac{\partial u}{\partial x_i}}(\mathcal{Q}^G; \mathcal{F}^{ZZ-1}; \mathcal{F}^{DIR}; \tau_i, T_h)$ for biquadratic elements shown in Fig. 10d. The points of interest in these regions are marked and enumerated for studying the relative error in the ZZ-recipe.

Fig. 20. *Comparison of the robustness of the "statically-admissible" recipes with the ZZ-recipe*: Laplace's equation, bi-cubic elements, mesh-cell ω^h_I.
(a) The regions $\mathcal{R}^{\eta\%}_{\frac{\partial u}{\partial x_i}}(\mathcal{Q}^H; \mathcal{F}^{ZZ-1}; \tau_i, T_h)$;

(b) The regions $\mathcal{R}^{\eta\%}_{\frac{\partial u}{\partial x_i}}(\mathcal{Q}^H; \mathcal{F}^{SA-1}; \tau_i, T_h)$;

(c) The regions $\mathcal{R}^{\eta\%}_{\frac{\partial u}{\partial x_i}}(\mathcal{Q}^H; \mathcal{F}^{SA-2}; \tau_i, T_h)$.

The levels of $\eta\%$ employed are: 0.5%, 1%, 2% (dark, light, lighter gray, respectively). Note that the 2%-superconvergence regions for the ZZ-1 recipe are almost non-existent.

Fig. 21. *Comparison of the robustness of the "statically-admissible" recipes with the ZZ-recipe*: Laplace's equation, bi-cubic elements, mesh-cell ω_{II}^h.
(a) The regions $\mathcal{R}^{\eta\%}_{\frac{\partial u}{\partial x_i}}(\mathcal{Q}^H; \mathcal{F}^{ZZ-1}; \tau_i, T_h)$;
(b) The regions $\mathcal{R}^{\eta\%}_{\frac{\partial u}{\partial x_i}}(\mathcal{Q}^H; \mathcal{F}^{SA-1}; \tau_i, T_h)$;
(c) The regions $\mathcal{R}^{\eta\%}_{\frac{\partial u}{\partial x_i}}(\mathcal{Q}^H; \mathcal{F}^{SA-2}; \tau_i, T_h)$.
The levels of $\eta\%$ employed are: 0.5%, 1%, 2% (dark, light, lighter gray, respectively). Note that the 2%-superconvergence regions for the ZZ-1 recipe do not exist in four elements from the mesh-cell.

Fig. 22. *Comparison of the robustness of the "statically-admissible" recipes with the ZZ-recipe*: Laplace's equation, bi-cubic elements, mesh-cell ω_{III}^h.
(a) The regions $\mathcal{R}^{\eta\%}_{\sigma_{ij}(u)}(\mathcal{Q}^{"H"}; \mathcal{F}^{ZZ-1}; \tau_i, T_h)$;
(b) The regions $\mathcal{R}^{\eta\%}_{\sigma_{ij}(u)}(\mathcal{Q}^{"H"}; \mathcal{F}^{SA-1}; \tau_i, T_h)$;
(c) The regions $\mathcal{R}^{\eta\%}_{\sigma_{ij}(u)}(\mathcal{Q}^{"H"}; \mathcal{F}^{SA-2}; \tau_i, T_h)$.
The levels of $\eta\%$ employed are: 0.1%, 0.5%, 1% (dark, light, lighter gray, respectively). Note that the 1%-superconvergence regions for the SA-2 recipe cover the elements almost entirely.

Rate of convergence of the error in the gradient		
Point $\bar{\mathbf{x}}_1$; $\tilde{\Theta}_1 = 19.7\%$		
h	$\left\| F(u) - \mathcal{F}^{ZZ-1}(u_h) \right\|$	$\dfrac{\left\| F(u) - \mathcal{F}^{ZZ-1}(u_h) \right\|}{h}$
0.25000	2.026	8.104
0.12500	1.179	9.432
0.06250	0.625	10.001
0.03125	0.333	10.640
Point $\bar{\mathbf{x}}_2$; $\tilde{\Theta}_2 = 20.92\%$		
h	$\left\| F(u) - \mathcal{F}^{ZZ-1}(u_h) \right\|$	$\dfrac{\left\| F(u) - \mathcal{F}^{ZZ-1}(u_h) \right\|}{h}$
0.25000	1.917	7.668
0.12500	1.143	9.144
0.06250	0.613	9.808
0.03125	0.317	10.144

Table 1. *Rate of convergence of the error in the gradient*: Laplace's equation, bilinear elements ($p = 1$), meshes consisting of mesh-cells shown in Fig.2a. The locations of the points $\bar{\mathbf{x}}_1, \ldots, \bar{\mathbf{x}}_6$ with respect to the mesh-cell are shown in Fig. 2b. Here $F(u)$ denotes the value of the derivative of the exact solution $\mathcal{F}^{ZZ-1}(u_h)$ denotes the recovered derivative using the recipe described in Section 4 and $\mathcal{F}^{DIR}(u_h)$ denotes the derivative of the finite element solution u_h.

Rate of convergence of the error in the gradient		
Point $\bar{x}_3$; $\tilde{\Theta}_3 = 0.0\%$		
h	$\left\| F(u) - \mathcal{F}^{ZZ-1}(u_h) \right\|$	$\dfrac{\left\| F(u) - \mathcal{F}^{ZZ-1}(u_h) \right\|}{h^2}$
0.25000	0.04993	0.800
0.12500	0.01840	1.178
0.06250	0.00449	1.149
0.03125	0.00116	1.188
Point $\bar{x}_4$; $\tilde{\Theta}_4 = 0.016\%$		
h	$\left\| F(u) - \mathcal{F}^{DIR}(u_h) \right\|$	$\dfrac{\left\| F(u) - \mathcal{F}^{DIR}(u_h) \right\|}{h^2}$
0.25000	0.27604	4.417
0.12500	0.06846	4.382
0.06250	0.01841	4.714
0.03125	0.00464	4.750

Table 1. (continued)

Rate of convergence of the error in the gradient		
Point $\bar{x}_5$; $\tilde{\Theta}_5 = 20.21\%$		
h	$\left\| F(u) - \mathcal{F}^{ZZ-1}(u_h) \right\|$	$\frac{\left\| F(u) - \mathcal{F}^{ZZ-1}(u_h) \right\|}{h}$
0.25000	0.05367	0.215
0.12500	0.01977	0.158
0.06250	0.00616	0.099
0.03125	0.00249	0.080
Point $\bar{x}_6$; $\tilde{\Theta}_6 = 30.25\%$		
h	$\left\| F(u) - \mathcal{F}^{ZZ-1}(u_h) \right\|$	$\frac{\left\| F(u) - \mathcal{F}^{ZZ-1}(u_h) \right\|}{h}$
0.25000	1.621	6.484
0.12500	0.933	7.464
0.06250	0.487	7.792
0.03125	0.242	7.744

Table 1. (continued)

η%-superconvergence for the recipe $\mathcal{F}^{DIR}$												
Mesh cell of three elements shown in Fig. 4a												
Elasticity problem												
τ_i	$F(\mathbf{u}) = \sigma_{11}(\mathbf{u})$				$F(\mathbf{u}) = I_1(\sigma_{ij}(\mathbf{u}))$				$F(\mathbf{u}) = \sigma_{ij}(\mathbf{u})$			
	$\eta^{\%}_{min}(\tau_i)$	$\tau^{\%}_{\mathcal{H}<5\%}$	$\tau^{\%}_{\mathcal{H}<10\%}$	$\tau^{\%}_{\mathcal{H}<25\%}$	$\eta^{\%}_{min}(\tau_i)$	$\tau^{\%}_{\mathcal{H}<5\%}$	$\tau^{\%}_{\mathcal{H}<10\%}$	$\tau^{\%}_{\mathcal{H}<25\%}$	$\eta^{\%}_{min}(\tau_i)$	$\tau^{\%}_{\mathcal{H}<5\%}$	$\tau^{\%}_{\mathcal{H}<10\%}$	$\tau^{\%}_{\mathcal{H}<25\%}$
1	0.14	0.11	2.03	26.19	1.34	0.01	0.69	14.33	11.42	0.00	0.00	4.04
2	0.92	0.89	6.92	64.27	12.62	0.00	0.00	7.84	13.99	0.00	0.00	3.87
3	1.23	0.01	1.24	9.09	3.19	0.01	0.57	12.96	14.06	0.00	0.00	9.19

Table 2a. *Influence of the measure on the η%-superconvergence regions*: Elasticity problem, "Harmonic" solutions, biquadratic elements ($p = 2$), mesh-cell ω^h_I. η%-superconvergence regions for the direct sampling. Values of $\eta^{\%}_{min}(\tau_i) = \eta^{\%}_{min}(F; \mathcal{F}^{DIR}; Q^{``H"}; \tau_i, T_h)$ and $\tau^{\%}_{\mathcal{H}<\eta\%}(F; \mathcal{F}^{DIR}; Q^{``H"}; \tau_i, T_h)$ for $\eta = 5$, 10 and 25 and for $F(u) = \sigma_{11}$, $F(u) = I_1(\sigma_{ij}(\mathbf{u}))$ and $F(u) = \sigma_{ij}(\mathbf{u})$.

η%-superconvergence for the recipe $\mathcal{F}^{ZZ-1}$												
Mesh-cell of three elements shown in Fig. 4a												
Elasticity problem												
τ_i	$F(\mathbf{u}) = \sigma_{11}(\mathbf{u})$				$F(\mathbf{u}) = I_1(\sigma_{ij}(\mathbf{u}))$				$F(\mathbf{u}) = \sigma_{ij}(\mathbf{u})$			
	$\eta^{\%}_{min}(\tau_i)$	$\tau^{\%}_{\mathcal{H}<5\%}$	$\tau^{\%}_{\mathcal{H}<10\%}$	$\tau^{\%}_{\mathcal{H}<25\%}$	$\eta^{\%}_{min}(\tau_i)$	$\tau^{\%}_{\mathcal{H}<5\%}$	$\tau^{\%}_{\mathcal{H}<10\%}$	$\tau^{\%}_{\mathcal{H}<25\%}$	$\eta^{\%}_{min}(\tau_i)$	$\tau^{\%}_{\mathcal{H}<5\%}$	$\tau^{\%}_{\mathcal{H}<10\%}$	$\tau^{\%}_{\mathcal{H}<25\%}$
1	0.04	60.13	76.34	96.67	1.33	24.17	82.13	95.50	0.82	60.37	76.12	96.14
2	1.06	56.39	74.22	94.33	1.29	22.14	80.36	90.18	1.46	20.17	31.33	86.87
3	0.83	50.36	75.00	89.74	1.04	23.84	79.17	89.94	2.17	21.39	64.41	94.39

Table 2b. *Influence of the measure on the η%-superconvergence regions*: Elasticity problem, "Harmonic" solutions, biquadratic elements ($p = 2$), mesh-cell ω^h_I. η%-superconvergence regions for the discrete ZZ recipe $\mathcal{F}^{ZZ-1}$, $\eta^{\%}_{min}(F; \mathcal{F}^{ZZ-1}; Q^{\text{"}H\text{"}}; \tau_i, T_h)$ and $\tau^{\%}_{\mathcal{H}<\eta\%}(F; \mathcal{F}^{ZZ-1}; Q^{\text{"}H\text{"}}; \tau_i, T_h)$ for $\eta = 5$, 10 and 25 and for $F(\mathbf{u}) = \sigma_{11}(\mathbf{u})$, $F(\mathbf{u}) = I_1(\sigma_{ij}(\mathbf{u}))$ and $F(\mathbf{u}) = \sigma_{ij}(\mathbf{u})$.

η%-superconvergence for the ZZ-recipes						
Mesh-cell of seven elements shown in Fig. 4b						
Elasticity problem						
	Discrete-ZZ with $a_{ijk\ell}$ $(ZZ-1)$		Continuous ZZ with $a_{ijk\ell}$ $(ZZ-2)$		Discrete-ZZ with $\delta_{ik}\delta_{j\ell}$ $(ZZ-3)$	
τ_i	$\eta^{\%}_{min}(\tau_i)$	$\tau^{\%}_{\mathcal{H}<10\%}$	$\eta^{\%}_{min}(\tau_i)$	$\tau^{\%}_{\mathcal{H}<10\%}$	$\eta^{\%}_{min}(\tau_i)$	$\tau^{\%}_{\mathcal{H}<10\%}$
1	2.45	11.96	0.19	61.37	2.17	12.94
2	13.21	0.00	2.74	22.27	13.62	0.00
3	14.10	0.00	3.32	37.16	13.89	0.00
4	1.72	43.30	1.61	54.01	1.95	42.22
5	2.16	48.37	3.11	68.94	2.09	48.81
6	9.31	0.18	7.59	10.47	9.33	0.18
7	8.93	3.27	4.30	39.31	8.84	3.33

Table 3a. *Influence of the definition of the recipe*: Elasticity problem, "Harmonic" solutions, biquadratic elements (p =2), mesh-cell ω^h_{II}. η%-superconvergence regions for the three versions of the ZZ recipe. The values of $\eta^{\%}_{min}(\tau_i) := \eta^{\%}_{min}(\sigma_{ij}; \mathcal{F}; \mathcal{Q}^{\text{"}H\text{"}}; \tau_i, T_h)$ and $\tau^{\%}_{\mathcal{H}<10\%}$ $(\sigma_{ij}; \mathcal{F}; \mathcal{Q}^{\text{"}H\text{"}}; \tau_i, T_h)$ for $\mathcal{F} = \mathcal{F}^{ZZ-1}$, $\mathcal{F}^{ZZ-2}$ and $\mathcal{F}^{ZZ-3}$.

Relative robustness of the ZZ-recipes with respect to direct sampling						
Mesh-cell of seven elements shown in Fig. 4b						
Elasticity problem						
τ	Discrete-ZZ with $a_{ijk\ell}$ $(ZZ-1)$		Continuous ZZ with $a_{ijk\ell}$ $(ZZ-2)$		Discrete-ZZ with $\delta_{ik}\delta_{j\ell}$ $(ZZ-3)$	
	$\mathcal{D}^{max}_{F(u)}$	$\tau^{\%}_{\mathcal{D}>1}$	$\mathcal{D}^{max}_{F(u)}$	$\tau^{\%}_{\mathcal{D}>1}$	$\mathcal{D}^{max}_{F(u)}$	$\tau^{\%}_{\mathcal{D}>1}$
1	1.87	4.81	0.64	0.00	1.80	4.79
2	2.31	11.21	1.79	5.15	2.09	11.09
3	1.44	9.44	1.32	3.20	1.46	9.52
4	1.39	6.47	0.83	0.00	1.36	6.33
5	2.09	10.39	1.54	5.61	1.98	10.34
6	1.61	3.01	0.94	0.00	1.59	3.01
7	2.42	17.00	1.05	0.13	2.42	17.59

Table 3b. *Influence of the definition of the recipe*: Elasticity problem, "Harmonic" solutions, biquadratic elements (p =2), mesh-cell ω^h_{II}. Regions of relative robustness of the ZZ-recipes with respect to direct sampling. The values of $\mathcal{D}^{max}_{F(u)} := \max_{x\in\tau} \mathcal{D}_{F(u)}(x; Q^{"H"}; \mathcal{F}', \mathcal{F}^{DIR}; \tau_i, T_h)$ and $\tau^{\%}_{\mathcal{D}>1}(Q^{"H"}; \mathcal{F}, \mathcal{F}^{DIR}; \tau_i, T_h)$ for $\mathcal{F} = \mathcal{F}^{ZZ-1}$, $\mathcal{F}^{ZZ-2}$ and $\mathcal{F}^{ZZ-3}$.

η%-superconvergence for the discrete ZZ-recipe								
Mesh-cell of seven elements shown in Fig. 4b								
Orthotropic heat-conduction								
τ_i	$\mathcal{Q}^{"H"}$				$\mathcal{Q}^{G}$			
	$\frac{K_{22}}{K_{11}} = 1$		$\frac{K_{22}}{K_{11}} = 2$		$\frac{K_{22}}{K_{11}} = 1$		$\frac{K_{22}}{K_{11}} = 2$	
	$\eta^{\%}_{min}(\tau_i)$	$\tau^{\%}_{\mathcal{H}<10\%}$	$\eta^{\%}_{min}(\tau_i)$	$\tau^{\%}_{\mathcal{H}<10\%}$	$\eta^{\%}_{min}(\tau_i)$	$\tau^{\%}_{\mathcal{H}<10\%}$	$\eta^{\%}_{min}(\tau_i)$	$\tau^{\%}_{\mathcal{H}<10\%}$
1	1.86	70.15	6.00	0.74	2.45	11.96	8.48	0.09
2	5.19	24.47	17.93	0.00	13.21	0.00	22.17	0.00
3	7.02	14.01	12.83	0.00	14.10	0.00	19.56	0.00
4	1.72	36.04	1.66	17.12	1.72	33.30	2.41	11.72
5	2.22	70.87	3.48	17.77	2.16	48.37	5.28	13.44
6	10.87	0.00	20.67	0.00	11.31	0.00	28.29	0.00
7	4.78	22.68	9.70	0.16	8.93	1.27	11.97	0.00

Table 4a. *Influence of the solution type and material orthotropy*: Orthotropic heat conduction problem, biquadratic elements ($p = 2$), mesh-cell ω^h_{II}. η%-superconvergence regions for the discrete ZZ recipe $\mathcal{F}^{ZZ-1}$. The values of $\eta^{\%}_{min}(\tau_i) := \eta^{\%}_{min}(q_i; \mathcal{F}^{ZZ-1}; \mathcal{Q}; \tau_i, T_h)$ and $\tau^{\%}_{\mathcal{H}<10\%}\ (q_i; \mathcal{F}^{ZZ-1}; \mathcal{Q}; \tau_i, T_h)$ for $\mathcal{Q} = \mathcal{Q}^{"H"}$ and $\mathcal{Q} = \mathcal{Q}^{G}$ with the principal material coefficients $\frac{K_{22}}{K_{11}} = 1$ and $\frac{K_{22}}{K_{11}} = 2$.

Relative robustness of $\mathcal{F}^{ZZ-1}$ with respect to $\mathcal{F}^{DIR}$			
Mesh-cell of seven elements shown in Fig. 4b			
Orthotropic heat-conduction			
τ_i	$\mathcal{Q}^{"H"}$		$\mathcal{Q}^G$
	$\frac{K_{11}}{K_{22}}=1$	$\frac{K_{11}}{K_{22}}=2$	$\frac{K_{11}}{K_{22}}=2$
1	1.21	14.53	42.72
2	1.04	38.58	67.43
3	1.11	56.05	77.83
4	1.31	14.81	27.82
5	1.19	7.25	17.15
6	1.37	23.73	59.40
7	1.16	7.06	19.27

Table 4b: *Influence of the solution-type and material orthotropy*: Orthotropic heat conduction problem, biquadratic elements ($p = 2$), mesh-cell ω_{II}^h. Regions of relative robustness of the ZZ-recipe $\mathcal{F}^{ZZ-1}$. The values of $\tau^{\%}_{\mathcal{D}>1}(q_i; \mathcal{Q}; \mathcal{F}^{ZZ-1}, \mathcal{F}^{DIR}; \tau_i, T_h)$ for $\mathcal{Q} = \mathcal{Q}^{"H"}$ and $\mathcal{Q} = \mathcal{Q}^G$ with material orthotropy $\frac{K_{22}}{K_{11}} = 1$ and $\frac{K_{22}}{K_{11}} = 2$.

η%-superconvergence and relative robustness of the ZZ-recipe with respect to direct sampling										
Quadratic triangles (p=2)										
Criss-Cross pattern										
τ_i	$\mathcal{F}^{ZZ-1}$				$\mathcal{F}^{DIR}$					
	$\frac{K_{11}}{K_{22}} = 1$		$\frac{K_{11}}{K_{22}} = 10$		$\frac{K_{11}}{K_{22}} = 1$		$\frac{K_{11}}{K_{22}} = 10$		$\frac{K_{11}}{K_{22}} = 10$	
	$\eta^{\%}_{min}(\tau_i)$	$\tau^{\%}_{\mathcal{H}<10\%}$	$\eta^{\%}_{min}(\tau_i)$	$\tau^{\%}_{\mathcal{H}<10\%}$	$\eta^{\%}_{min}(\tau_i)$	$\tau^{\%}_{\mathcal{H}<10\%}$	$\eta^{\%}_{min}(\tau_i)$	$\tau^{\%}_{\mathcal{H}<10\%}$	$\mathcal{D}^{max}_{F(u)} \times 100$	$\tau^{\%}_{\mathcal{D}>1}$
1	2.86	6.45	2.58	1.96	26.71	0.00	25.87	0.00	144.90	6.08
2	2.99	7.00	2.65	8.94	31.24	0.00	24.55	0.00	173.78	7.59
3	2.86	6.45	2.58	1.96	26.71	0.00	25.87	0.00	144.90	6.08
4	2.99	7.00	2.65	8.94	31.24	0.00	24.55	0.00	173.78	7.59

Table 5. *Influence of material-orthotropy*: Criss-Cross pattern. Orthotropic heat-condiction, quadratic triangles ($p = 2$). Values of $\eta^{\%}_{min}(\tau_i)$ and $\tau^{\%}_{\mathcal{H}<10\%}$ for the class of general solutions and the recipe $\mathcal{F}^{ZZ-1}$ (columns 1-4) and the recipe $\mathcal{F}^{DIR}$ (columns 5-8). In columns 9-10 we give the values of $\mathcal{D}^{max}_{F(u)}$ and $\tau^{\%}_{\mathcal{D}>1}$ for the case $\frac{K_{22}}{K_{11}} = 10$.

Relative robustness of $\mathcal{F}^{ZZ-1}$ with respect to $\mathcal{F}^{DIR}$						
Mesh-cell of seven elements shown in Fig. 4b						
Elasticity problem						
τ	$p=1$		$p=2$		$p=3$	
	$\mathcal{D}^{max}_{F(u)}$	$\tau^{\%}_{\mathcal{D}>1}$	$\mathcal{D}^{max}_{F(u)}$	$\tau^{\%}_{\mathcal{D}>1}$	$\mathcal{D}^{max}_{F(u)}$	$\tau^{\%}_{\mathcal{D}>1}$
1	0.94	0.00	1.14	9.37	3.34	42.36
2	0.58	0.00	2.28	15.53	2.92	79.31
3	0.61	0.00	2.12	19.04	5.65	82.91
4	0.50	0.00	1.50	13.64	3.64	33.17
5	0.47	0.00	2.95	6.24	3.38	20.97
6	0.57	0.00	1.54	20.98	4.82	67.92
7	0.55	0.00	1.36	10.53	2.90	29.76

Table 6. *Influence of the p-order of the element*: Elasticity problem, bi-p elements, mesh-cell ω^h_{II}. Regions of relative robustness of the ZZ-recipe $\mathcal{F}^{ZZ-1}$ with respect to direct sampling. The values of $\mathcal{D}^{max}_{F(u)} := \max_{x \in \tau} \mathcal{D}_{F(u)}(x; \mathcal{Q}^{"H"}; \mathcal{F}^{ZZ-1}, \mathcal{F}^{DIR}; \tau_i, T_h)$ and $\tau^{\%}_{\mathcal{D}>1}\ (q_i; \mathcal{Q}; \mathcal{F}^{ZZ-1}, \mathcal{F}^{DIR}; \tau_i, T_h)$ for $p = 1$, 2 and 3.

η%-superconvergence and relative robustness of the ZZ-recipe with respect to direct sampling.						
Isotropic heat-conduction						
Linear triangles ($p = 1$)						
Chevron pattern						
	$\mathcal{F}^{ZZ-1}$		$\mathcal{F}^{DIR}$			
τ_i	$\eta^{\%}_{min}(\tau_i)$	$\tau^{\%}_{\mathcal{H}<10\%}$	$\eta^{\%}_{min}(\tau_i)$	$\tau^{\%}_{\mathcal{H}<10\%}$	$\mathcal{D}^{max}_{F(u)}$	$\tau^{\%}_{\mathcal{D}>1}$
1	0.00	43.97	43.68	0.00	23.20	0.00
2	0.00	43.97	43.68	0.00	23.20	0.00
3	0.00	43.97	41.91	0.00	22.59	0.00
4	0.00	43.97	41.91	0.00	22.59	0.00

Table 7. *Influence of the topology of the mesh*: Chevron pattern. Isotropic heat-conduction, linear triangles ($p = 1$). Values of the minimum relative error $\eta^{\%}_{min}(\tau_i) := (\frac{\partial u}{\partial x_i}; \mathcal{F}; \mathcal{Q}^G; \tau_i, T_h)$ in the elements for the class of general solutions and percentage area of the element $\tau^{\%}_{\mathcal{H}<10\%}$ $(\frac{\partial u}{\partial x_i}; \mathcal{F}; \mathcal{Q}^G; \tau_i, T_h)$ in which the relative error in the recovered gradient is less than 10% for $\mathcal{F} = \mathcal{F}^{ZZ-1}$ and $\mathcal{F} = \mathcal{F}^{DIR}$ (columns 3, 4). In columns 5, 6 we give the values $\mathcal{D}^{max}_{F(u)} := \max_{\mathbf{x}\in\tau_i} \mathcal{D}_{F(u)}(\mathbf{x}; \mathcal{Q}^G; \mathcal{F}^{ZZ-1}, \mathcal{F}^{DIR}; \tau_i, T_h)$ and of $\tau^{\%}_{\mathcal{D}>1}$ defined in (74).

η%-superconvergence and relative robustness of the ZZ-recipe with respect to direct sampling.						
Isotropic heat conduction						
Quadratic triangles ($p = 2$)						
	$\mathcal{F}^{ZZ-1}$		$\mathcal{F}^{DIR}$			
τ_i	$\eta^{\%}_{min}(\tau_i)$	$\tau^{\%}_{\mathcal{H}<10\%}$	$\eta^{\%}_{min}(\tau_i)$	$\tau^{\%}_{\mathcal{H}<10\%}$	$\mathcal{D}^{max}_{F(u)} \times 100$	$\tau^{\%}_{\mathcal{D}>1}$
Regular Pattern						
1	0.0	100.00	26.07	0.00	13.02	0.00
2	0.0	100.00	26.07	0.00	13.02	0.00
Chevron Pattern						
1	5.90	61.72	29.34	0.00	41.35	0.00
2	5.90	61.72	30.09	0.00	41.35	0.00
3	5.90	61.72	29.10	0.00	41.49	0.00
4	5.90	61.72	29.10	0.00	41.49	0.00
Union Jack Pattern						
1	2.86	6.83	31.77	0.00	131.51	1.56
2	2.86	6.83	31.77	0.00	131.51	1.56
3	2.99	6.91	28.51	0.00	112.83	0.93
4	2.95	6.91	28.51	0.00	112.83	0.93
5	2.95	6.93	28.51	0.00	112.83	0.93
6	2.99	6.94	28.51	0.00	112.83	0.93
7	2.86	6.83	31.77	0.00	131.51	1.56
8	2.86	6.83	31.77	0.00	131.51	1.56
Criss-Cross Pattern						
1	2.86	6.45	26.71	0.00	133.76	1.58
2	2.99	7.00	31.24	0.00	134.29	0.88
3	2.86	6.45	26.71	0.00	133.76	1.58
4	2.99	7.00	31.24	0.00	134.29	0.88

Table 8. *Influence of the mesh-topology*: Regular, Chevron, Union-Jack and Criss-Cross patterns. Isotropic heat-conduction, quadratic triangles ($p = 2$). Values of $\eta^{\%}_{min}(\tau_i)$ and $\tau^{\%}_{\mathcal{H}<10\%}$ for the recipes $\mathcal{F}^{ZZ-1}$ (columns 1, 2) and $\mathcal{F}^{DIR}$ (columns 3, 4). In columns 5, 6 we give the values of $\mathcal{D}^{max}_{F(u)}$ and $\tau^{\%}_{\mathcal{D}>1}$.

Comparison of the values of the relative errors from the periodic and the finite mesh					
Point k	$\tilde{\mathcal{H}}(\bar{\mathbf{x}}_k; \frac{\partial u}{\partial x_i}; \mathcal{F}^{DIR}; Q^H; \tilde{\tau}_i, \tilde{T})$	$\left\| \frac{\partial e_h}{\partial x_i}(\bar{\mathbf{x}}_k) \right\|$	$\left\| \left(\frac{\partial u}{\partial x_i} - \mathcal{F}^{ZZ-1}(u_h)\right)(\bar{\mathbf{x}}_k) \right\|$	$\Psi(\tau)$	$\Theta(\bar{\mathbf{x}}_k; \frac{\partial u}{\partial x_i}; \mathcal{F}^{ZZ-1}; Q; \tilde{\tau}, \tilde{T})$
1	1.86	.6137E-03	.1874E-04	.9307E-03	2.01
2	5.19	.2149E-03	.1567E-04	.4563E-03	3.43
3	7.02	.1730E-03	.2131E-04	.3617E-03	5.89
4	1.72	.3306E-03	.8311E-05	.4719E-03	1.76
5	2.22	.4019E-03	.1486E-04	.6846E-03	2.17
6	10.87	.3116E-03	.2973E-04	.2951E-03	10.08
7	4.78	.4885E-03	.1605E-04	.3252E-03	4.94

Table 9a. *An example which shows that the results obtained using the method of freezing the periodicity hold in the actual meshes.* Isotropic heat-conduction, biquadratic elements ($p = 2$), mesh-cell ω_{II}^h. The points are shown in Fig. 18. The values of $\tilde{\mathcal{H}}(\bar{\mathbf{x}}_k; \frac{\partial u}{\partial x_i}; \mathcal{F}^{DIR}; Q^H; \tilde{\tau}_i, \tilde{T})$ are given in column 2. In column 3 (resp. column 4) we give the values of $\left\| \frac{\partial e_h}{\partial x_i}(\bar{\mathbf{x}}_k) \right\|$ (resp. $\left\| \left(\frac{\partial u}{\partial x_i} - \mathcal{F}^{ZZ-1}(u_h)\right)(\bar{\mathbf{x}}_k) \right\|$. In column 5 we give the value of $\Psi(\tau_i)$ and in column 6 the values of $\Theta(\bar{\mathbf{x}}_k; \frac{\partial u}{\partial x_i}; \mathcal{F}^{ZZ-1}; Q; \tilde{\tau}, \tilde{T})$.

Coefficients of the cubic harmonic solutions used in Table 9a		
$u(x_1, x_2) = \alpha_1(x_1^3 - 3x_1x_2^2) + \alpha_2(x_2^3 - 3x_1^2x_2)$		
Point k	α_1	α_2
1	1.000	0.714
2	1.000	0.688
3	-0.577	1.000
4	-1.000	-0.796
5	-1.000	-0.796
6	-0.578	.1.000
7	-1.000	-0.578

Table 9b. *An example which shows that the results obtained using the method of freezing the periodicity hold in the actual meshes.* Isotropic heat-conduction, biquadratic elements ($p = 2$), mesh-cell ω_{II}^h. The coefficients of the solutions employed to compute the errors at the points $\bar{\mathbf{x}}_k$ in table 9a (by solving a Dirichlet boundary-value problem over the square-domain $\Omega = (0,1)^2$ using the mesh shown in Fig. 5a).

Comparison of the errors in the finite element flux and the recovered flux						
Point k	$\Psi(\tau_i)$	$\left\vert \left(F(u) - \mathcal{F}^{DIR}(u_h)\right)(\mathfrak{X}_k) \right\vert$	$\Theta(\mathfrak{X}_k; F, \mathcal{F}^{DIR}; u_i, u_h; \tau_i, T_h)$	$\left\vert \left(F(u) - \mathcal{F}^{ZZ-1}(u_h)\right)(\mathfrak{X}_k) \right\vert$	$\Theta(\mathfrak{X}_k; F, \mathcal{F}^{ZZ-1}; u_i, u_h; \tau_i, T_h)$	$\dfrac{\left\vert \left(F(u) - \mathcal{F}^{ZZ-1}(u_h)\right)(\mathfrak{X}_k) \right\vert}{\left\vert \left(F(u) - \mathcal{F}^{DIR}(u_h)\right)(\mathfrak{X}_k) \right\vert}$
1	.1391E-03	.1004E-04	7.22	.1936E-04	13.92	1.93
2	.2774E-03	.2416E-04	8.71	.5100E-04	18.41	2.11
3	.1049E-03	.3112E-04	29.67	.3166E-04	30.18	1.02
4	.4912E-03	.1109E-04	2.26	.1418E-04	2.89	1.28
5	.3314E-03	.1517E-04	4.58	.2019E-04	6.09	1.33
6	.3006E-03	.3816E-05	1.27	.3952E-04	13.15	10.35
7	.1945E-03	.2124E-04	10.92	.2816E-04	14.48	1.33

Table 10a. *An example which shows that the results obtained using the method of freezing the periodicity hold in the actual meshes.* Isotropic heat conduction, biquadratic elements ($p = 2$), mesh-cell ω_{II}^h. In column 2 we give the maximum error in the finite element solution in the elements of ω_{II}^h. Column 3 shows the error in the finite element solution at these points. Column 4 shows the relative error in the finite element solution with respect to the maximum error in the element. In Column 5 we give the error in the recovered solution at these points. In column 6 we give the relative error in the recovered solution with respect to the maximum error in the finite element solution in the element. In Column 7 we give the ratio of the error in the recovered solution $\mathcal{F}^{ZZ-1}$ with respect to the error in finite element solution $\mathcal{F}^{DIR}$ at these points.

Coefficients for the cubic solutions used in Table 10a				
$u(x_1, x_2) = a_1 x_1^3 + a_2 x_1^2 x_2 + a_3 x_1 x_2^2 + a_4 x_2^3$				
Point	a_1	a_2	a_3	a_4
1	1.00000000	.27931142	-.88763169	.92384722
2	-.05439094	-.02646028	.84947474	-1.00000000
3	.43162747	-1.00000000	-.93122513	.45706703
4	-.75131974	-.61557397	.42834683	1.00000000
5	.95275077	-.75780325	-1.00000000	-.79558135
6	-.24876338	.27911873	1.00000000	.59140203
7	-.29648689	-1.00000000	-.21416015	.97156428

Table 10b. ***An example which shows that the results obtained using the method of freezing the periodicity hold in the actual meshes***: Isotropic heat conduction, biquadratic elements ($p = 2$), mesh-cell ω_{JI}^h. The coefficients of the solutions employed to compute the errors at the points $\bar{\mathbf{x}}_k$ in Table 10a (by solving a Dirichlet boundary value problem over the square-domain $\Omega = (0,1)^2$ using the mesh shown in Fig. 5a). For example, to compute the errors at point $\bar{\mathbf{x}}_1$ in Table 10a we employed the exact solution $u(x_1, x_2) = x_1^3 + 0.27931142 x_1^2 x_2$ - $0.88763169 x_1 x_2^2 + 0.92384722 x_2^3$.

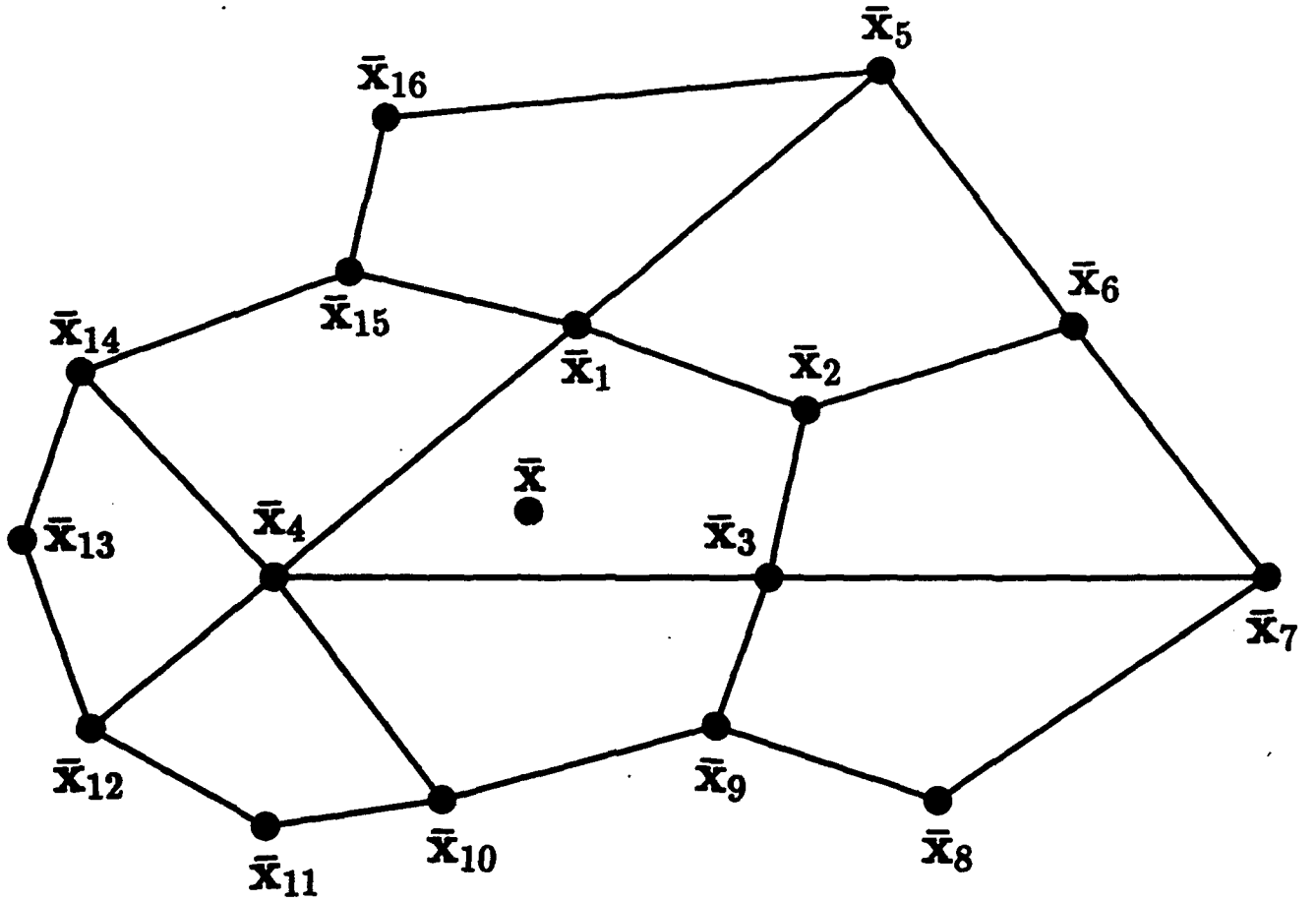
$\bar{x}_5$
$\bar{x}_{16}$
$\bar{x}_6$
$\bar{x}_{15}$
$\bar{x}_{14}$
$\bar{x}_1$
$\bar{x}_2$
$\bar{x}$
$\bar{x}_{13}$
$\bar{x}_4$
$\bar{x}_3$
$\bar{x}_7$
$\bar{x}_{12}$
$\bar{x}_9$
$\bar{x}_{11}$
$\bar{x}_{10}$
$\bar{x}_8$

Fig. 1

(a)

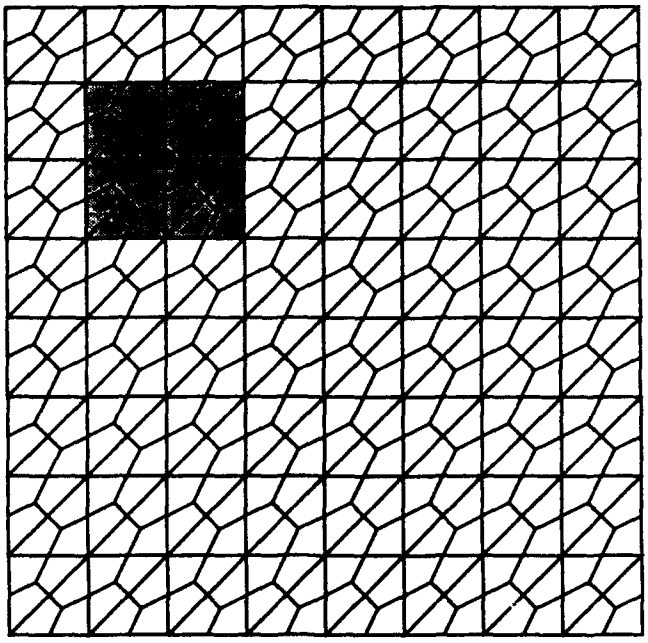

(b)

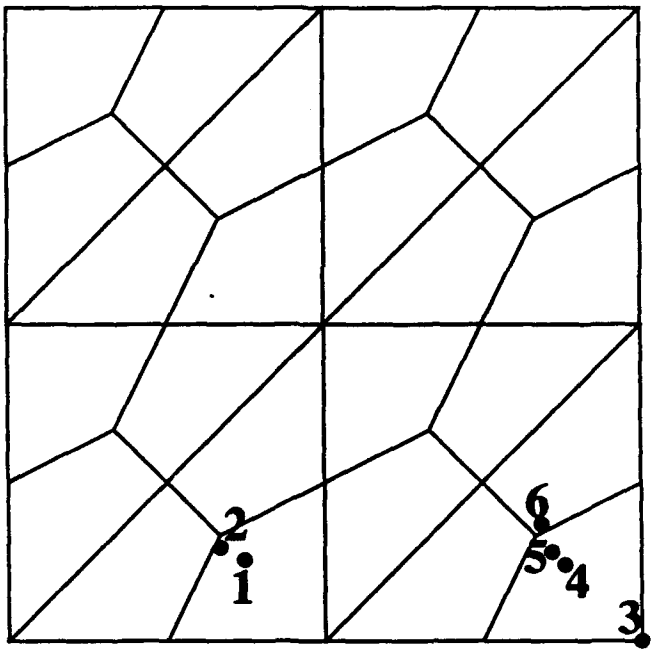

Fig. 2

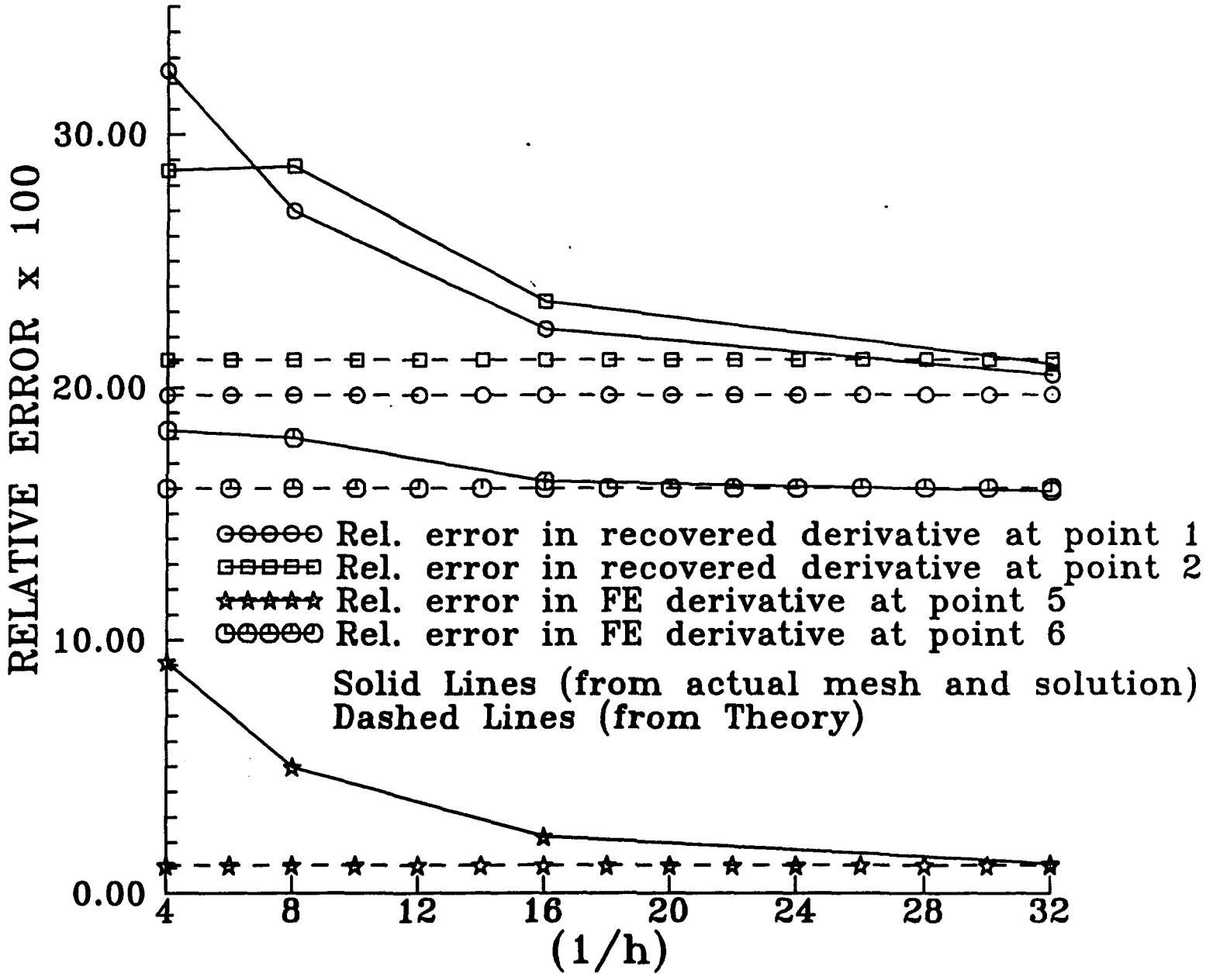
RELATIVE ERROR x 100
30.00
20.00
10.00
0.00
4
8
12
16
20
24
28
32
(1/h)
Rel. error in recovered derivative at point 1
Rel. error in recovered derivative at point 2
Rel. error in FE derivative at point 5
Rel. error in FE derivative at point 6
Solid Lines (from actual mesh and solution)
Dashed Lines (from Theory)

Fig. 3

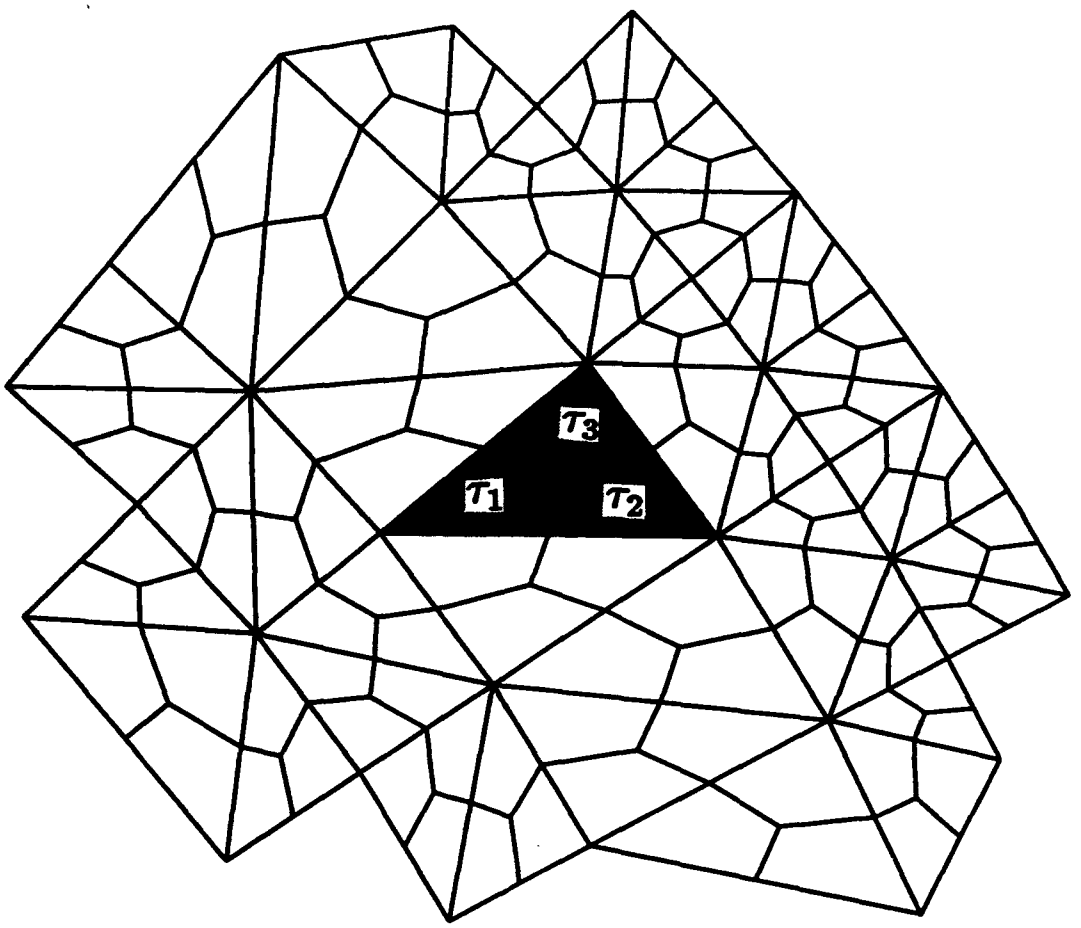

Fig. 4a

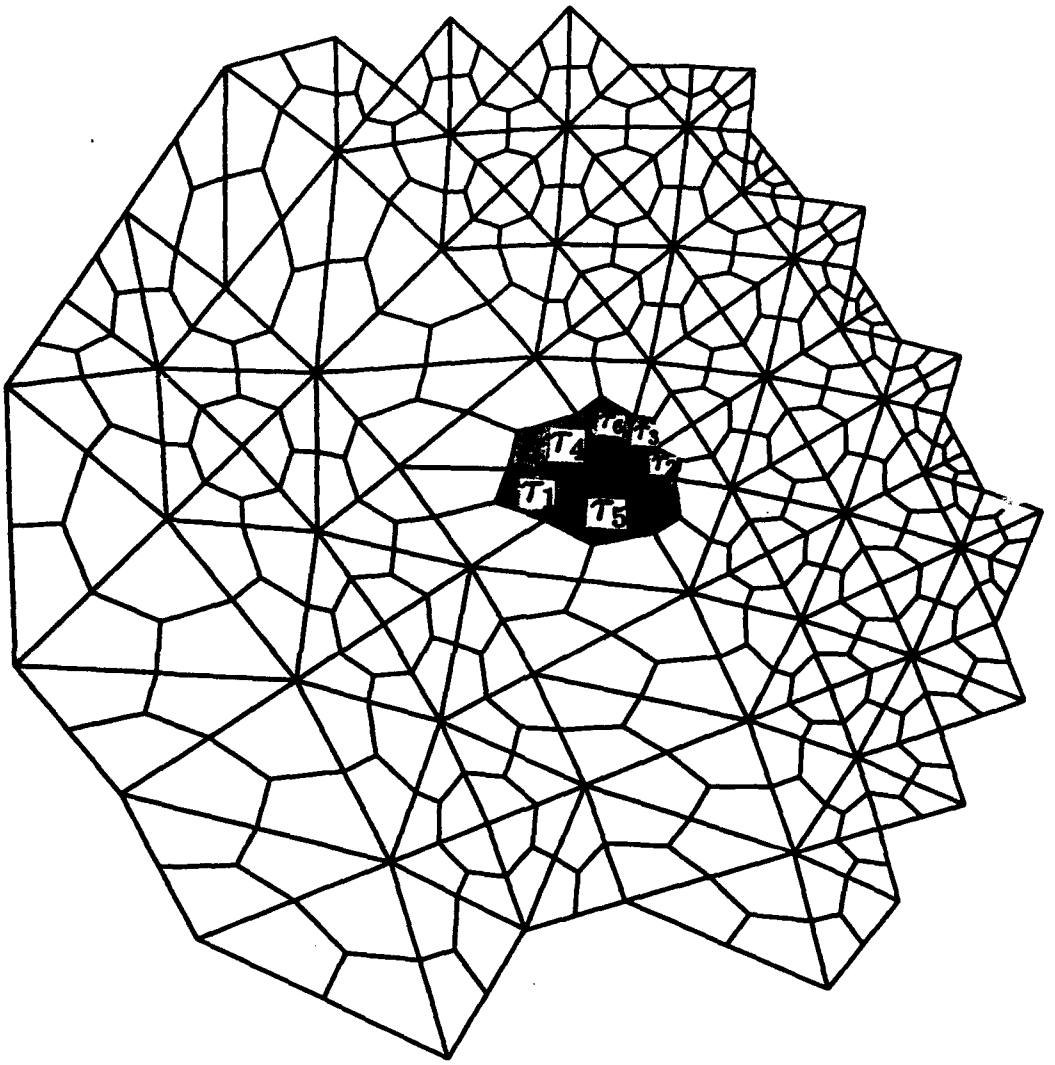

Fig. 4b

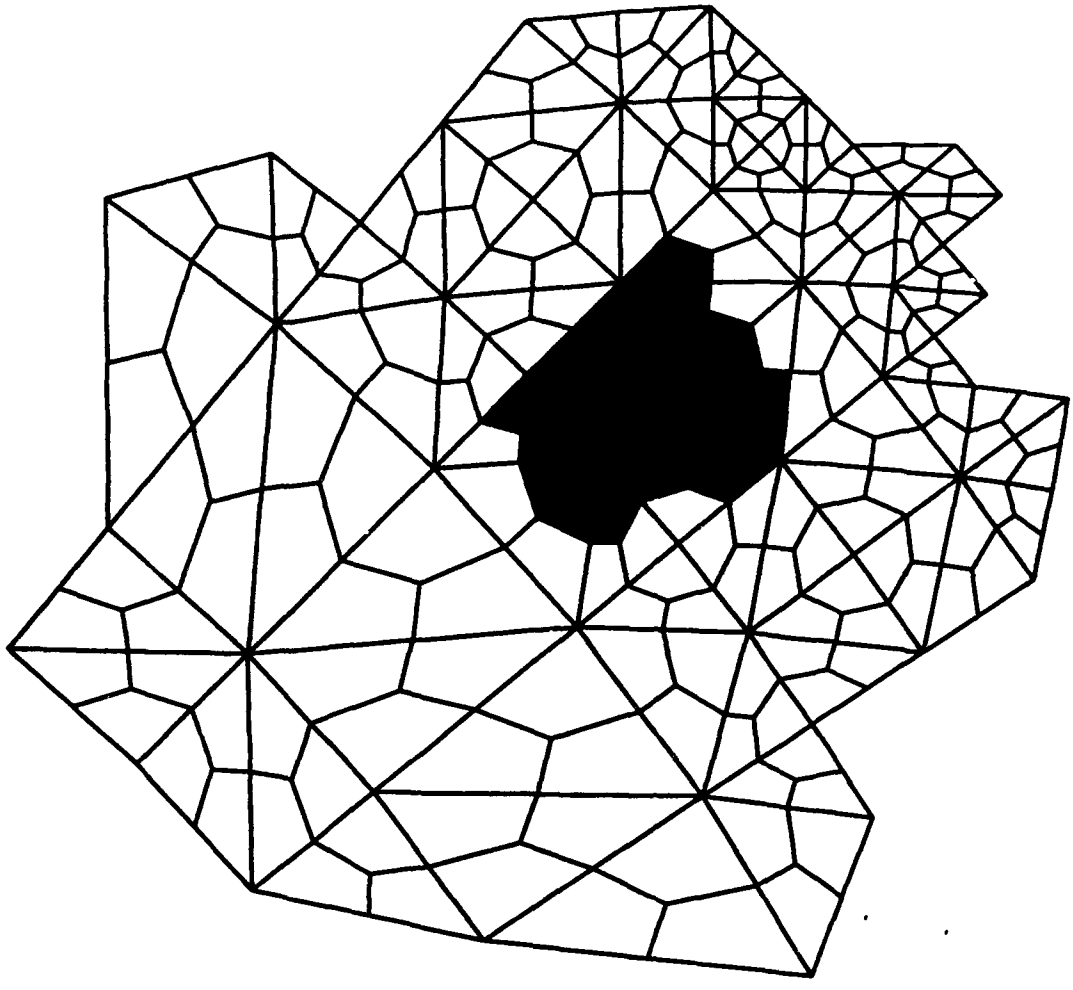

Fig. 4c

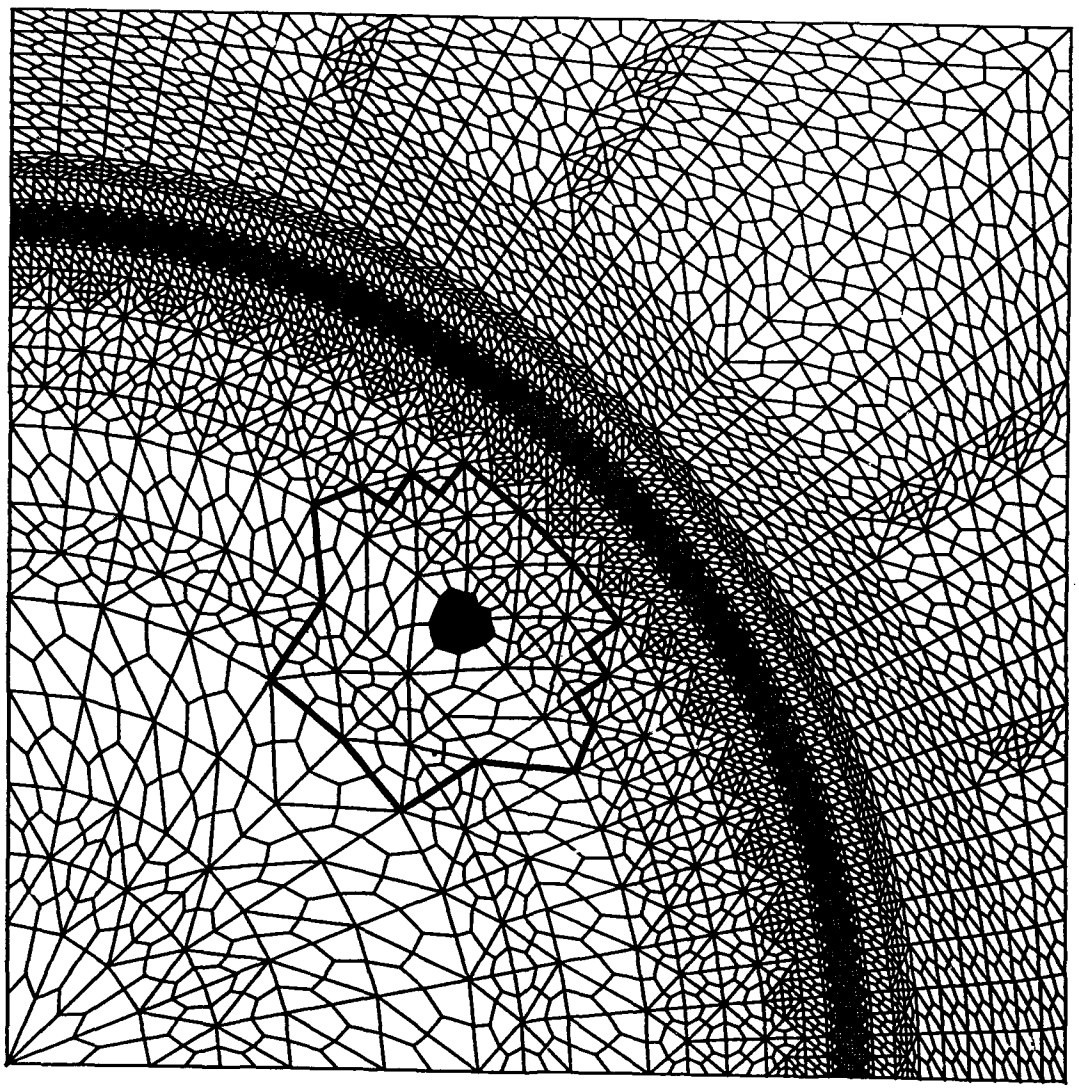

Fig. 5a

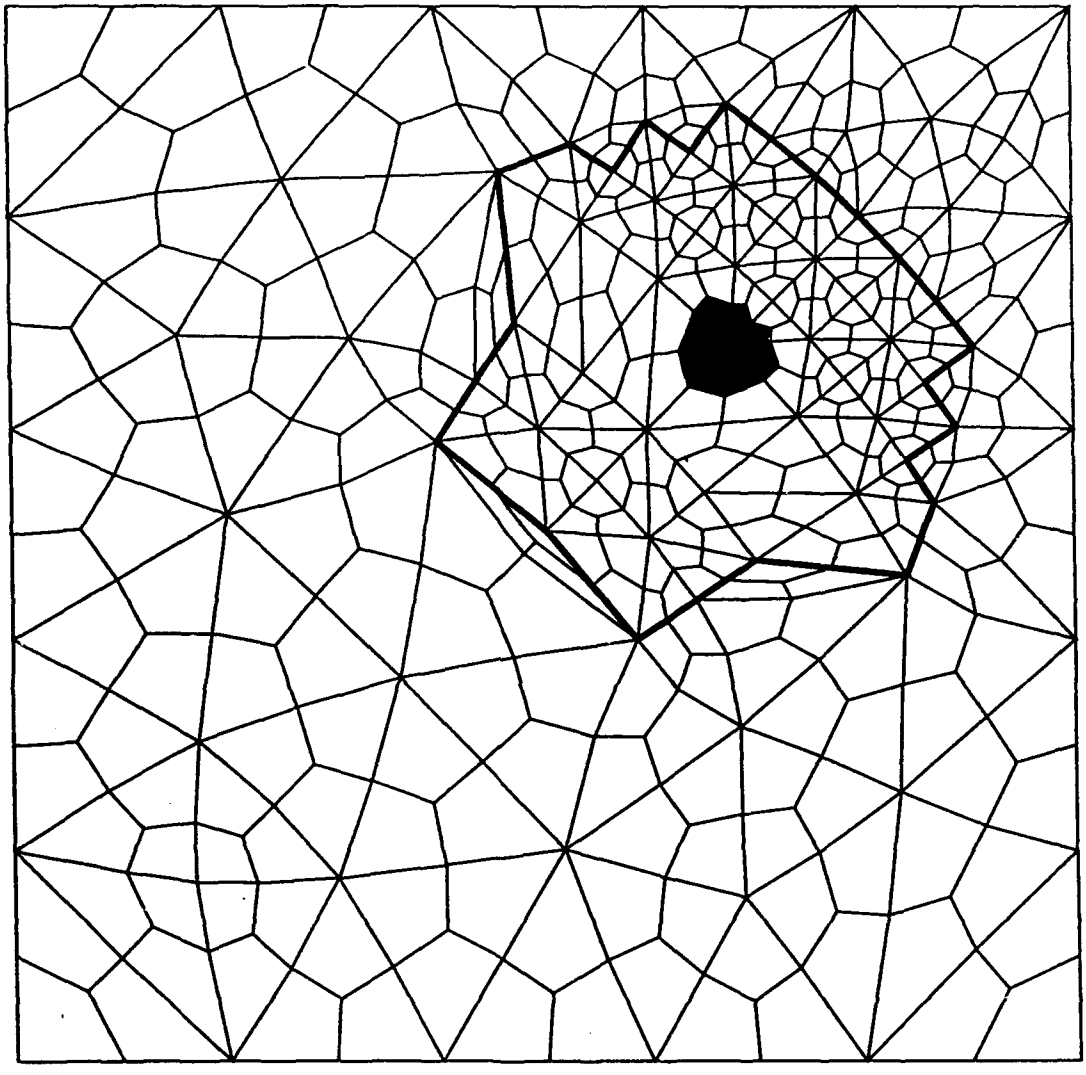

Fig. 5b

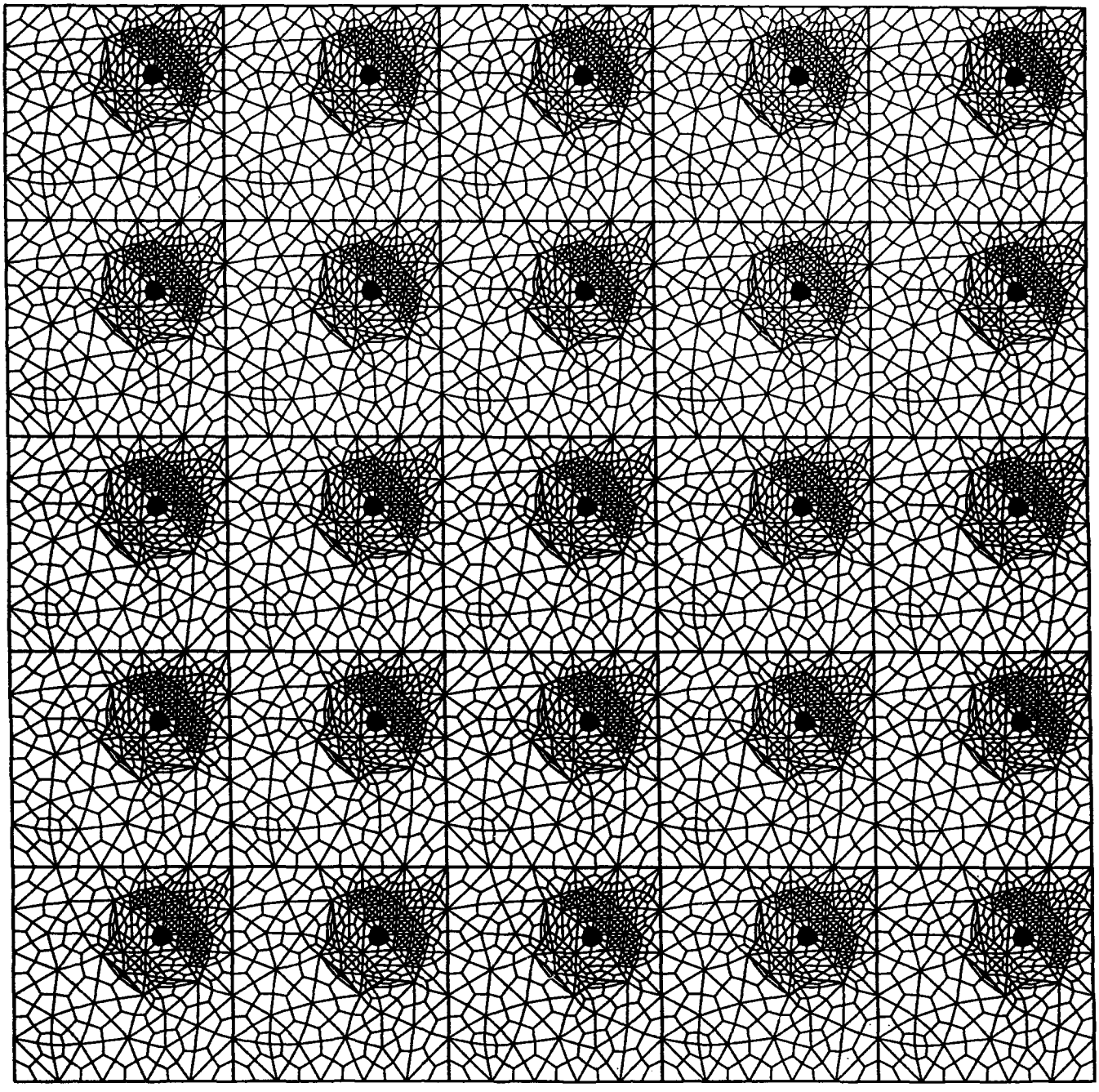

Fig. 5c

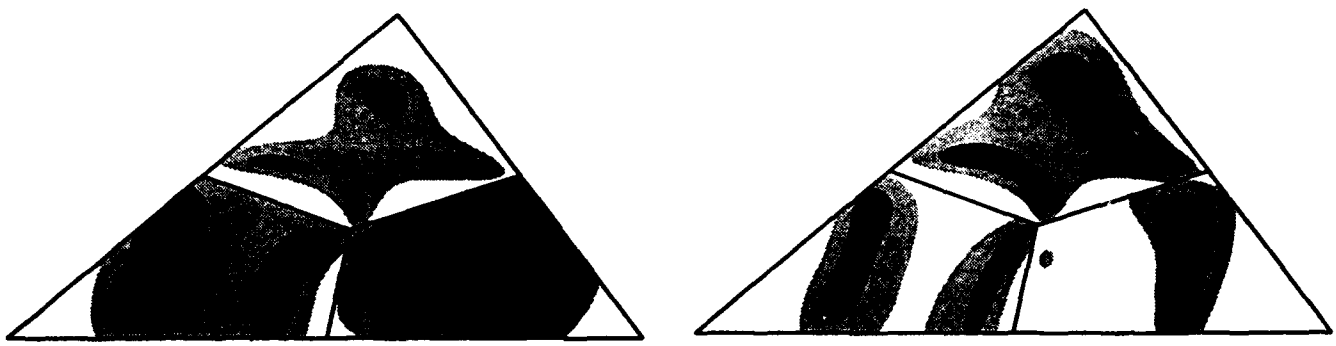

(a)

(b)

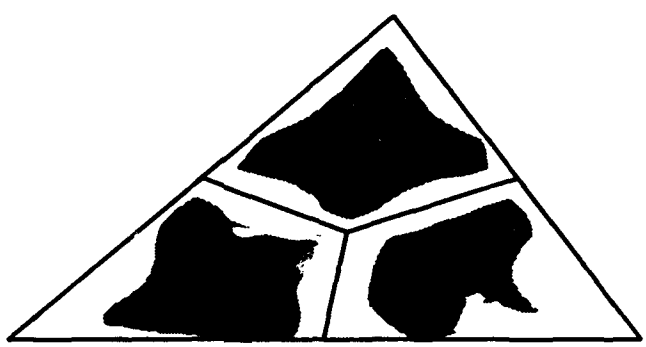

(c)

Fig. 6

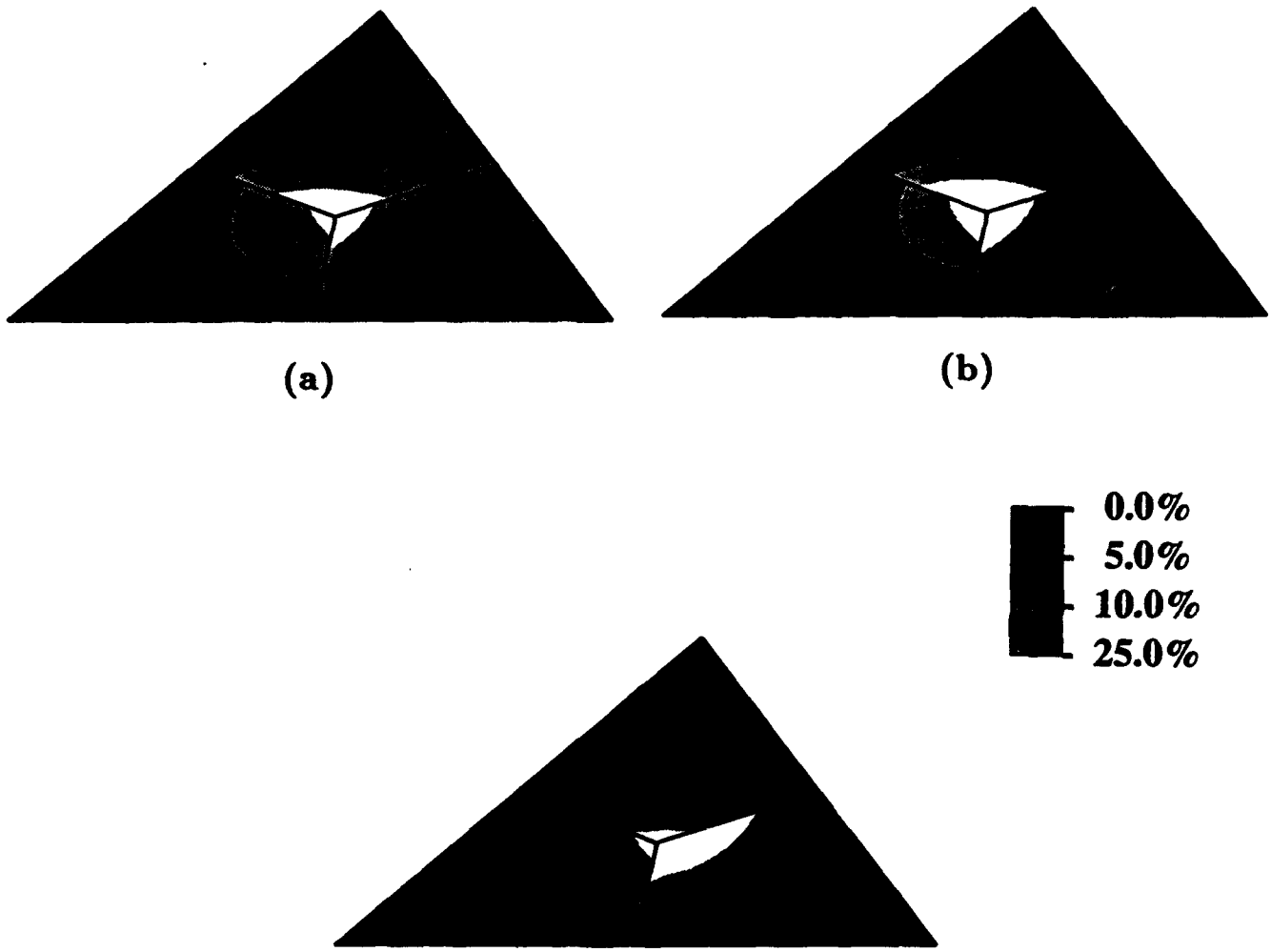

Fig. 7

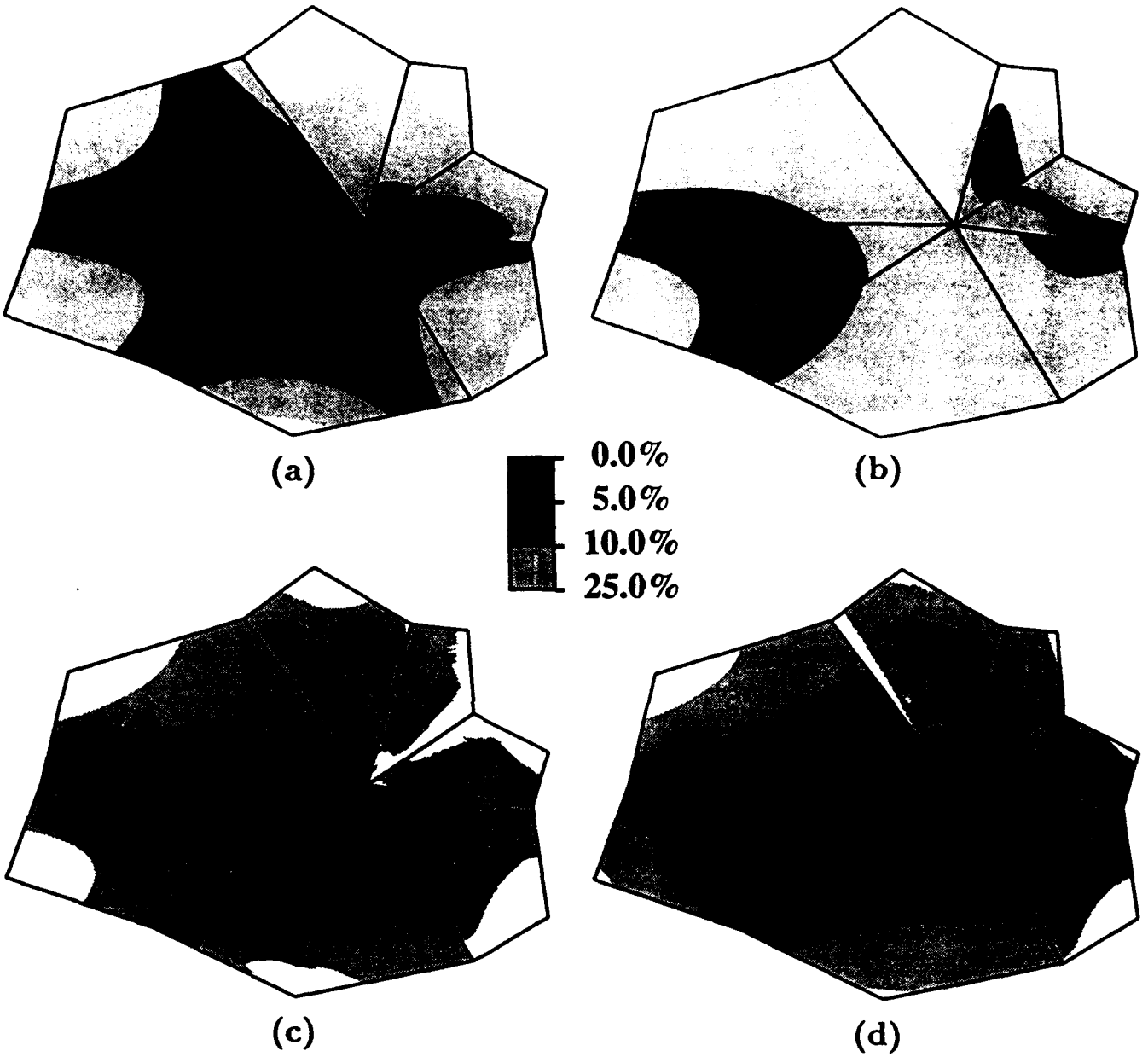

Fig. 8

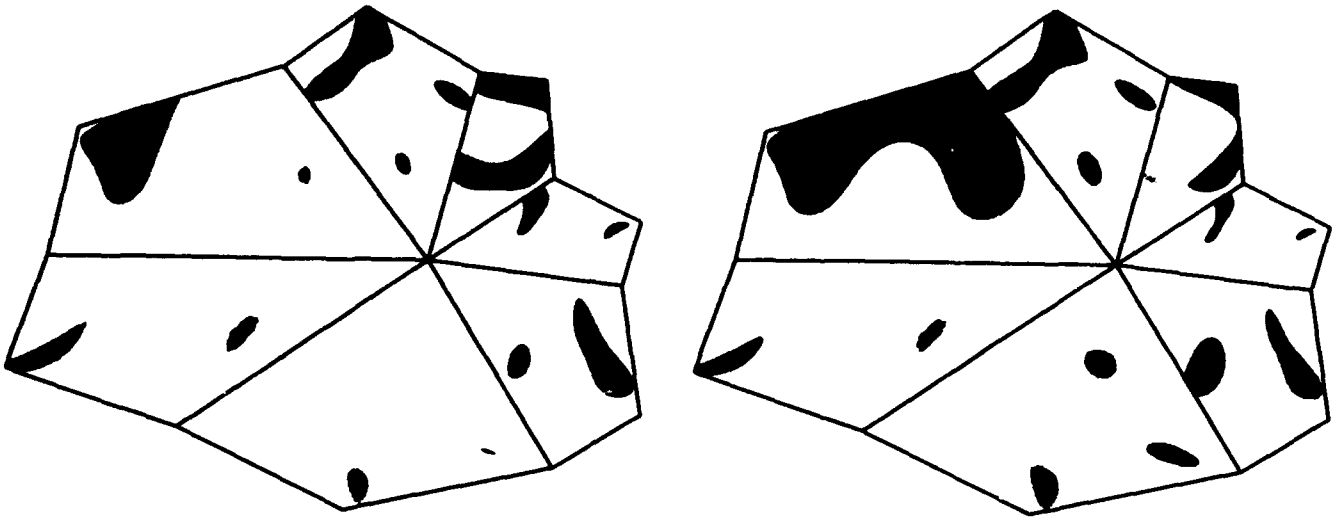

(a) (b)

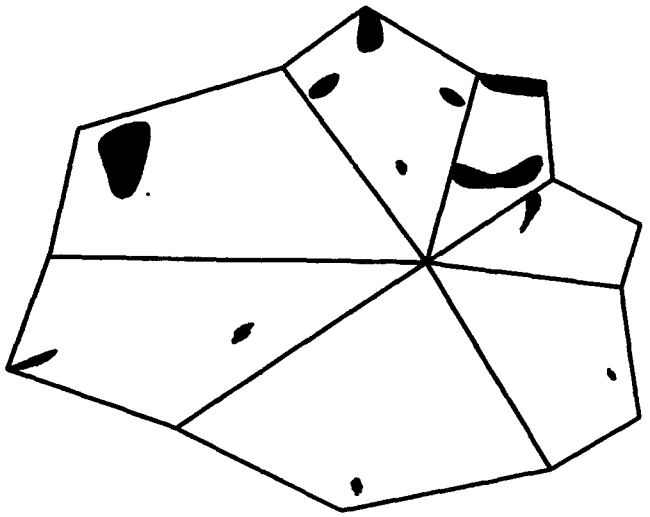

(c)

Fig. 9

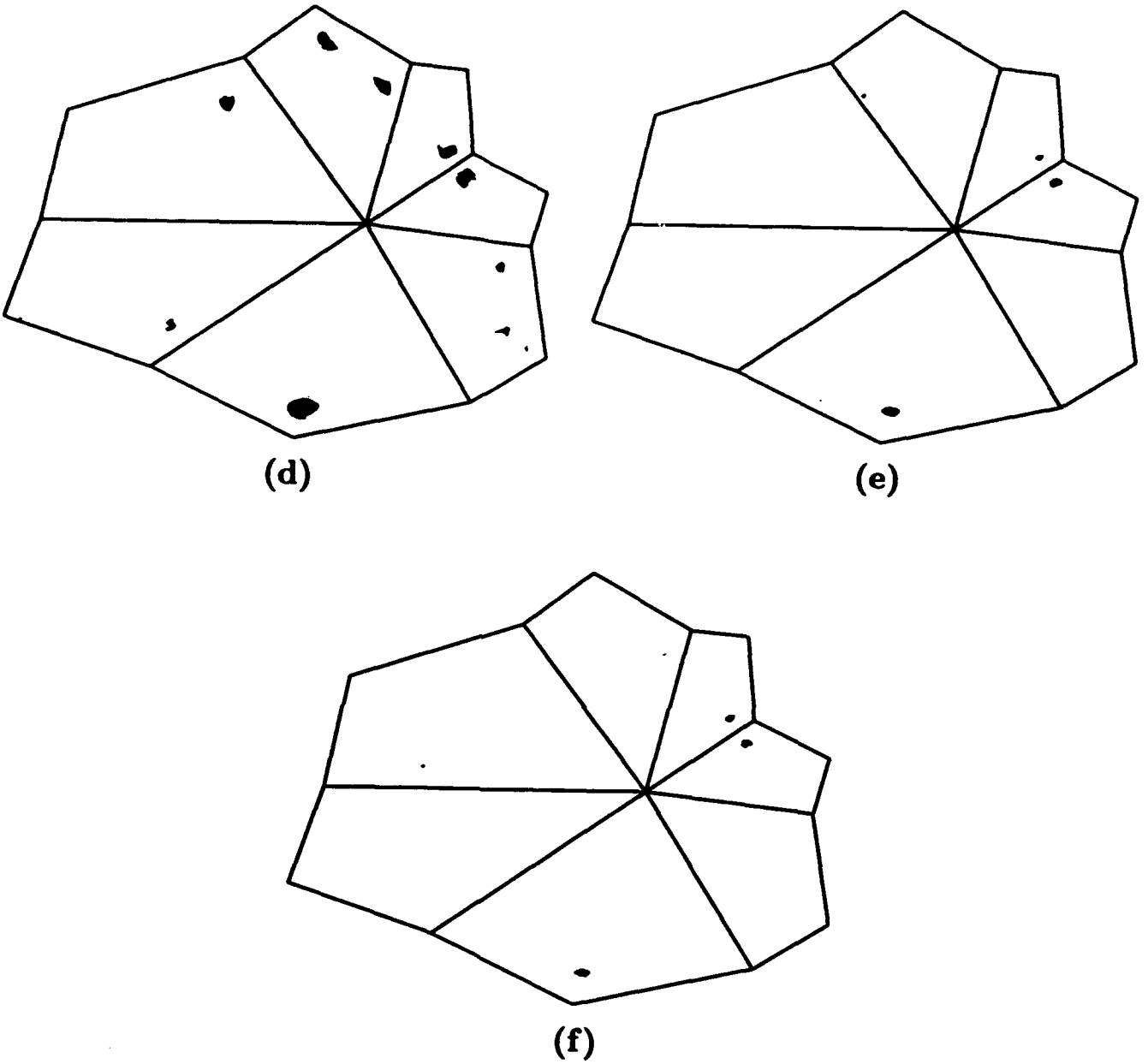

Fig. 9 (continued)

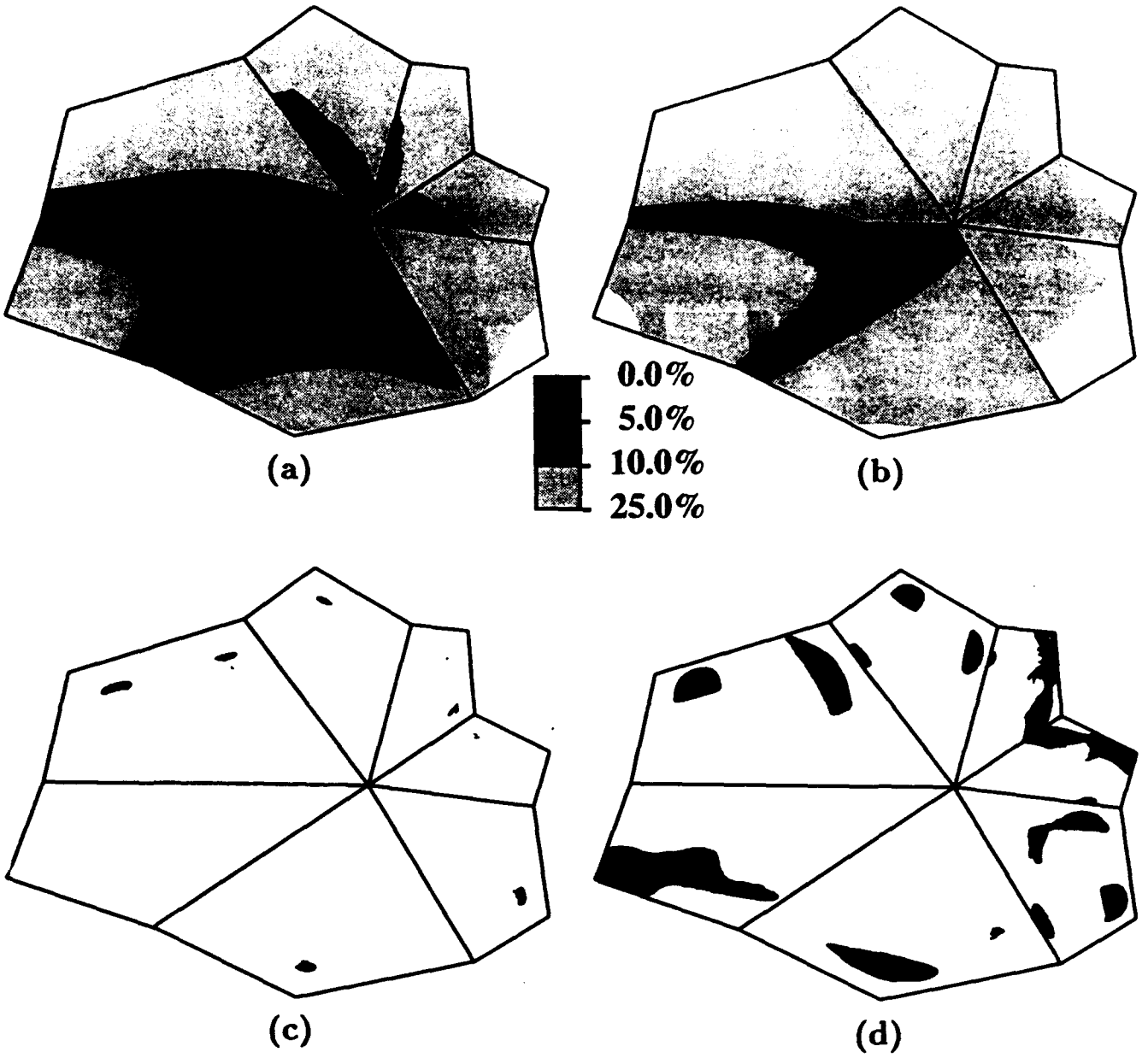

Fig. 10

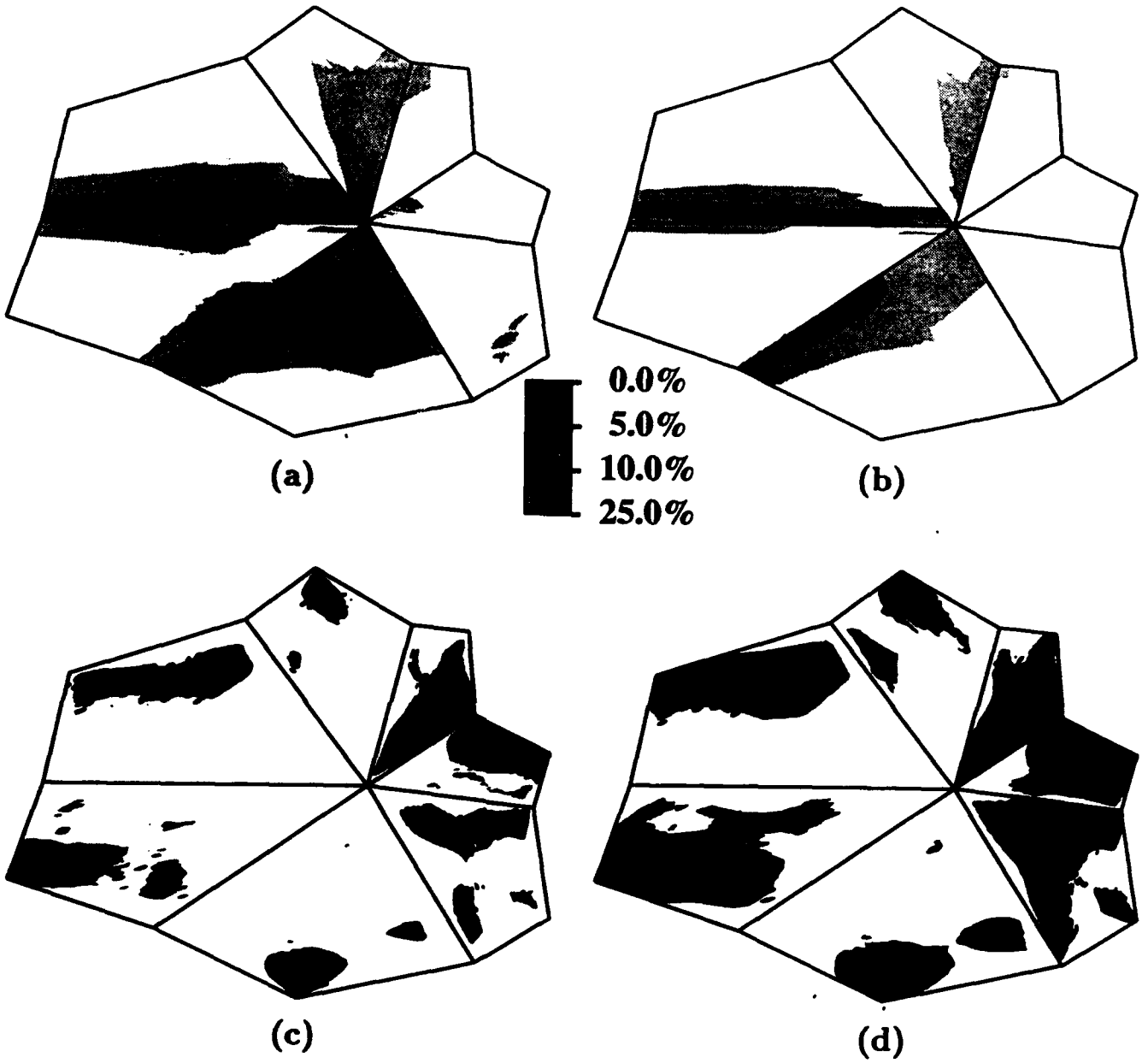

Fig. 11

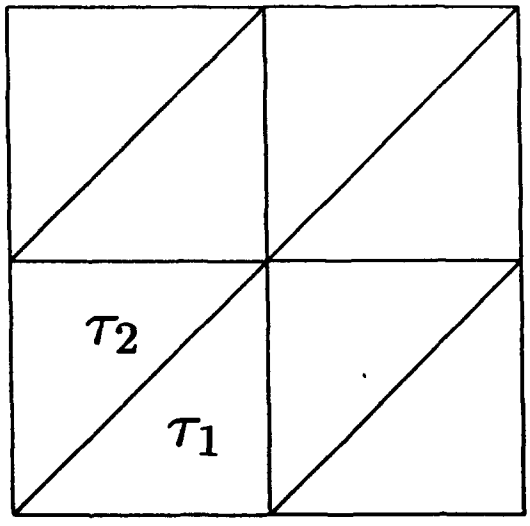
τ_2
τ_1

(a)

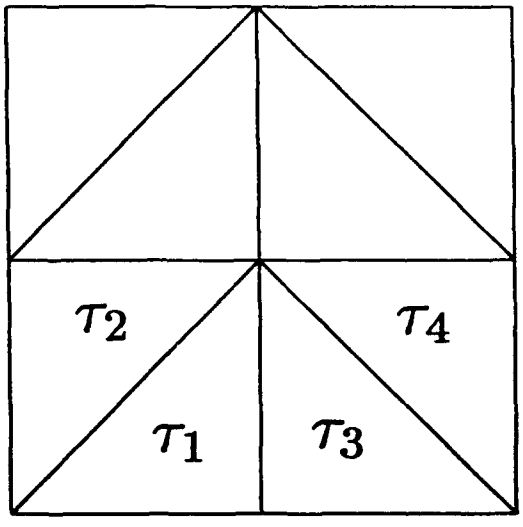
τ_2
τ_4
τ_1
τ_3

(c)

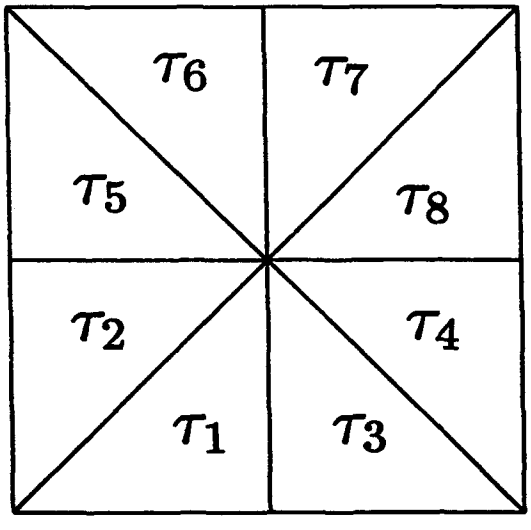
τ_6
τ_7
τ_5
τ_8
τ_2
τ_4
τ_1
τ_3

(b)

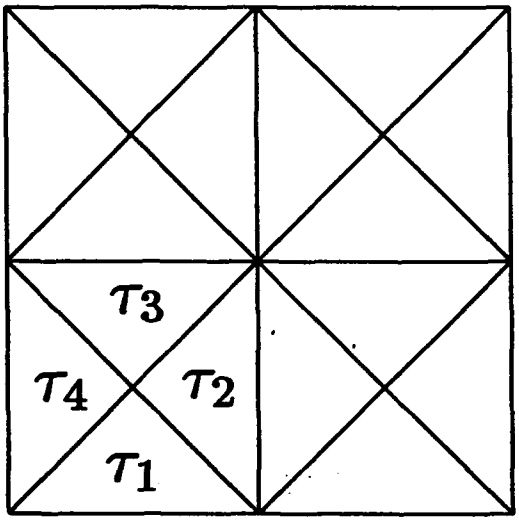
τ_3
τ_4
τ_2
τ_1

(d)

Fig. 12

(a)

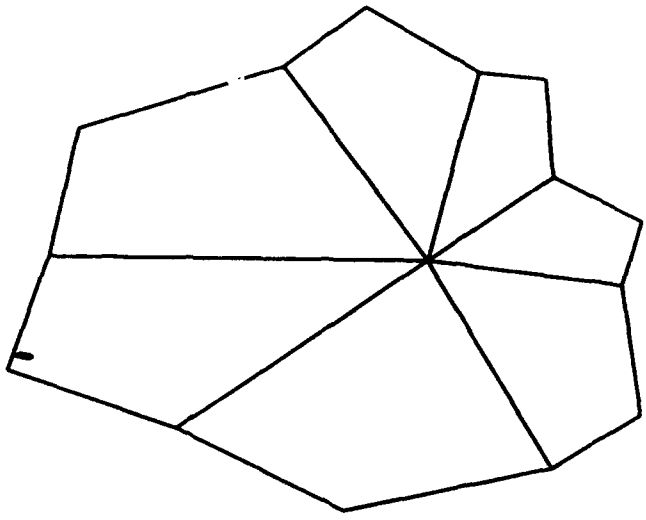

(b)

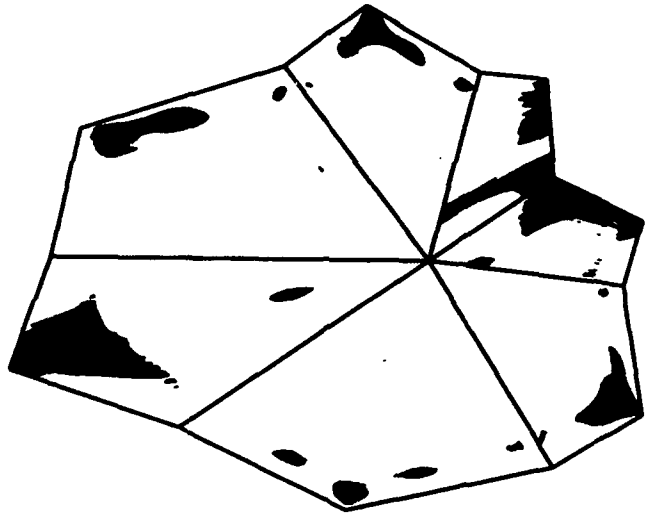

Fig. 13

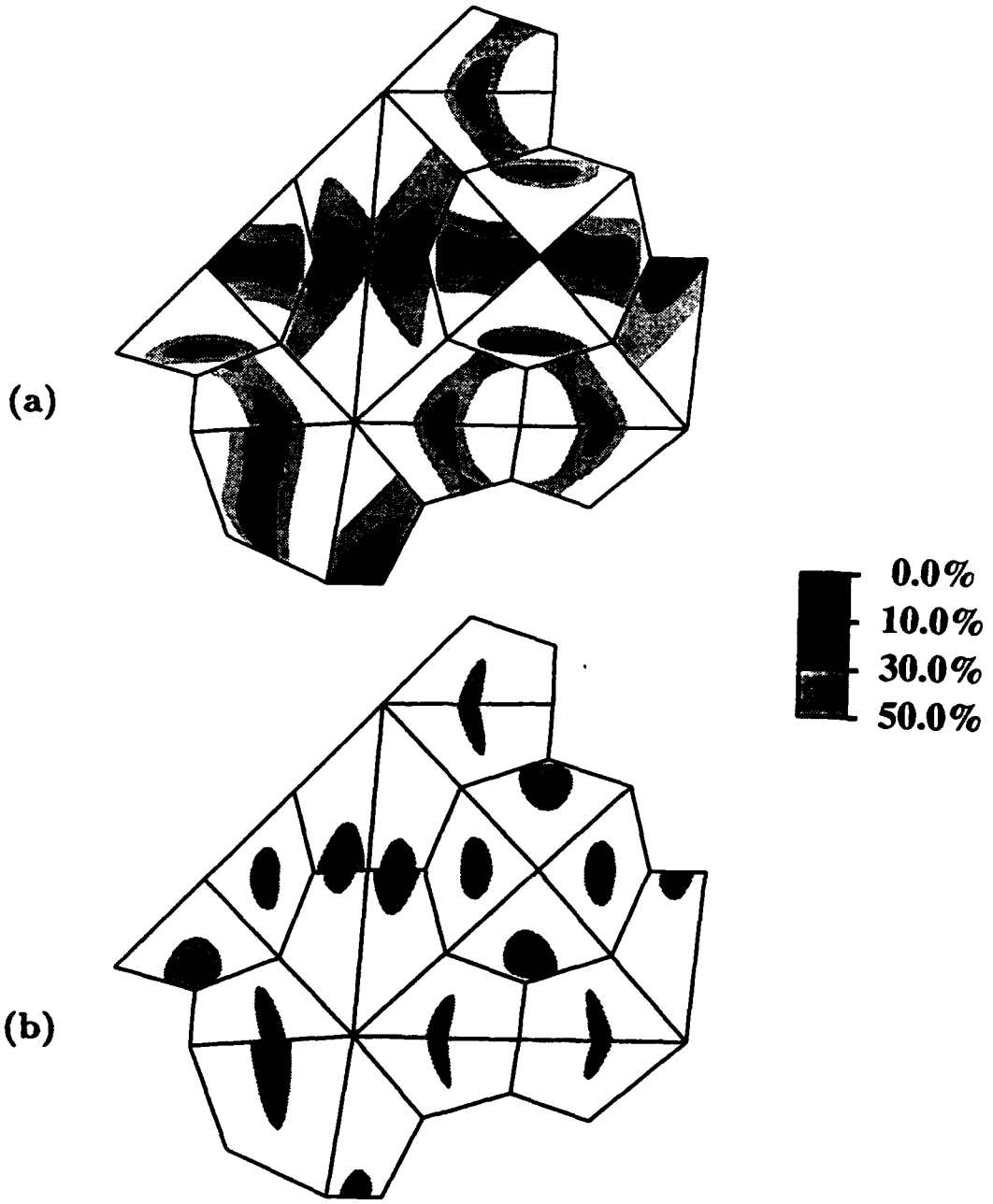

Fig. 14

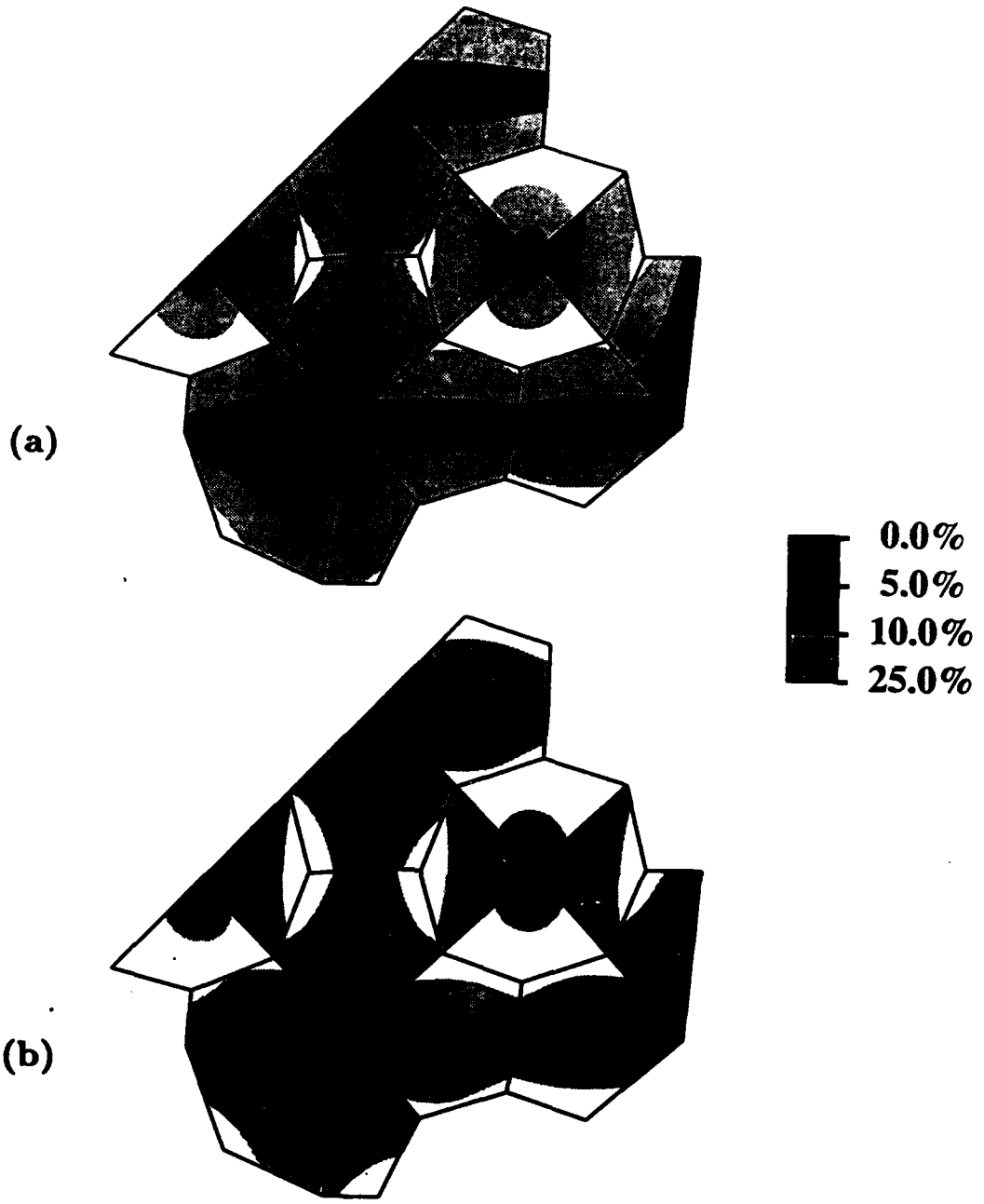

Fig. 15

(c)

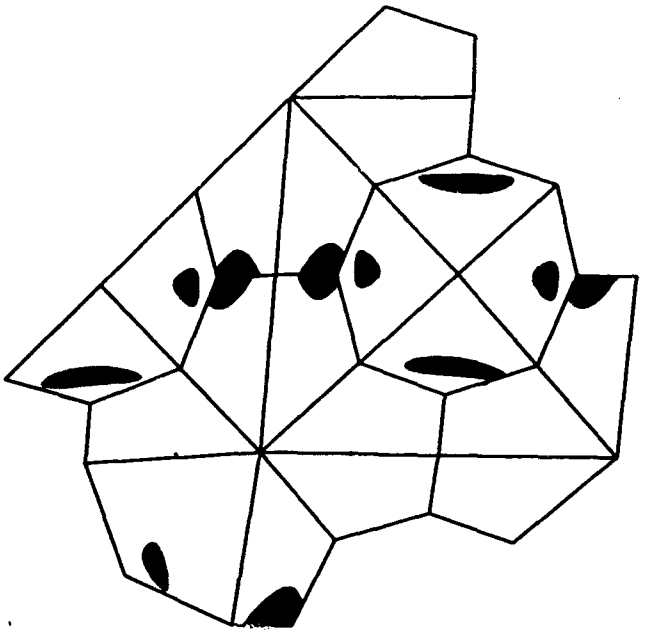

(d)

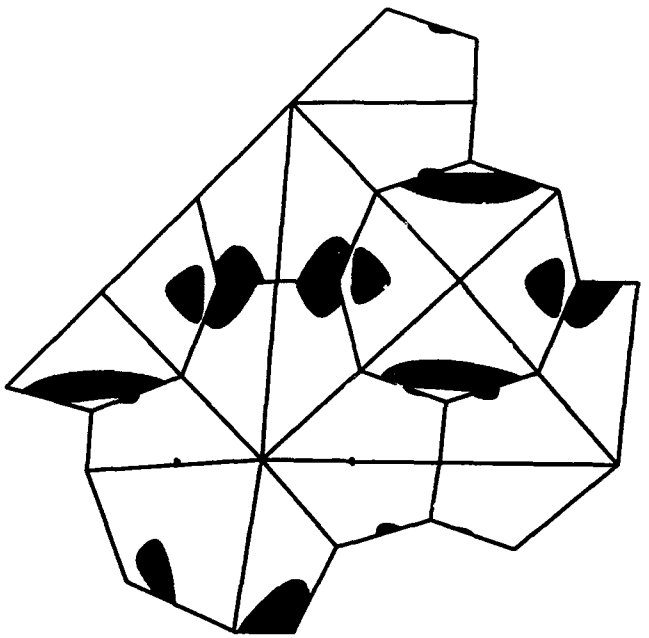

Fig. 15 (continued)

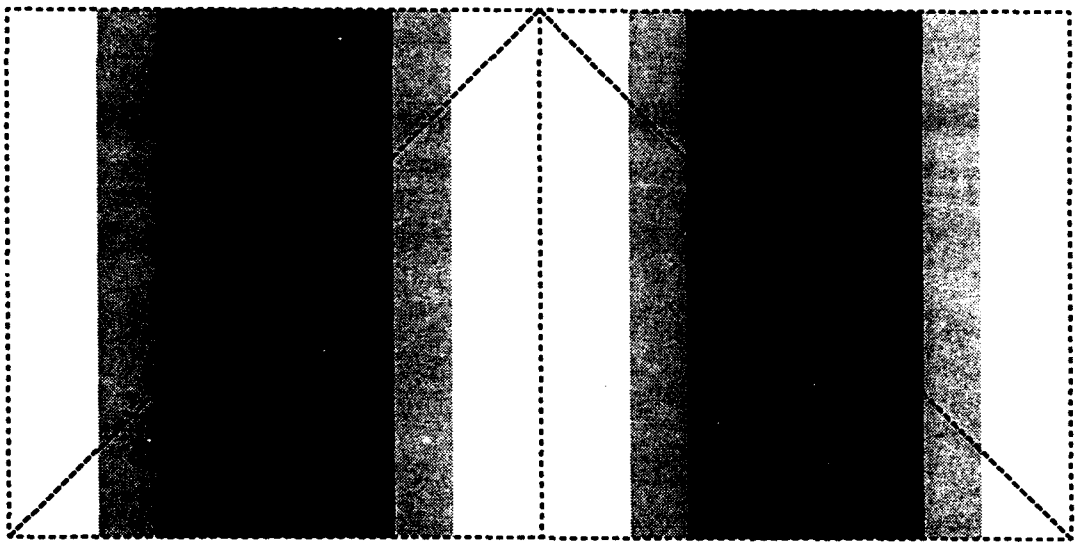

Fig. 16

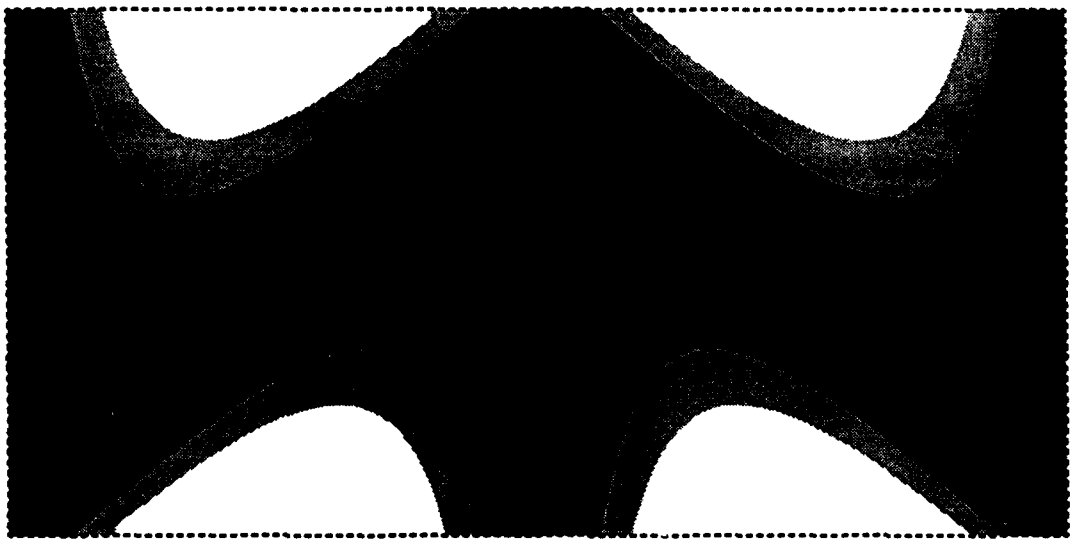

MAX ETA= 31.20

MIN ETA= 5.90

0.0%
5.0%
10.0%
15.0%

General solution **P = 2**

Fig. 17a

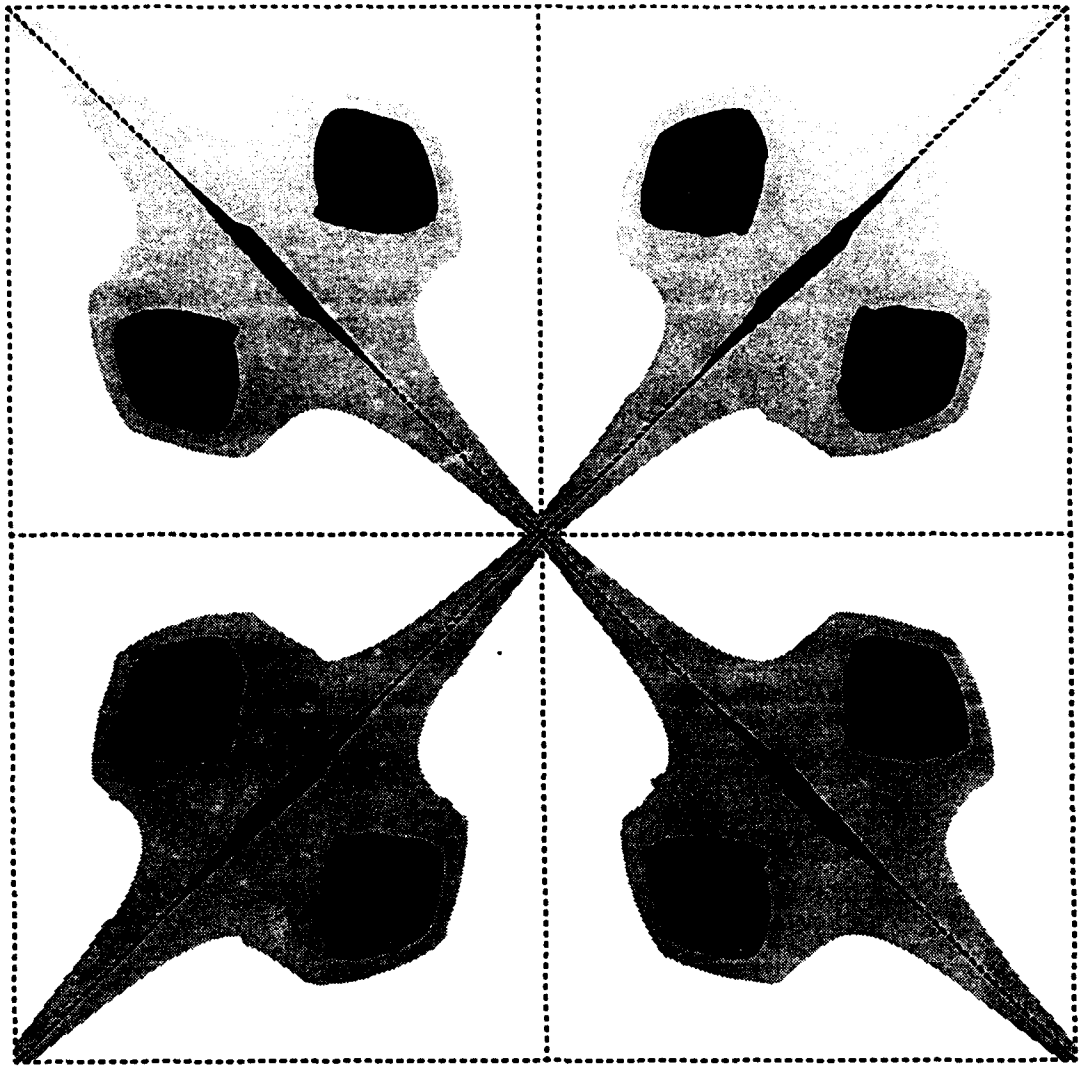

MAX ETA= 83.95

MIN ETA1= 2.86 *MIN ETA2= 2.99*

0.0%
5.0%
10.0%
15.0%

General solution **P = 2**

Fig. 17b

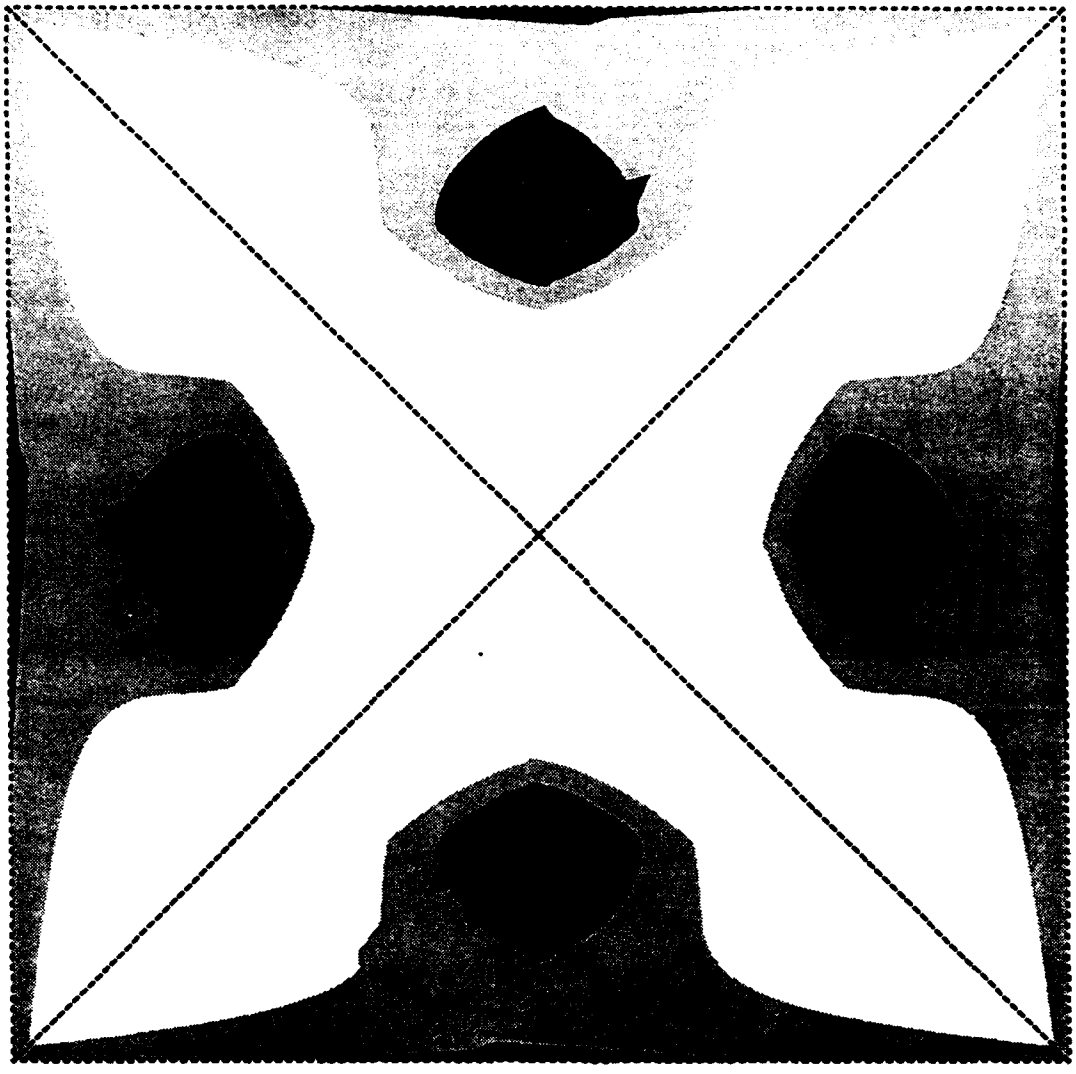

Fig. 17c

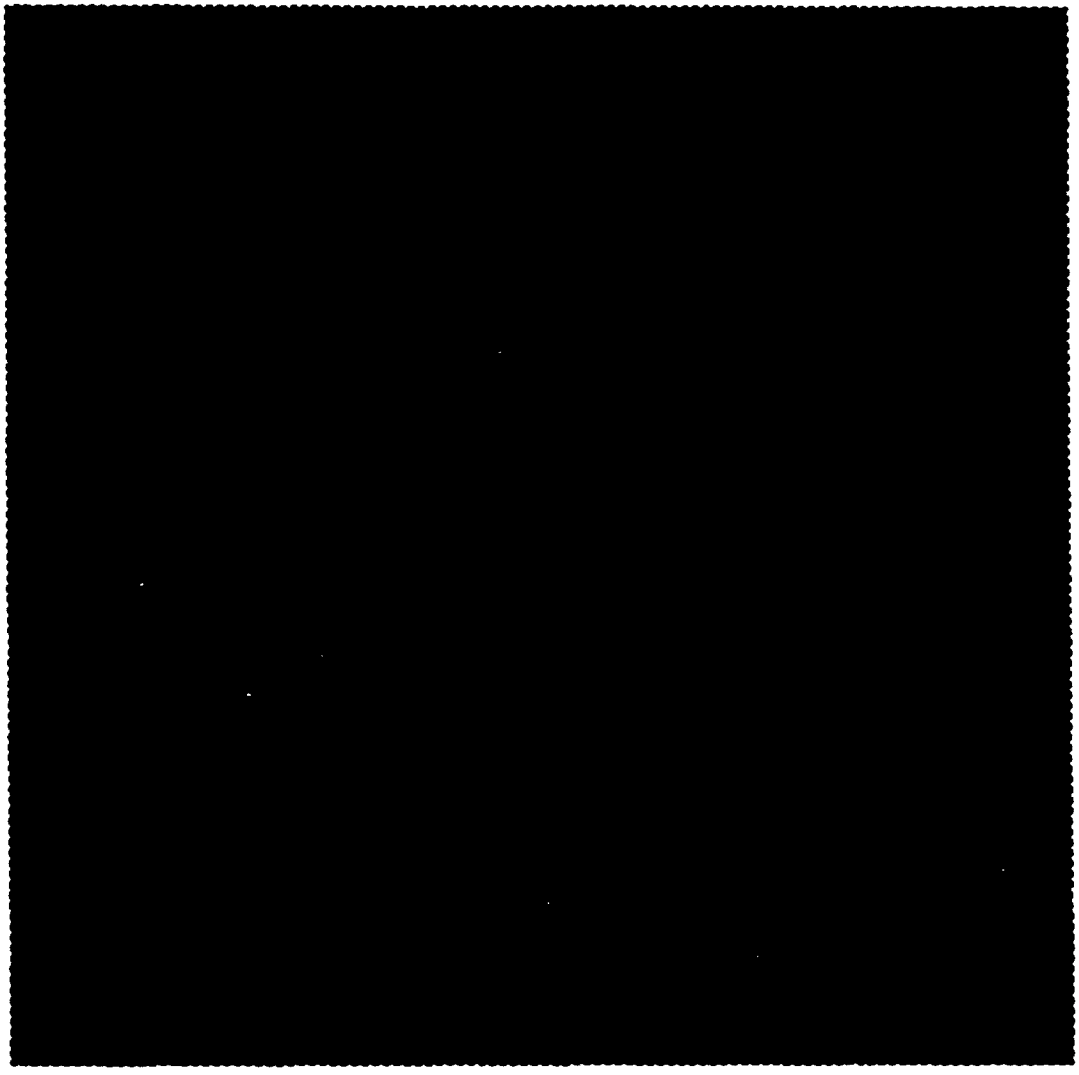

MAX ETA= 9.09

MIN ETA= .00

0.0%

5.0%

10.0%

15.0%

General solution **P = 2**

Fig. 17d

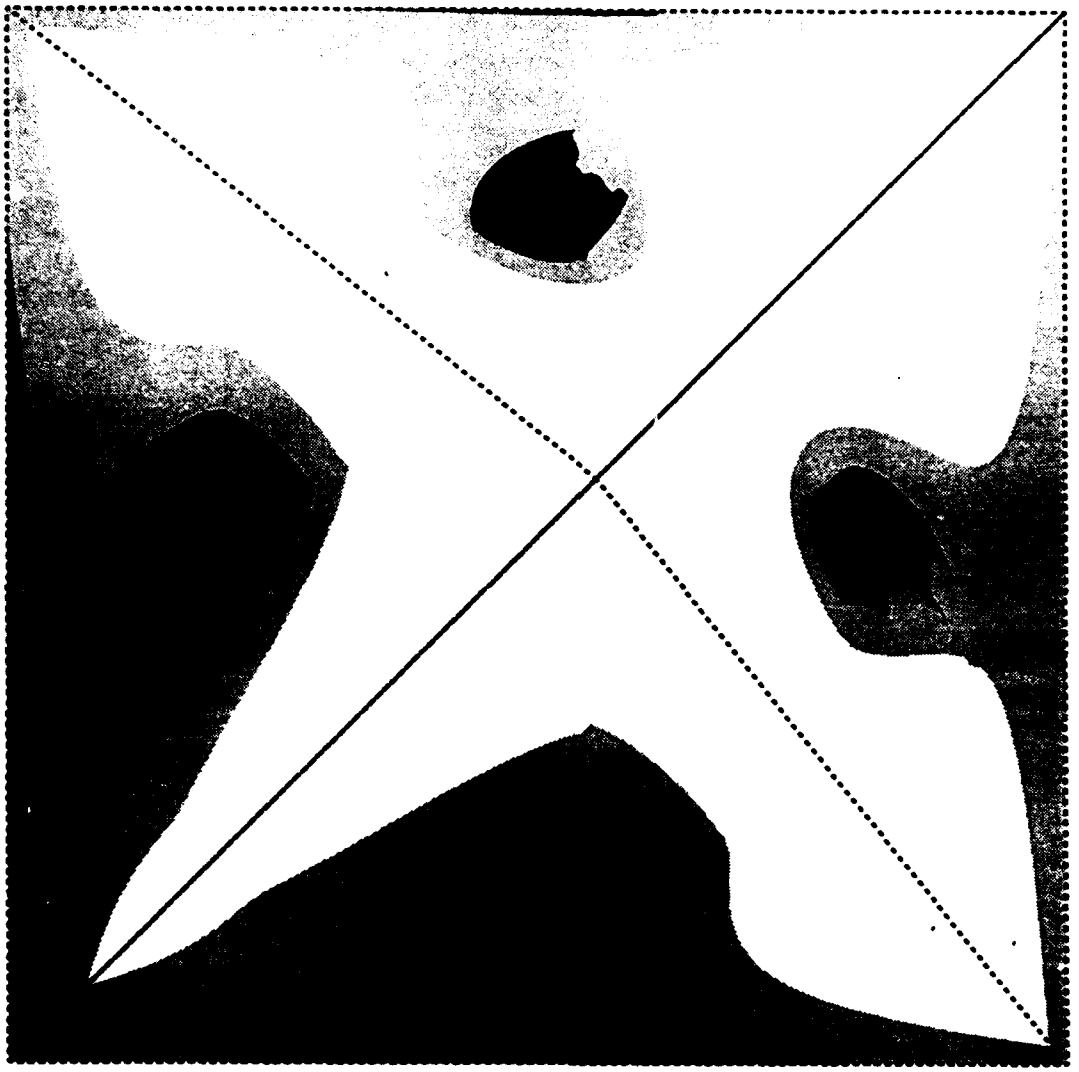

MAX ETA= 83.11 *MAX ETA= 88.02* *MAX ETA= 88.02* *MAX ETA= 80.78*

MIN ETA= 1.86 *MIN ETA= 4.98* *MIN ETA= 6.08* *MIN ETA= 2.39*

0.0%
5.0%
10.0%
15.0%

General solution **P = 2**

Fig. 17e

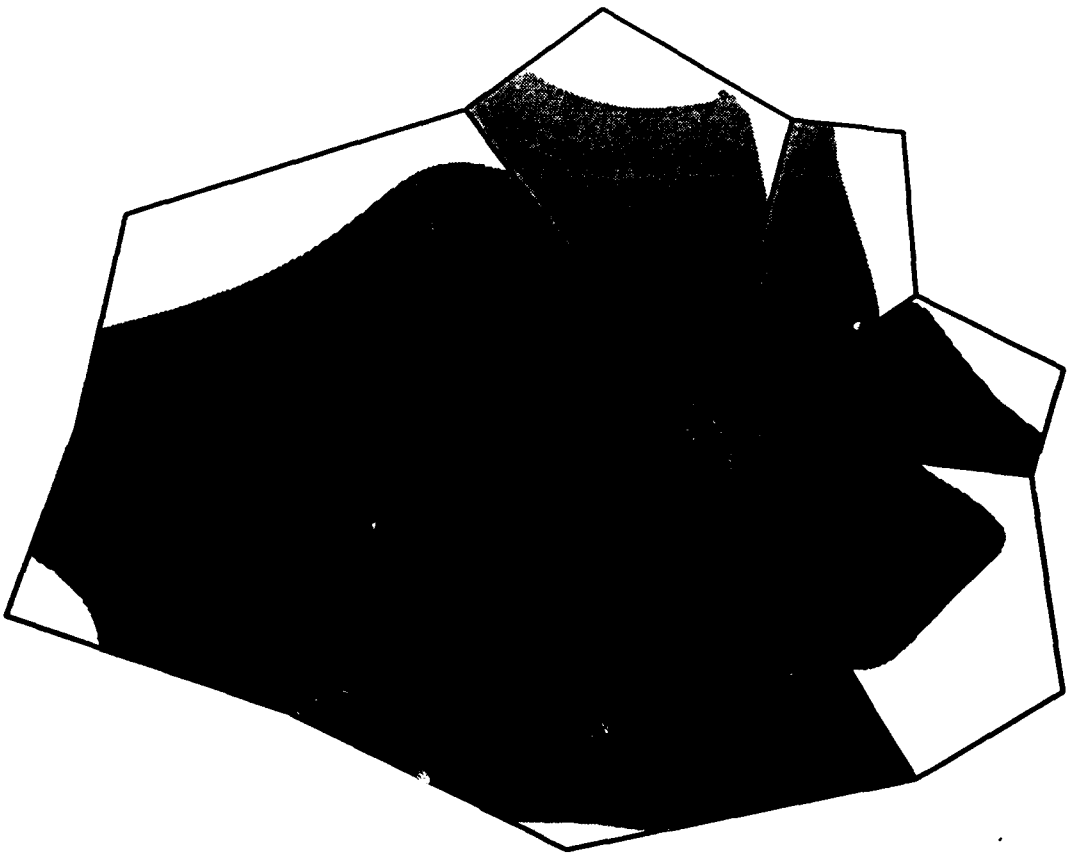

Fig. 18

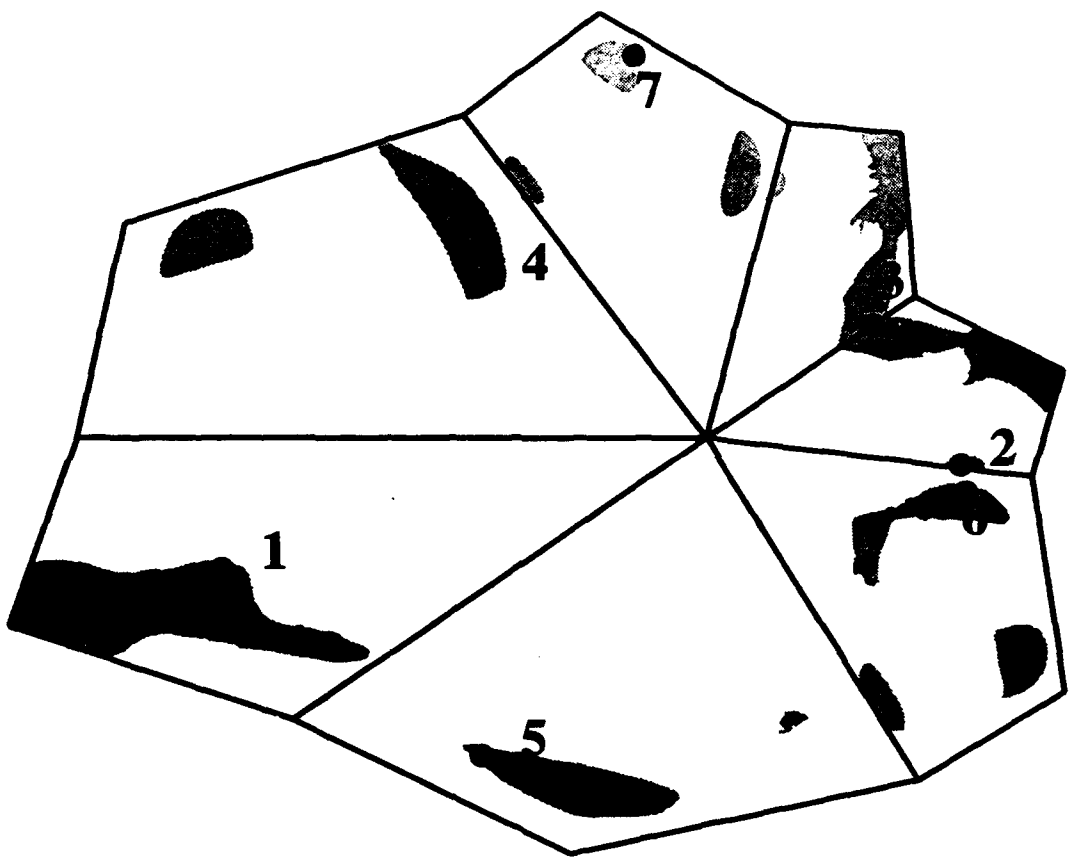

Fig. 19

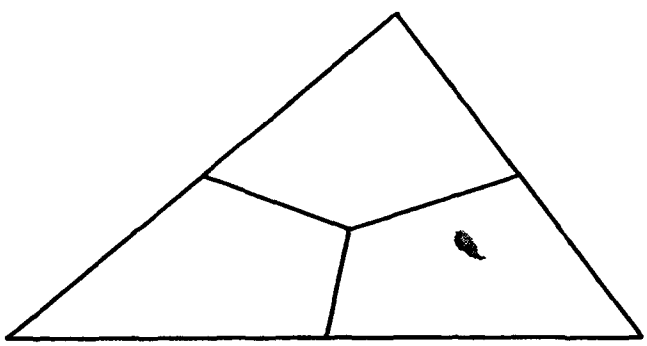

(a)

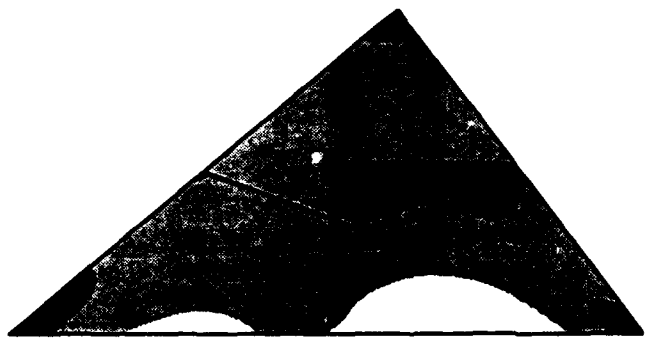

(b)

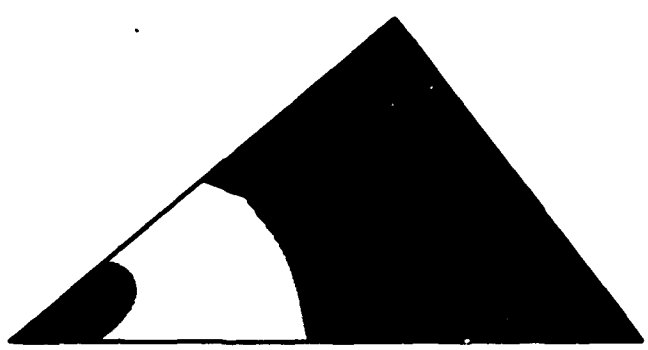

(c)

Fig. 20

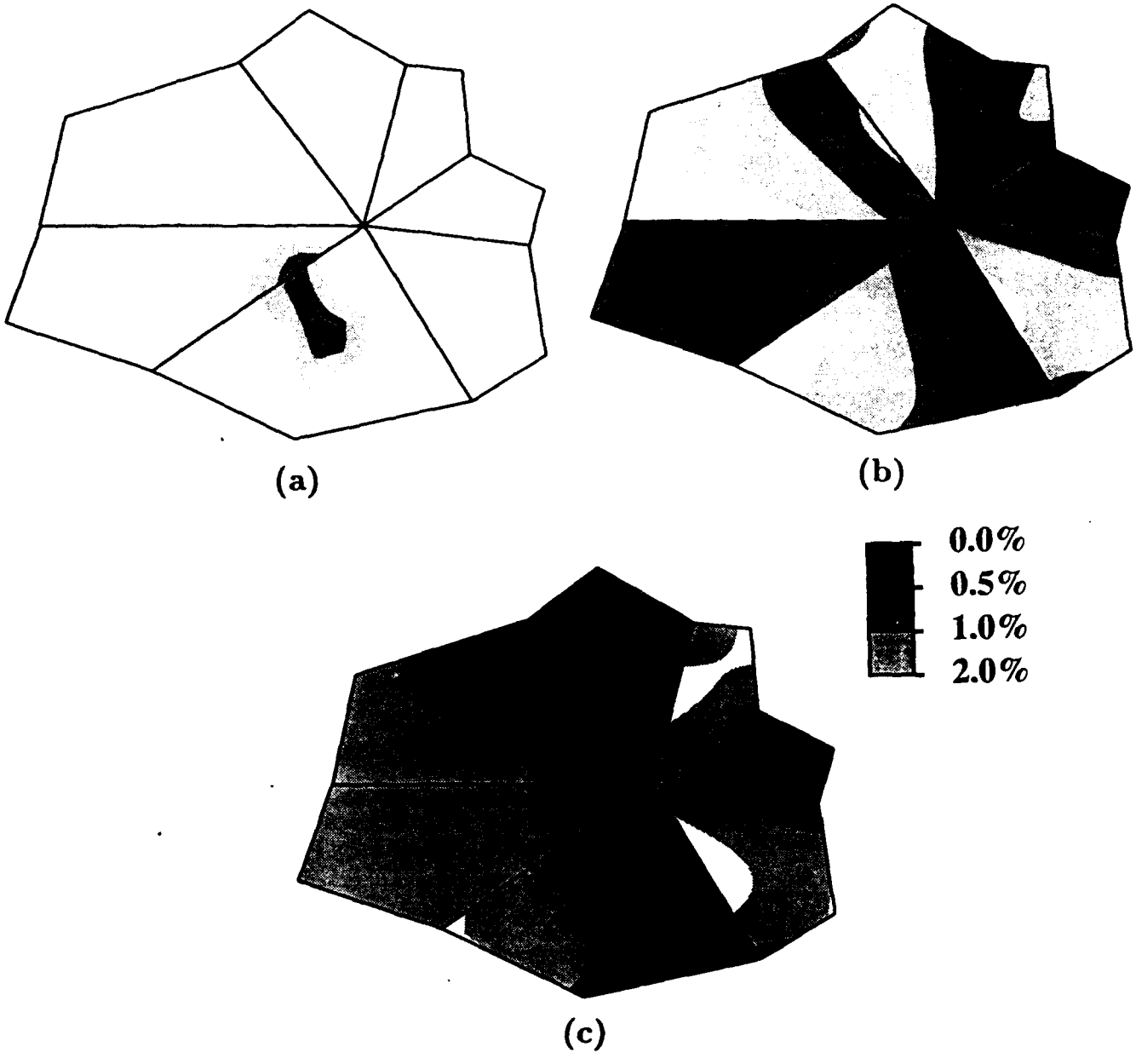

Fig. 21

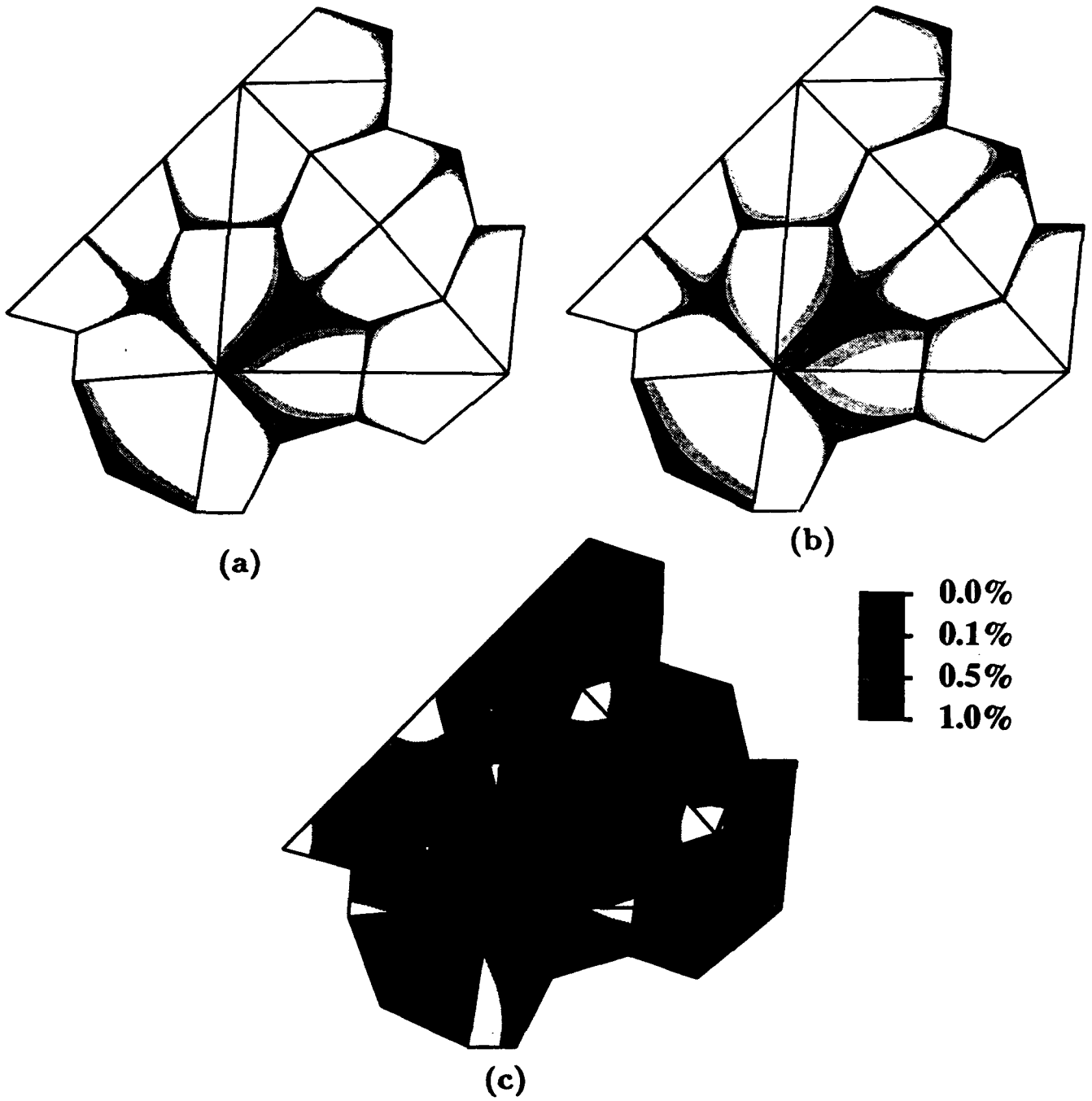

Fig. 22

The Laboratory for Numerical Analysis is an integral part of the Institute for Physical Science and Technology of the University of Maryland, under the general administration of the Director, Institute for Physical Science and Technology. It has the following goals:

To conduct research in the mathematical theory and computational implementation of numerical analysis and related topics, with emphasis on the numerical treatment of linear and nonlinear differential equations and problems in linear and nonlinear algebra.

To help bridge gaps between computational directions in engineering, physics, etc., and those in the mathematical community.

To provide a limited consulting service in all areas of numerical mathematics to the University as a whole, and also to government agencies and industries in the State of Maryland and the Washington Metropolitan area.

To assist with the education of numerical analysts, especially at the postdoctoral level, in conjunction with the Interdisciplinary Applied Mathematics Program and the programs of the Mathematics and Computer Science Departments. This includes active collaboration with government agencies such as the National Institute of Standards and Technology.

To be an international center of study and research for foreign students in numerical mathematics who are supported by foreign governments or exchange agencies (Fulbright, etc.).

Further information may be obtained from **Professor I. Babuška**, Chairman, Laboratory for Numerical Analysis, Institute for Physical Science and Technology, University of Maryland, College Park, Maryland 20742-2431.